Design Control and Power Management of Small Satellite Microgrids

Yaqoob, Mohammad

DOI (link to publication from Publisher):
10.54337/aau527274534

Publication date:
2022

Document Version
Publisher's PDF, also known as Version of record

DESIGN CONTROL AND POWER MANAGEMENT OF SMALL SATELLITE MICROGRIDS

BY
MOHAMMAD YAQOOB

DISSERTATION SUBMITTED 2022

AALBORG UNIVERSITY
DENMARK

DESIGN CONTROL AND POWER MANAGEMENT OF SMALL SATELLITE MICROGRIDS

Ph.D. DISSERTATION

by

Mohammad Yaqoob

AALBORG UNIVERSITY
DENMARK

Dissertation submitted to the Faculty of Engineering and Science at
Aalborg University for the Degree of Doctor of
Philosophy in Electrical Engineering

Dissertation submitted: December 5, 2022

PhD supervisor: Prof. Josep M. Guerrero,
Aalborg University

Assistant PhD supervisor: Prof. Juan C. Vasquez,
Aalborg University

PhD committee: Associate Professor Jayakrishnan Radhakrishna Pillai
Aalborg University, Denmark

Professor Ahmed M. M. R. Abdou
Qatar University, Qatar

Professor Ausias Garrigós Sirvent
Miguel Hernández University of Elche, Spain

PhD Series: Faculty of Engineering and Science, Aalborg University

Department: AAU Energy

ISSN (online): 2446-1636
ISBN (online): 978-87-7573-777-2

Published by:
Aalborg University Press
Kroghstræde 3
DK – 9220 Aalborg Ø
Phone: +45 99407140
aauf@forlag.aau.dk
forlag.aau.dk

Printed in Denmark by Stibo Complete, 2023

CV

Mohammad Yaqoob received his B.S degree in Electrical Engineering from Balochistan University of Engineering and Technology Khuzdar (BUETK), Pakistan, and his M.S degree in Telecommunication Engineering from Asian Institute of Technology (AIT), Bangkok Thailand in the year 2006 and 2012, respectively.

He is currently working towards a Ph.D. degree in design, control, and power management of small satellite microgrids at the Center for Research on Microgrids (CROM), Department of AAU Energy, Aalborg University, Denmark. His research interests include the design, modeling, control, and management of space microgrids and DC microgrids in general.

ENGLISH SUMMARY

Within the last decades, a significant boost in the interest in space exploration has emerged among scientists, commercial organizations, governments, and in different sectors of society. The present-day efforts of space explorations from low Earth orbit to adjacent planets like the Moon, and Mars up to deep space have triggered an influx in the class of Small Satellite (SmallSat) a particular class of satellites. Due to its small volume and size, low price, and quick development time, the Cube Satellite (CubeSat) has experienced an extraordinary expansion within this class of mini-, micro-, and nanosatellites. Additionally, the advancements in integrated circuits and digital signal processing units, as well as the cost and accessibility of COTS components, have made it particularly well-positioned for rapid expansion. For scientific, earth observation, and remote sensing purposes, these satellites are fascinating. It is valuable due to its low cost, cubic shape, quick production, lightweight, and modular structure. The space operators pay remarkable attention to it.

The Electrical Power System (EPS) is the most important of the numerous subsystems that make up the SmallSat since an unstable power supply to the others frequently compromises the mission. The EPS is made up of electrical sources, storage units, and loads that are all connected via various power converters. The operation of the various power converters that make up the EPS must be carefully coordinated to achieve efficient photovoltaic power use, reliable power delivery, and ideal battery management. Due to the coordination and control of distributed generation (DG), storage, and loads in a small-scale electrical network, a SmallSat EPS can be viewed as a space microgrid in terms of power systems. At the same time, managing the charge/discharge cycle of the battery, pulse, peak, and transient power demand to prevent instability and performance degradation of the spacecraft is difficult due to the demanding requirements of their design, which include harsh radiation, space, weight, and varying temperatures. Therefore, selecting an appropriate EPS design, control, and power management are major elements for a long-lasting and successful satellite mission. In this respect, this thesis presents a comprehensive review of EPS architectures, converter topologies, and technologies dedicated to the SmallSat microgrids. Relevant technical challenges will be identified and addressed by considering space conditions to guarantee the extended satellite mission life. Besides, sophisticated design, control, and power management strategies are introduced and analyzed. As opposed to the current specific mission designs, a generalized and full-scale EPS design will be proposed where the design and modeling of PV, converter, and battery sizing will be considered and examining the power supply and demand of the satellite, which is dependent on PV array cyclic power generation and battery cell nonlinear behavior. To guarantee that necessary duties are carried out effectively and without power shortages throughout the satellite mission, first, the suitable EPS model with solar panel converter architectures and configurations including battery energy storage will be derived. The proposed design considers load profile, operating modes,

eclipse, and altitude. A 3U CubeSat configuration operating under various load, temperature, and irradiance circumstances show the effectiveness of this design and power management. The design verification demonstrated good results in several operational modes across a wide range of temperatures and irradiance. Secondly, for tiny satellite applications, a comparative analysis of Maximum Power Point Tracking (MPPTs) in spinning situations will be developed. Due to the volume and mass limitations of the Nano Satellite (NanoSat), which have solar panels installed on their bodies, these satellites are designed to operate in a variety of unusual orientation scenarios. As a result, the PV system's unpredictable solar irradiation is caused, and an efficient PPT technique is required to extract the most power possible to transfer to the loads in the NanoSat Electrical Power System (EPS). To confirm the best MPPT extractions for NanoSat applications, several well-known MPPT approaches are analyzed for optimal power extraction. These include the traditional Perturb and Observe (P&O), Incremental Conductance (IC), and Ripple Correlation Control (RCC) methods. In contrast to the IC and RCC, the P&O extracts less power while oscillating more. In comparison to RCC, the IC method extracts greater power. RCC, in contrast to IC, is smoother and exhibits fewer oscillations. A power management control technique has lastly been established for SmallSat microgrid applications to avoid overcharging batteries while monitoring the PV Maximum Power Point (MPP) and Battery State of Charge (SOC) limits under a variety of solar and load scenarios. This suggested power management system uses an intelligent algorithm that can switch between maximum power point tracking and current control mode depending on the battery's state of charge to optimally manage solar power generation. The implied control and management system tends to prolong battery life through controlled charging in addition to enabling the best solar power extraction. For a seamless inter-mode transition, a local link is in charge of transmitting data about the battery's state of charge. To prevent battery overcharging, the suggested control and energy management system under incident load needs can limit PV power extraction. At various profiles of load and incident irradiance, the results are examined for power-sharing among solar PV, battery, and load to validate the effectiveness of the proposed full-scale EPS design, MPPT, and power management system for SmallSat applications. The proposed EPS design, power electronic control, and power management systems are modeled in MATLAB/SIMULINK.

DANSK RESUME

Inden for de sidste årtier er der opstået et betydeligt løft i interessen for udforskning af rummet blandt videnskabsmænd, kommercielle organisationer, regeringer og i forskellige sektorer af samfundet. Nutidens bestræbelser på rumudforskninger fra lav kredsløb om Jorden til tilstødende planeter som Månen og Mars op til det dybe rum har udløst en tilstrømning i klassen Small Satellite (SmallSat), en bestemt klasse af satellitter. På grund af dens lille volumen og størrelse, lave pris og hurtige udviklingstid, har Cube Satellite (CubeSat) oplevet en ekstraordinær udvidelse inden for denne klasse af mini-, mikro- og nanosatellitter. Derudover har fremskridt inden for integrerede kredsløb og digitale signalbehandlingsenheder, såvel som omkostningerne og tilgængeligheden af COTS-komponenter, gjort det særligt godt positioneret til hurtig udvidelse. Til videnskabelige, jordobservations- og fjernmålingsformål er disse satellitter fascinerende. Det er værdifuldt på grund af dets lave omkostninger, kubiske form, hurtige produktion, lette og modulære struktur. Rumoperatørerne er bemærkelsesværdige opmærksomme på det.

Electrical Power System (EPS) er det vigtigste af de mange undersystemer, der udgør SmallSat, da en ustabil strømforsyning til de andre ofte kompromitterer missionen. EPS består af elektriske kilder, lagerenheder og belastninger, der alle er forbundet via forskellige strømomformere. Driften af de forskellige strømomformere, der udgør EPS'en, skal omhyggeligt koordineres for at opnå effektiv fotovoltaisk strømforbrug, pålidelig strømforsyning og ideel batteristyring. På grund af koordineringen og styringen af distribueret generation (DG), lagring og belastninger i et lille elektrisk netværk, kan en SmallSat EPS ses som et rummikronet i form af strømsystemer. Samtidig er det vanskeligt at styre batteriets opladnings-/afladningscyklus, puls, peak og transient effektbehov for at forhindre ustabilitet og ydeevneforringelse af rumfartøjet på grund af de krævende krav til deres design, som omfatter hård stråling, plads, vægt og varierende temperaturer. Derfor er valg af et passende EPS-design, kontrol og strømstyring vigtige elementer for en langvarig og vellykket satellitmission. I denne henseende præsenterer denne afhandling en omfattende gennemgang af EPS-arkitekturer, konvertertopologier og teknologier dedikeret til SmallSat-mikronettene. Relevante tekniske udfordringer vil blive identificeret og behandlet ved at overveje pladsforhold for at garantere den forlængede satellitmissions levetid. Desuden introduceres og analyseres sofistikerede design-, kontrol- og strømstyringsstrategier. I modsætning til de nuværende specifikke missionsdesign vil der blive foreslået et generaliseret og fuldskala EPS-design, hvor design og modellering af PV, konverter og batteristørrelser vil blive overvejet og undersøge satellittens strømforsyning og -efterspørgsel, som er afhængig af PV array cyklisk strømgenerering og battericelle ikke-lineær adfærd. For at sikre, at nødvendige opgaver udføres effektivt og uden strømmangel i hele satellitmissionen, vil først den passende EPS-model med solpanelkonverteringsarkitekturer og -konfigurationer, inklusive batterienergilagring, blive udledt. Det foreslåede design

tager hensyn til belastningsprofil, driftstilstande, formørkelse og højde. En 3U CubeSat-konfiguration, der fungerer under forskellige belastnings-, temperatur- og irradiansforhold, viser effektiviteten af dette design og strømstyring. Designverifikationen viste gode resultater i flere driftstilstande på tværs af en lang række temperaturer og irradians. For det andet, for små satellitapplikationer, vil der blive udviklet en sammenlignende analyse af Maximum Power Point Tracking (MPPT'er) i spinningssituationer. På grund af volumen- og massebegrænsningerne af Nano Satellite (NanoSat), som har solpaneler installeret på deres kroppe, er disse satellitter designet til at fungere i en række usædvanlige orienteringsscenarier. Som følge heraf forårsages PV-systemets uforudsigelige solbestråling, og der kræves en effektiv PPT-teknik for at udtrække mest mulig strøm til at overføre til belastningerne i NanoSat Electrical Power System (EPS). For at bekræfte de bedste MPPT-udtrækninger til NanoSat-applikationer analyseres flere velkendte MPPT-tilgange for optimal strømudvinding. Disse omfatter de traditionelle Perturb and Observe (P&O), Incremental Conductance (IC) og Ripple Correlation Control (RCC) metoder. I modsætning til IC og RCC udtrækker P&O mindre strøm, mens den oscillerer mere. I sammenligning med RCC udvinder IC-metoden større kraft. RCC, i modsætning til IC, er glattere og udviser færre svingninger. En strømstyringskontrolteknik er endelig blevet etableret for SmallSat mikronetapplikationer for at undgå overopladning af batterier, mens PV Maximum Power Point (MPP) og Battery State of Charge (SOC) grænser overvåges under en række forskellige sol- og belastningsscenarier. Dette foreslåede strømstyringssystem bruger en intelligent algoritme, der kan skifte mellem maksimal power point-sporing og strømstyringstilstand afhængigt af batteriets ladetilstand for optimalt at styre solenergiproduktion. Det underforståede kontrol- og styringssystem har en tendens til at forlænge batteriets levetid gennem kontrolleret opladning ud over at muliggøre den bedste solenergiudvinding. For en sømløs inter-mode overgang er en lokal forbindelse ansvarlig for at sende data om batteriets ladetilstand. For at forhindre overopladning af batteriet kan det foreslåede kontrol- og energistyringssystem under indfaldsbelastningsbehov begrænse PV-strømudvindingen. Ved forskellige profiler for belastning og hændelsesstråling undersøges resultaterne for strømdeling mellem solcelle-PV, batteri og belastning for at validere effektiviteten af det foreslåede fuldskala EPS-design, MPPT og strømstyringssystem til SmallSat-applikationer. Det foreslåede EPS-design, effektelektronikstyring og strømstyringssystemer er modelleret i MATLAB/SIMULINK.

PREFACE

This thesis is a summary of outcomes from my Ph.D. project "*Design, Control, and Power Management of Small Satellite Microgrids*", carried out at the Center for Research on Microgrids (CROM), AAU Energy Department, Aalborg University, Denmark.

This thesis work is an overview of the several papers the author has produced in association with co-authors while pursuing his Ph.D. A large part of this thesis is established from the outcome of these publications, which are discussed in the main part of the thesis.

My sincere gratitude to my supervisor, Prof. Josep M. Guerrero, for providing me with this opportunity to be part of the CROM for this nice experience. I am also thankful to him for the supervision and guidance throw-out this project. Many thanks to my co-supervisors Prof. Juan C. Vasquez, and Abderezak Lashab for their help and support, which were with me during the entire duration of my Ph.D. studies.

Special thanks to Prof. Jose Matas Alcala for hosting me as a visiting researcher and supervising me for the duration of my study abroad at the Technical University of Catalonia, in Barcelona, Spain.

Moreover, I am obliged for the absolute support and cooperation that I received from my friends and colleagues, especially, Noor Hussain, José Maurilio Raya-Armenta, Hussain Abubakar, Mashood Nasir, and the entire Aalborg University staff during this project.

For the successful accomplishment of this degree, I must acknowledge the Balochistan University of Engineering and Technology Khuzdar for funding my Ph.D. studies. Likewise, for partially funding this thesis and my Ph.D. studies my honest thanks to AAU Energy, Aalborg University, and Otto Mønsteds Fond in Denmark.

Mohammad Yaqoob
November 2022

DEDICATION

To my *parents* for their endless love, support, and motivation from the beginning, when I was very young until now.

To my son *Yaleen Yaqoob Baloch*, and daughter *Zamur Yaqoob Baloch* who are my happiness and energy since they have come into my life.

To my wife, *Murwarid Murad Baloch* for her support, and cooperation throughout this project, without which it was not possible to complete this mission.

To my *siblings* for their good wishes and prayers in every mode of life.

TABLE OF CONTENTS

CHAPTER 1. INTRODUCTION

In this chapter, the motivation and introduction, together with the background of SmallSat microgrids will be presented. Next, the research questions, the hypothesis, and the thesis outline are presented. Finally, the publications derived from the Ph.D. research project are listed.

1.1. MOTIVATION

Exploring space from low Earth orbit to deep space and other alien planets in the future is one of the main desires of mankind. Besides as we are moving closer to that future, several societal sectors are currently spending time and resources to create new spacecraft technology based on cutting-edge scientific investigations. Especially, satellite technology in the way to space exploration is a vital element and solution for the human being. In this regard, the new concept of a small satellite (SmallSat) the Cube Satelite (CubeSat) is a thrilling solution, due to its miniature and compact size, inexpensive parts, and cubic shape. These satellites consist of some critical subsystems for satellite operational requirements including a transponder, satellite ADCS, CDH, OBC, and more prominently the EPS. The CubeSat architecture is shown in Fig. 1-1. In this regard, recently space microgrids (SMGs) a new concept have been proposed for EPSs of satellites [1]. SMGs concept is an inspiration of widely applied terrestrial microgrids, but with higher reliability, stability, resiliency, and optimization for individual elements and the whole system. In the case of the SmallSat, the energy generation, storage, and distribution systems are restricted by systems modularity, mass, and specific volume. The SmallSat EPS being so scalable

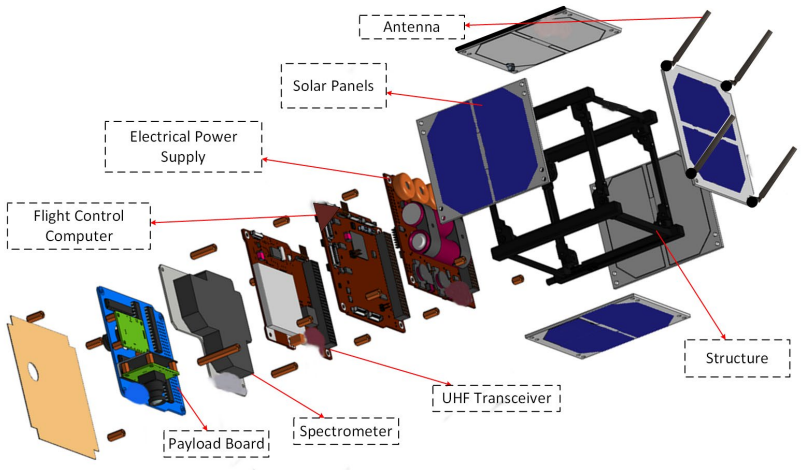

Figure 1-1: Architecture of the Small Satellite [J1].

requires high efficiency, resiliency, and reliability. Moreover, the EPS systems are mostly custom-built with COTS components which are vulnerable to space radiations, volatile temperatures, etc., and require special shielding from environmental effects [2]. These factors have compelled the researchers to search for extra alternatives. The core technology for energy harvesting in SmallSat is PV technology. Besides, for harvesting energy PV technology has been recognized as the most appropriate technology, which is not very mature enough and modular, therefore requires some special shielding to sustain and reduce the risk of degradation [3]. As a result, further research is required in the field of SmallSat operational, technological, control, and power management advances.

1.2. BACKGROUND

Exploring the universe since the beginning of time has been the dream of humans. Discovery and exploration of other worlds, stretching the bounds of the known, and the expansion in knowledge to discover scientific and technical myths have thrilled the curiosity of man. States and space agencies have been involved in space exploration since the first space launch. Sputnik I, the first man-made satellite, was launched by the USSR (now Russia) on October 4th, 1957, and it sparked the dormant U.S. program into action, sparking a worldwide competition that became known as the "space race." On January 31, 1958, the first American satellite Explorer I, was launched into space. Though earth-orbiting satellites have by far made up most launches in the space program, space probes have gathered even more knowledge about the moon, other planets, and the sun. While Explorer 1 was compact, most orbiters and spacecraft that followed it weighed thousands of pounds (or multiple tons) [4]. This makes launching them into space very expensive. The emergence of tiny constellations of lightweight satellites known as CubeSat is one approach that appears to be gaining popularity, a demonstration is shown in Fig. 1-2. These 4-inch cubes can perform complex calculations, whereas the electrical equipment required to conduct actual science experiments on spacecraft had to be very bulky and heavy in the past. These satellites open-up fresh possibilities for tackling global issues by building skills to start new collaborations. Young people are inspired by space exploration to study and work in the fields of science, technology, engineering, and mathematics disciplines. To help people all over the world and enhance the quality-of-life scientists use airborne satellite missions, and ground-based observations to collect data about the Earth's land, air, water, and ongoing natural and human-made changes to the planet. For a wide range of industries, including health care, utilities, enterprise, maritime, and more, the companies provide a wide range of satellite solutions. Sending satellites into orbit or space will become considerably more affordable because of the recent developments in rocket science made possible by private businesses like SpaceX and the reduction in the size of satellites. The future of space exploration is thrilling. It is clear that SmallSats, and in particular NanoSats, have grown quickly; as shown in Fig. 1-3, 690 missions were expected to be launched by the end of 2021, despite only 294 NanoSat missions having been launched as of

Figure 1-2: CubeSat missions. The figure is an illustration only.

2017 [5]. For instance, SpaceX's Starlink fleet, which seeks to launch thousands of satellites into orbit to supply remote areas of Earth with an internet connection, is undergoing testing [6]. In 2016, 58 nanosatellites between 1 and 10 kg were launched, 44 of which were commercial launches by Planet Labs [7]. These nanosatellites were launched into various Low Earth Orbits (LEOs).

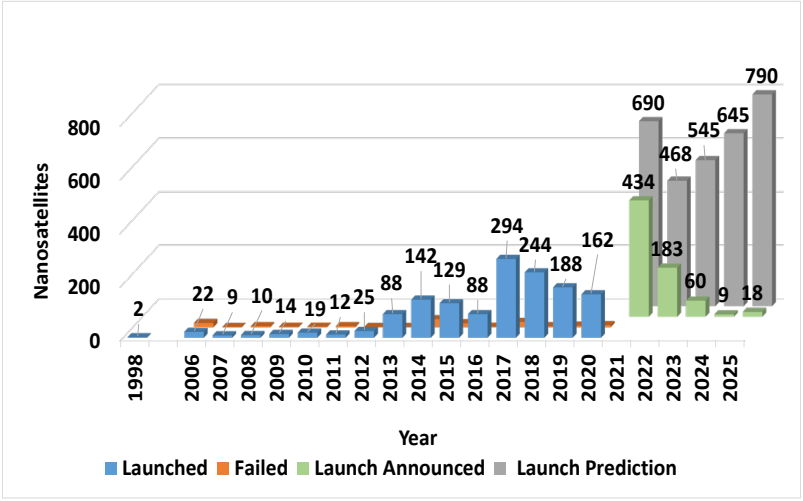

Figure 1-3: NanoSat mission launches and future predictions [5].

Apart from all these missions, under NASA's Educational Launch of Nanosatellites (ELaNa) 39 project, two tiny research CubeSats are getting ready to launch aboard Virgin Orbit's LauncherOne rocket, which aims to measure total solar irradiance by this mission to determine how much incident solar energy from the Sun reaches the Earth [8]. Both regional and global climate change are impacted by these irradiance levels. Besides, Planet Labs a startup company which is based in Sunnyvale, California is planning CubeSats launches which are called Doves. They are interested in collecting images of the planet. A flock is a collection of Dove that was released all at once and each Dove satellite weighs 3U [9]. Moreover, CanX-7 is a Canadian satellite with defense funding that uses a modular storable sail to study the effects of drag. This sail is employed in the deorbiting of tiny satellites [10]. The AAUSAT4 is a cube satellite with an Automated Identification System (AIS) receiver created by a student team at Aalborg University for sea vessels. This system is used to transmit and receive signals at a frequency of 162 MHz that carry data on identification, position, course, and speed [11]. Likewise, the Johns Hopkins Applied Physics Laboratory constructed a 3U CubeSat RAVAN, as a technology demonstration. This satellite will gauge the radiation from Earth. There are hundreds of other individual and specific CubeSat missions from different organizations and agencies launched or in the process to be launched.

1.2.1. SMALL SATELLITE STRUCTURE AND ARCHITECTURE

The recent shift in SmallSat missions from academic and experimental studies to commercial endeavors has altered the outlook for the specs and dependability of the CubeSat. The mission lives have been increased from months to years, and the specific orbits have been widened. A diverse community like universities, research institutes, and small companies are provided affordable access to space by these SmallSats. Recently, the CubeSat market has also gained the attention of diverse vendors and commercial organizations. Less development time, smaller mass, volume, and lower cost have been achieved as a result of recent advancements and developments in SmallSat subsystem technologies such as digital signal processing, additive built-up, microelectromechanical systems, integrated circuits (ICs), and affordable Commercial-Off-The-Shelf (COTS) and accessibility of innovative technologies [12] [13]. The CubeSat got its name from the cubic shape of its fundamental construction piece, a unit (U), which has dimensions of 10 x 10 x 10 cm, a weight of 1.33 kg, and a volume of one litter [14]. This satellite is expandable for greater payload requirements by adding several cubic units, as illustrated in Fig. 1-4 and Table 1-1. Notably, although being included in the same class as nanosats, which can weigh up to 10 kg of mass and range from 1 kg, CubeSats are not constrained by this weight range (e.g. the heaviest CubeSat is comprised of 27 U and weights 40 kg, as reported) [15]. A classification of spacecraft has been shown in Table 1-2. Initially, Prof. Bob Twiggs from Stanford University in the USA and Prof. Jordi Puig-Suari from California Polytechnic State University began working together on a specific standard for CubeSats in 1999 [16]. Since then, there have been several SmallSat missions

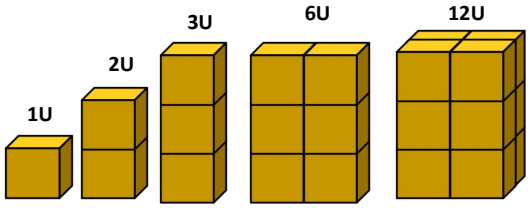

Figure 1-4: CubeSat from basic to extended forms.

TABLE 1-1: CLASSIFICATION OF CUBESAT PER THEIR MASS AND VOLUME [J1].

Specifications of CubeSat	Max Mass (kg)	Max Volume
1U	1.33	10×10×10
2U	2.66	10×10×20
3U	4.00	10×10×30
6U	8.00	10×20×30
12U	16.00	20×20×30

TABLE 1-2: CLASSIFICATION OF SPACECRAFT AS PER MASS AND MANUFACTURING BUDGET [J1].

Satellite Types	Mass (kg)	Production Expense (US $)
Large	>1000	0.1-2 B
Medium	500 - 1000	50-100 M
Mini	100 - 500	10-50 M
Micro	10 - 100	02-10 M
Nano	1 - 10	0.2-02 M
Pico	0.1 - 1	20-200 K
Femto	<0.1	0.1-20 K

including Earth observation, technology development, communication, space science, and some other applications, from the year 1974 up to 2016 missions are illustrated in Fig. 1-5. CubeSats have been launched to serve a variety of communication applications, astronomy, and Earth observations, where even continuous monitoring or short revisit intervals are necessary, even though they are primarily thought of as a teaching tool for students [17] [18]. The development of constellations of these satellites to provide space-based telecommunication networking used for mobile communications and global internet coverage is one of the future goals for NanoSat applications [19] [20]. The majority of nanosats are made to be launched for a variety of tasks into Low Earth Orbit (LEO). While keeping the cost cheap, these satellites

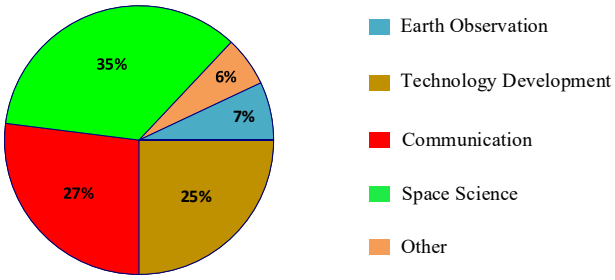

Figure 1-5: Classification of SmallSat missions 1974 - 2016 [18].

must carry out several difficult duties in space exploration, science, education, space weather, Earth observation, high-resolution photography, and airplane and ship monitoring [21] [22]. Because of their modular architecture, subsystems can be stacked together under the requirements of the mission and are readily available off-the-shelf from various suppliers. Because of this, CubeSat missions may be prepared for flight very fast - usually in just one or two years. Due to the propensity of CubeSats to use spare space on rockets, there are numerous launch options and inexpensive launch costs. They are contained in a unit that, when activated by a button, uses a spring mechanism to launch them into space. CubeSats are launched from the Japanese module Kibo onboard the International Space Station (ISS) and are deployed using a similar procedure.

1.2.2. SMALL SATELLITE MICROGRID CHALLENGES

Some of the crucial subsystems found in SmallSat microgrids are the attitude determination and control system (ADCS), communication transmitter (COM TX), communication receiver (COM RX), command and data handling system (CDH), on-board computer (OBC), electrical power system (EPS) and payload. EPS contains photovoltaic (PV) panels, DC-to-DC power electronic converters, Lithium-ion (Li-ion) cells, power distribution, and a protection system. All the required DC-DC converters like maximum power point tracking (MPPT) of PV panels battery charge regulators (BCR), dc bus voltage regulator (VR), and point-of-load (POL) converters for load equipment are part of EPS. The satellite payload is made up of devices including particle detectors, sensors, cameras, telescopes, gauges, and other electrical equipment, and it is used to collect the measurements and data that a satellite is designed to collect. Hence, the EPS is the most important subsystem among the others that fuels all the other subsystems. This assertion is supported by reliability analyses conducted in [23] and [24], which show that the EPS causes the second-most fatal failures in the first four weeks after launch while causing the most fatal failures thereafter. While 25% of all spacecraft failures are caused by EPS breakdowns. The SmallSat EPS that functions in an islanded manner is a tiny remote electrical network

and is referred to as a space microgrid system. The term microgrid is an autonomous distributed network, with the coordinated generation, battery storage systems, and loads. [25] [26].

The demand for capable components with high reliabilities, small size, mass, lower power, and simple EPS architecture, limits present the biggest design challenges for SmallSat. While the more powerful, volumetric, and massive systems need more resources to be able to operate in space [27]. The design of SmallSats uses COTS components which are mostly not focused on the space weather. The COTS parts lack the capacity to withstand hostile environments but often perform better than space-rated parts [28]. Contrarily, military-grade electronic parts for aerospace and avionics applications are designed in the environment of radiations present in the upper atmosphere, the extreme temperature of up to 100 °C in LEO, vacuum conditions, and intense vibrations during the left-off process [21]. Lacking these requirements not only shortens the lifespan of the satellite's routine electrical components but also impairs its normal operational capability. According to the standard in [29], testing in a vacuum is required per the specification for SmallSat rate of change of temperatures and severe temperatures. Between the maximum and minimum temperature boundaries, eight thermal cycles must be completed. Cosmic rays energize electrical components of the spacecraft a constant barrage of extremely energetic particles with the potential to energize due to carrying energy ions and cause damage and malfunction, presenting an additional problem in addition to temperature. Low-altitude satellites are particularly susceptible to these radiations [30]. Single event effects (SEEs) and total ionizing dose (TID) are the two main ways that radiations can affect satellite electronics. The TID is rated by mean time to failure, which is a long-term failure mechanism, while the SEE is represented in terms of a random failure rate which is an instantaneous failure mechanism. While for the protection of electronics there is less structural mass. Outer space vacuum causes whiskers to grow. Whiskers are conductive filaments that develop on the metal surfaces of tin, cadmium, and zinc. While the whiskers are as thin as spiderwebs. For a short circuit, a channel is created in Tin between metal-plated surfaces. Because Tin appears to be more likely to develop whiskers over time in the vacuum condition [31]. Conversely, at the time of launch, the thrust is applied suddenly to the satellite and the left-off vibration of 9.2 million pounds [32]. The high failure rate of SmallSat has been attributed to several factors, including lack of testing and aggressive technology infusion, which may be related to low budgets in the academic hobbyist sectors.

In this regard, robust design, control, and power management techniques are discussed in various articles to reduce the risk of EPS failures and mission losses. The following publications highlight the most recent research that is accessible regarding EPS. A modular EPS for SmallSats has been given by Timothy et al. [25], who also included operational details, control problems, and future work on the EPS design. An EPS that can be deployed to satellites for power demand spans of 1W to 1kW requirements, has been proposed by Johnston-Lemke et al. [26], which is scalable, modular, and

highly efficient. A thorough design and control technique for SmallSats EPS has been proposed by Khan et al. [33] in which a strategy is specified for scaling important EPS components like the photovoltaic (PV) array and storage system. The irradiance predictions, PV cell characteristics, PV array geometry, state-of-charge (SOC) of the battery, and the round trip efficiency, are all considered in the suggested design. A review article presented in [2], on SmallSat EPS provides an in-depth analysis of the literature on the most recent breakthroughs in the most important areas of SmallSat EPS topologies, EPS energy transfer systems, new technological developments, and design and operational issues. Moreover, a review study on traditional and cutting-edge CubeSat EPS topologies was published by Edpuganti in [34]. Based on the DC-bus regulation, conversion stages, and interface with PV panels, seventeen categories of EPS topologies are identified. Additionally, a qualitative comparison is used to show the advantages and disadvantages of the various EPS topologies. On the other hand, Yost [35] offers a useful overview of the cutting-edge SmallSat EPS technology and key EPS components readily available from several commercial vendors. Bintoudi [36] has suggested that the EPS subsystem be classified as a microgrid to treat it holistically. More particularly, Lashab [1] introduced space microgrids, providing an overview of Energy Storage Systems (ESS), energy generation, and EPS for satellite-based microgrids. Moreover, the sizing recommendations and insight into protection strategies have been presented. However, there are still challenges to overcoming long-stay SmallSat deployments in outer space conditions for a reliable and robust EPS design, control, and power management.

1.3. RESEARCH QUESTIONS OBJECTIVES AND HYPOTHESES

Based on the discussed challenges, the following research questions can be formulated:

- ✓ What are the challenging aspects of SmallSat microgrids from the point of view of energy transfer architectures, the main challenges indicated in recent research development studies of the latest technologies and converter topologies? In addition to that, what are some potential solutions described in the literature, which will enable building a more robust, resilient, and efficient EPS?

- ✓ How to analyze the MPPT technique among some well-known MPPT strategies of conventional Perturb and Observe (P&O), Incremental Conductance (IC), and Ripple Correlation Control (RCC) and find an optimal MPP technique under the spinning conditions for SmallSat applications in varying irradiance and temperatures?

- ✓ How to efficiently coordinate solar power generation together with battery energy storage, power distribution, and payloads in a SmallSat microgrid, for

proper coordination and efficient resource utilization among the satellite DGs and loads?

To address the above-formulated research questions, The main objective of this project is to develop a new research framework related to analysis, EPS modeling and control design approaches for optimal operation and energy management for Small Sat microgrids.

The specific objectives of this thesis are listed as follows:

- To address the challenges regarding control, operation, and energy management for SmallSat microgrid technologies.
- To design a full-scale SmallSat microgrid including performance analysis under a realistic orbital environment and invariant load conditions.
- To investigate new MPPT methods for the proposed SmallSat microgrid.
- To develop an adaptive control algorithm for power management to avoid battery overcharging.
- To design a control architecture to shift the PV MPPT mode into the current control mode for prevention of battery state of health issues.

To achieve the research project objectives stated above, several hypotheses are provided:

- ❖ By exploring the type of challenges faced by the available technologies, EPS configurations, and converter controls, it is possible to discover solutions to mitigate the SmallSat microgrid issues.
- ❖ By designing the SmallSat microgrid with state-of-the-art technologies, EPS architectures, converter topologies and design verification, testing in different environments, and load conditions risk of EPS failures can be minimized.
- ❖ By implementation and analyzing the important MPP tracking techniques in SmallSat orientation and environment the optimal MPPT technique can be selected for SmallSat applications to increase power generation efficiency.
- ❖ By designing a new resilient control architecture in conjunction with advanced power management strategies between PV generation, battery storage systems, and loads, a coordinated operation for resource sharing is possible.

1.4. OUTLINE OF THE THESIS

This thesis is divided into two main sections: the first section includes the thesis report, and the second one comprises the publications derived from the Ph.D. research work. Each chapter and its associated publication are corresponded in Fig. 1-6. The summary of each chapter is given as follows:

Chapter 1. Introduction

Chapter 2. Small satellite orbital parameters

In this chapter, the orbital period parameters such as inclination, altitude, and methods to draw orbital trajectory periods will be discussed which determines the solar irradiation level, eclipse, and illumination time of the SmallSat microgrids. Next, the important orientations of Sun-pointing, Nadir-pointing, and Free-orientation will be analyzed for a 3U CubeSat case study to discover the harvested energy from the SmallSat PV panels.

Chapter 3. EPS architectures, converter topologies, and technologies

This chapter will discuss the SmallSat EPS architectures and an overview of the control and configuration of energy transfer and power conditioning architectures. The power conversion topologies, which are the backbone for the transition of power to fulfill load demands will be comprehensively reviewed. Moreover, the PV, the PV degradation analysis, and the storage technologies for SmallSat microgrids will be discussed and comprehensively reviewed which will enable the building of more resilient and robust space microgrids from the efficient, and state-of-the-art SmallSat microgrid technologies.

Chapter 4. Design and design verification of full-scale small satellite microgrid

In this chapter, an EPS design architecture will be verified in different operating modes considering all the design requirements and main features of the mission, including power budget, orbital environment, the PV, converter, and battery designs and models. The design and sizing of key EPS elements and the coordinated control strategy will be implemented to attain efficient and stable system operation in the space volatile environment.

Chapter 5. An optimized control MPPT for Small Satellite Microgrid

In this chapter, some MPPT techniques such as, perturbed and observe (P&O), incremental conductance (IC), and ripple correlation control (RCC) will be considered in a comparative study for SmallSat microgrid applications. While the important

orbital parameters and space environment scenarios will be considered for optimal power extraction.

Chapter 6. Power Management and Control of Small Satellite Microgrid

In this chapter, a novel adaptive control algorithm for battery and load management will be introduced in order to achieve coordinated and efficient resource utilization in SmallSat applications. The adaptive control algorithm is in charge of battery voltage regulation and the control coordination to shift MPPT mode to load current control for PV power curtailment purposes.

Chapter 7. Conclusions

The overall Ph.D. project contributions and future perspectives will be presented in this section.

1.5. LIST OF PUBLICATIONS

The outcome of the Ph.D. thesis work is based on two first-author journal publications and two conference papers, and one co-authored journal and two conferences as listed below.

Journal papers

J1. **M. Yaqoob,** A. Lashab, J. C. Vasquez, J. M. Guerrero, M. E. Orchard and A. D. Bintoudi, "A Comprehensive Review on Small Satellite Microgrids," in *IEEE Transactions on Power Electronics*, vol. 37, no. 10, pp. 12741-12762, Oct. 2022, doi: 10.1109/TPEL.2022.3175093.

J2. **M. Yaqoob,** A. Hussain, J. Maurilio, A. Lashab, J. C. Vasquez, J. M. Guerrero, "Design and Power Management of a Full-scale LEO Small Satellite Microgrid," Submitted in IEEE Access.

Conference papers

C1. **M. Yaqoob,** H. Abubakr, J. M. Alcala, A. Lashab, J. M. Guerrero, and J. C. Vasquez, "A Comparative Study of MPPTs for Nano-Satellite Microgrid Applications under Spinning Flight Scenarios," *in 48th Annual Conference of the Industrial Electronics Society, IECON 2022.* (Presented in October 2022).

C2. **M. Yaqoob,** M. Nasir, J. C. Vasquez, and J. M. Guerrero, "Self-directed Energy Management System for an Islanded Cube Satellite Nanogrid," *2020 IEEE Aerospace Conference*, 2020, pp. 1-7, doi: 10.1109/AERO47225.2020.9172754.

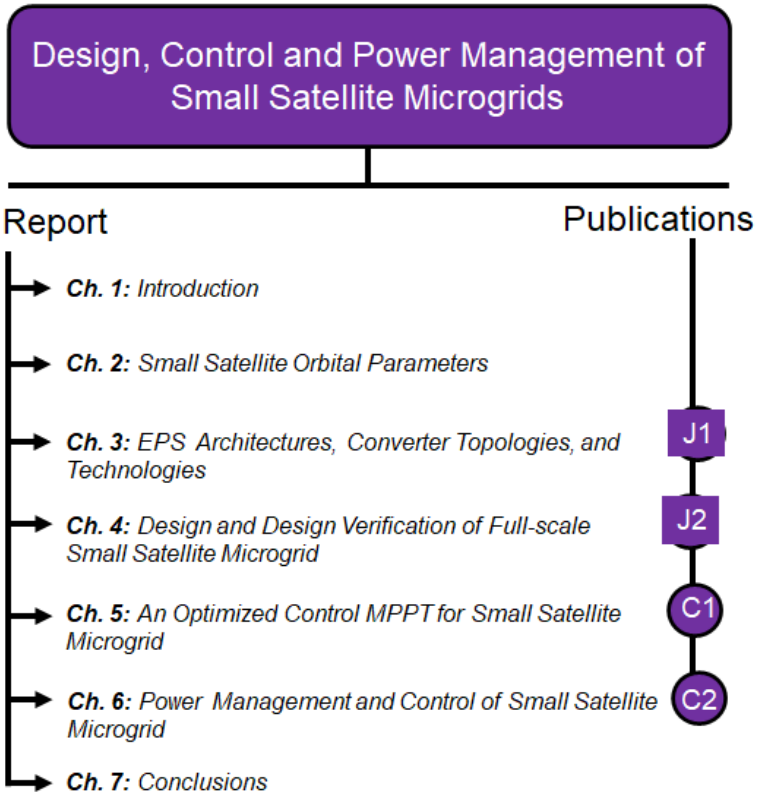

Figure 1-6: The structure of the thesis report and corresponding publications.

Finally, during the Ph.D. project additional co-authored publications were published:s

J. A. Lashab, **M. Yaqoob,** Y. Terriche, J. C. Vasquez and J. M. Guerrero, "Space Microgrids: New Concepts on Electric Power Systems for Satellites," in IEEE Electrification Magazine, vol. 8, no. 4, pp. 8-19, Dec. 2020, doi: 10.1109/MELE.2020.3026436.

C. A. Hussain, **M. Yaqoob,** M. Barrios, G. Agundis-Tinajero, H. Farag, J. C. Vasquez and J. M. Guerrero, "Inclusion of V2G and Power System Stabilizer for Residential Microgrid Applications," in IEEE Conference on Power Electronics and Renewable Energy, 2023. (Accepted for presentation).

C. H. Abubakr, A. Lashab, **M. Yaqoob,** Y. Yalman, J. C. Vasquez, and J. M. Guerrero, "Adaptive Control as a Hierarchical System," in Proc. of the Interdisciplinary Conference on Mechanics, Computers and Electrics (ICMECE 2022). (Presented in October 2022).

CHAPTER 2. SMALL SATELLITE ORBITAL PARAMETERS

In this chapter, the orbital period parameters such as inclination, altitude, and methods to draw orbital trajectory periods have been discussed which determines the solar irradiation level, eclipse, and illumination time of the SmallSat microgrids. Next, the important orientations of Sun-pointing, Nadir-pointing, and Free-orientation are analyzed for a 3U CubeSat case study to discover the harvested energy from the SmallSat PV panels.

2.1. INTRODUCTION

The orbital period determines the solar irradiation level, eclipse, and illumination time. Therefore, the orbital consideration for a satellite serves as the primary mission requirement while constructing a mission. Typically, CubeSats are launched into low earth orbit (LEO), which has an orbital period of 90 to 120 minutes and an altitude of 2000 kilometers or less [37]. However, the most suitable orbit for the SmallSat mission is low earth orbit which has a constant illumination of 1367 W/m2. The inclination angle of the LEO CubeSat's orbit concerning the equatorial plane can range from 0 to 98 degrees. In each orbit, the satellite is briefly visible to the Earth station. The CubeSat experiences both sunny and eclipse phases as it rotates in an orbit around the earth. In the irradiation period, the angle of incidence of Sunlight varies from 66.55 to 90 degrees on the photovoltaic (PV) arrays of CubeSat. While during the eclipse, the Sunlight is blocked by the Earth and CubeSat is not illuminated in every revolution around the earth repeatedly in all seasons of the year and which causes a sharp drop in the temperature. Typically, the orbit period for an LEO SmallSat has an eclipse of 1/3 of the total orbit [38].

2.1.1. ORBITAL INCLINATION AND ALTITUDE FOR SMALL SATELLITE

The eclipse duration depends on the inclination and altitude of the orbit, and the incident angle of the Sunlight on the orbit plane is recognized as a beta (β) angle [37]. The increase and decrease of β vary the eclipse period to longest and shortest, $\beta = 0$ with maximum eclipse, and an increase in β shortens the eclipse duration up to the non-eclipse condition, which occurs in polar orbits. When resolving the β angle profile to determine the mission life, the altitude and inclination of the satellite orbit are applied. As exemplified in Fig. 2-1, β in the coordination system is the inclination of the orbit and the Sun always lays at the XY plane. The angle is continually changing because of session changes and orbital perturbations. The arrangement for definitions is provided in full in [39] and β is calculated as (1).

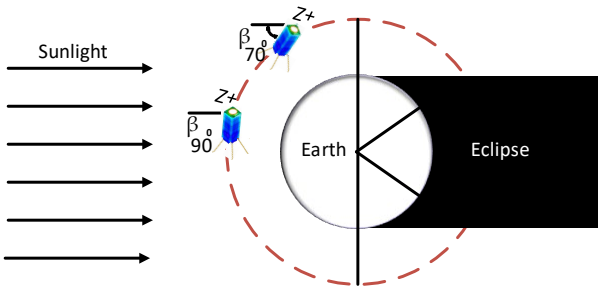

Figure 2-1: Beta angle (β) profile drawn by the satellite altitude and inclination.

$$\beta = \sin^{-1}(\cos\Gamma \sin\Omega \sin i - \sin\Gamma \cos\varepsilon \cos\Omega \sin i + \sin\Gamma \sin\varepsilon \cos i) \quad (1)$$

Where Γ is the change in seasons, Ω is the right ascension of the ascending node, ε is ecliptic obliquity and i is the inclination of the orbit. The approximation of the earth's circular orbit around the sun is used to calculate the rate of change of Γ with a time equal to 2π/365.25 rad/day. Whereas, for the calculation of the time rate of change of Ω, equation (2) is used.

$$\Omega = -x\frac{3}{2} j_2 \left(\frac{R_{eq}}{p}\right)^2 \sqrt{\frac{\mu}{R_0^3}} \cos i \quad (2)$$

Here J_2 is the ellipticity perturbation, R_{eq} planet equatorial radius, p parameter, μ is the mass of the planet, i is the inclination, and R is the radius of the orbit.

2.1.2. ORBITAL TRAJECTORY PERIODS

The satellite revolving in the orbit passes through two orbital trajectory periods, the Sun illumination radiation period, and the eclipse stage. The satellite receives radiation for adequate generation during the period of sunlight, charging the energy storage system and powering load requirements. When Earth blocks sunlight from reaching the satellite during the second stage, it is referred to as the eclipse stage or dark stage and is when the storage is used to power the spacecraft. The length of irradiation and eclipse stages vary on the season; However, we demonstrate an idealized scenario in which every region is highlighted as depicted in Fig. 2-2, and it is also possible to calculate both orbital periods from this figure data.

The orbital period, T is derived from Kepler's third law, and the orbital period is calculated as given in (3) [40].

$$T = 2_{\pi}\sqrt{\frac{rE + A^2}{\mu}} \quad (3)$$

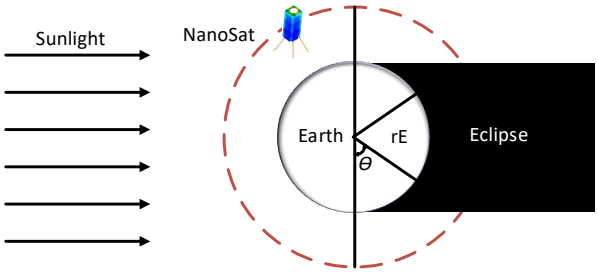

Figure 2-2: Sun-synchronous orbital trajectory periods of Sun and eclipse.

Where *rE* is the radius of the Earth, *A* is the orbital altitude, μ is the celestial body's standard gravitational parameter, and *rE+A* is the orbit semimajor in kilometers.

To demonstrate the design usability for a case study at 700km altitude in LEO orbit the total orbital period becomes 99 minutes and the inclination angle is 98.20. The satellite at an angle Θ enters and leaves the eclipse at an angle of (1800 - Θ), and Θ is equal to as given in equation (4). In this case albedo radiation is not considered because using only direct radiation in each scenario simplifies the analysis of the energy behavior, however, albedo will be considered realistically.

$$\theta = \arccos\frac{rE}{rE+A} \tag{4}$$

Where, Te is the eclipse time ratio and Te is = (180 - 2Θ)/360, which is 36.4% of the orbit and 36.27 minutes of the total orbit timing. While the Sunlight time ratio Ts is = (180 + 2Θ)/360, which is 63.36% of the orbit and 62.73 minutes of the total orbit timing.

2.2. ORIENTATION DETERMINATIONS

The CubeSats follow different orientations among Sun-pointing, Nadir-pointing, and Free-orientation depending on the purpose of the mission and load requirements. Three cases will be discussed in this section to study the behavior of energy when radiation is incident on different faces of a satellite at different times with varying incident angles [41].

2.2.1. SUN-POINTING SCENARIO

The Sun-pointing scenario is the first possible outcome, as depicted in Fig. 2-3 (a). The body reference frame is invariant about the reference frame of the Earth when an attitude control system is assumed. Thus, during the period of the simulation, only one face designated as X- receives sunshine with maximal radiation while the other faces do not. The harvested irradiation resulting from simulating this scenario is shown in

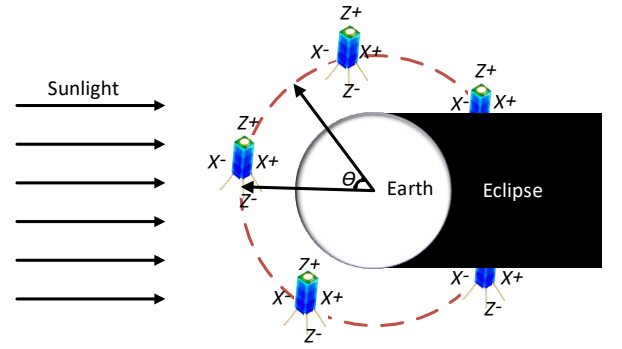

(a)

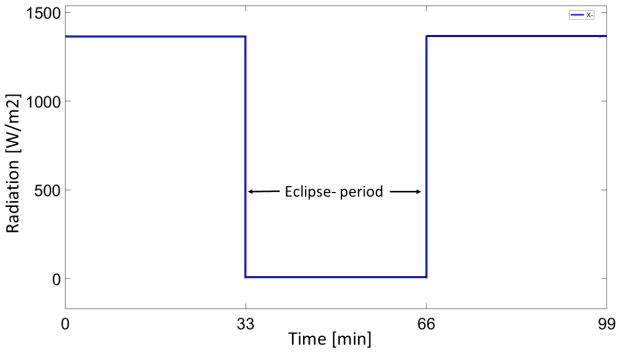

(b)

Figure 2-3: Satellite at Sun-pointing orientation scenario, (a) the orientation, (b), the PV harvested energy [J2].

Fig. 2-3 (b). It can be observed by simulation that in the Sun-pointing scenario only one of the satellite's 3U faces, X- is absorbing the maximum irradiation from the Sun during the entire Sunshine period and remains in zero energy harvesting mode during the eclipse period.

2.2.2. NADIR-POINTING SCENARIO

In the Nadir-pointing scenario, the X+ face is constantly pointing toward the center of the Earth, as shown in Fig. 2-4 (a). This scenario enables sinusoidal radiation behavior on the four faces exposed to sunlight. At the initial condition, the X- face has the maximum irradiation value, which slightly reduces with angular separation. The change in a position towards the maximum 900 increases the radiation level over X-

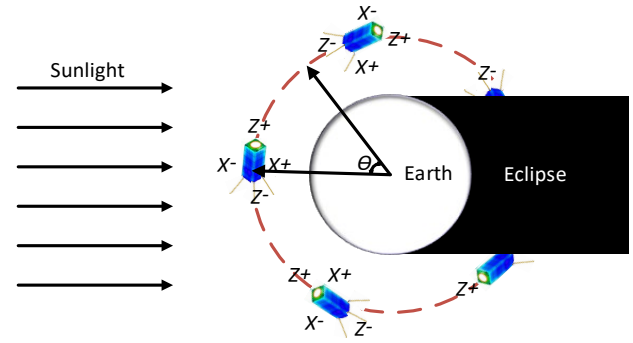

(a)

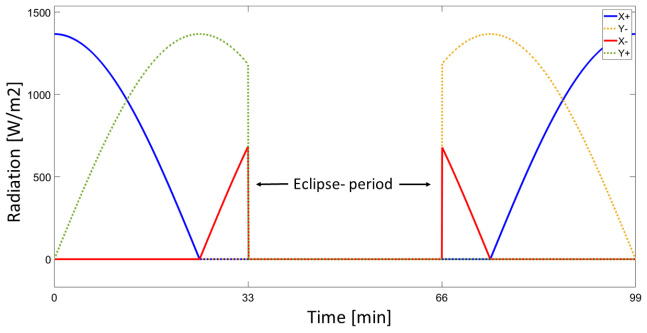

(b)

Figure 2-4: Nadir-pointing orientation scenario, (a) the orientation, (b), the PV harvested energy.

and X+ faces after and before the eclipse receives the full radiation over a small period of entrance and exit of the eclipse. Hence, the X- face receives irradiation at the rest of the orbital trajectory later than the eclipse condition and will return to its starting location. As a result, in nadir-pointing, the solar radiation illuminates the four faces of the CubeSat which are illuminated by solar radiation with a sinusoidal behavior. The harvested irradiation resulting from simulating this scenario is shown in Fig. 2-4 (b).

2.2.3. FREE-ORIENTATION

The attitude control system is nonexistent and the satellite face arbitrary revolutions in the free-orientation scenario, as shown in Fig. 2-5 (a). This scenario let the CubeSat faces a random irradiance strike and could be used as a reference for energy analysis

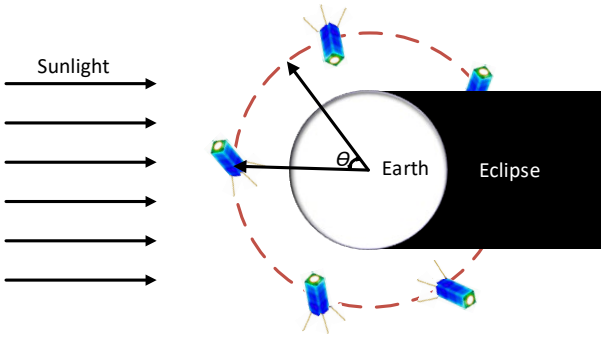

(a)

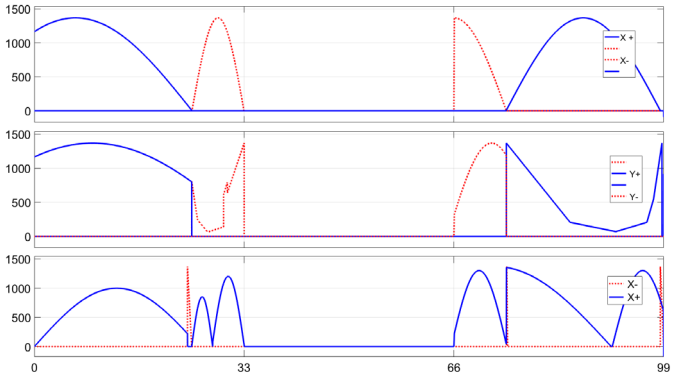

(b)

Figure 2-5: Free-orientation scenario, (a) the orientation, (b), the PV harvested energy.

to the previously discussed scenarios because the satellite faces arbitrary revolutions. Moreover, as for the radiation behavior of the cubic shape, the opposite side does not get any radiation while one face is in irradiation already. Different shifts in irradiation magnitude can be seen in Fig. 2-5 (b), for an opposite number of faces (X+, X-), (Y+, Y-), and (Z+, Z-).

2.3. SUMMARY

This chapter discus the basic mission requirements for the SmallSat microgrid orbital period determination, satellite altitude, the solar irradiation level, eclipse, and illumination time. The analysis has been done in terms of different mission-based satellite orientations for Sun-pointing, Nadir-pointing, and Free orientation for the

case study of a 3U CubeSat with PV panels on the X and Y axis to determine the harvested energy from the PV panels in different orientations.

CHAPTER 3. EPS ARCHITECTURES, TOPOLOGIES, AND TECHNOLOGIES

This chapter introduces a scientific approach to the SmallSat EPS architectures and an overview of the control and configuration of energy transfer and power conditioning architectures. The power conversion topologies, which are the backbone for the transition of power to fulfill load demands have been comprehensively reviewed. Moreover, the PV, the PV degradation analysis, and the storage technologies for SmallSat microgrids have been discussed and comprehensively reviewed which will enable the building of more resilient and robust space microgrids from the efficient, and state-of-the-art SmallSat microgrid technologies.

3.1. INTRODUCTION

The EPS of a Small Satellite which includes generation, power distribution, management system (PDMS), storage, and loads, is essentially the lifeblood of the other subsystems. The EPS architecture and its basic building blocks are illustrated in Fig. 3-1. The major purpose of the EPS is to keep the satellite bus powered continuously during the mission time span, providing sufficient power even during eclipses when no solar power is produced and safeguarding against faults. The EPS controls the electrical power input from the solar panels, charges, and discharges the onboard batteries, and distributes at the necessary voltage levels the power to the satellite's subsystem components. The onboard computer is also alerted of the monitoring, general health of the EPS subcomponents, and operation status [42]. As mentioned in the previous chapter, due to the EPS composition of distributed energy

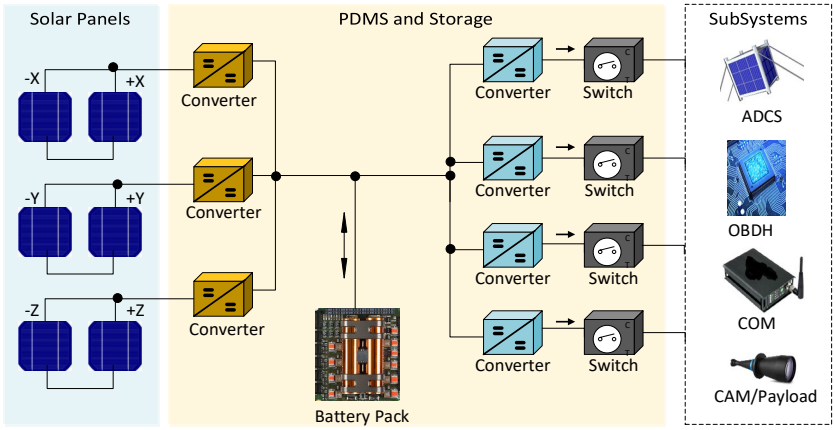

Figure 3-1: EPS architecture and its basic building blocks.

sources, modular DC-DC micro converters, and numerous loads, the satellite EPS can be interpreted as a microgrid, and one-third of the satellite mass is made up of the EPS approximately [43], [35]. An important aspect of the EPS design is to provide sufficient power required by the satellite subsystems and payloads. The efficiency of EPSs is crucial since it encourages having a greater power reserve, which feeds payloads whenever needed. Researchers have paid close attention to the EPS of satellites due to a variety of demanding requirements, including its impossibility of maintenance, restricted weight and volume, harsh radiation environment, and volatile temperature ranges. These requirements can be addressed by utilizing sophisticated control techniques to produce a resilient and stable EPS design [1]. However, some external factors like satellite orbit altitude, orientation scenarios, and information on payload power demands are very important characteristics to be considered in the design process.

3.2. EPS ARCHITECTURES

One of the crucial aspects of mission-specific requirements for EPS design is the choice based on a comparison of overall system reliability, the selection of appropriate EPS architecture, battery size, cost, and efficiency. State-of-the-art EPS architectures are classified based on energy conversion at the generation side, the interface of PV arrays, bus voltage regulation, stages of power conversion, and placement of converters in the architecture, various mission-specific EPS architectures have been presented by the researchers in [34], [44], [45]. The EPS architectures are broadly classified into power conversion and power distribution architectures.

3.2.1. POWER CONVERSION ARCHITECTURES

On the generation side, depending on the solar power exploitation mode and based on how the PV panels are interfaced the EPS architectures are divided into direct energy transfer (DET) and peak power tracking (PPT) architectures [46]. The DET CubeSat EPS architecture is shown in Fig. 3-2, in which diodes are used to connect the PV

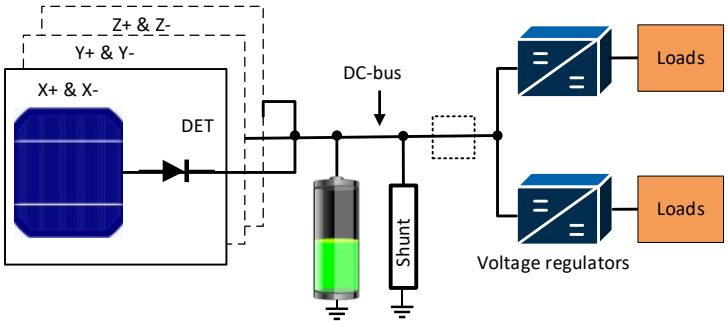

Figure 3-2: The DET EPS architecture.

panels directly to the battery and/or load equipment [47]. In addition, a shunt regulator is placed in parallel to the PV panels for absorbing the extra power when the load demand decreases or the battery achieves full-charge condition. If a resistor is used in the shunt regulator, the surplus power is dissipated as heat inside the CubeSat; otherwise, it is dissipated on the PV panel. It offers the simplest and most affordable solution with fewer parts and, as a result, greater reliability in radiation environments. DET architecture delivers the required power to the loads in a regulated manner by adding a voltage regulator shown in Fig. 3-2, with dotted lines or unregulated DC-bus, and shunts extra power while operating at a fixed voltage. This converting process is easy but un-effective. DET architectures are used in applications with power budgets under 100 W, frequently [37]. To generate the maximum possible power, the PV panel characteristics, and the DC-bus voltage is matched in DET architectures, which is challenging for space missions due to the limited power generating and storage capacity of CubeSats [48]. The main disadvantage of this design is the underutilization of PV panel generation capacity. In addition, the PV I-V curve is a direct consequence of the temperature, irradiance, and deterioration of the solar cells, DET systems are not making the most of the solar energy that the solar arrays are harvesting. To overcome the limitations of DET, the PPT-based architecture is proposed [49], as shown in Fig. 3-3. The PPT essentially pushes the output voltage of the PV array in a value where the maximum transfer of the power is resulted, regardless of the solar cell degradation degree and temperature. The PPT takes place from the array to the aggregated loads.

To achieve maximum power either the analog controllers or digital micro-controllers (MCUs) can be implemented for MPPT. An MCU provides the benefits of simplicity and tuning flexibility, but it is more prone to malfunction owing to radiation damage. The MCU is more efficient, however, the analog controller with discrete components is thought to be more reliable. The CubeSats may use analog as a backup controller if the MCU fails or as the primary controller [42], [50]. To extract the maximum output power PPT architecture demands a minimum of a dedicated series DC-DC converter for driving the PV array at the operating voltage of the PV cell and, the solar array

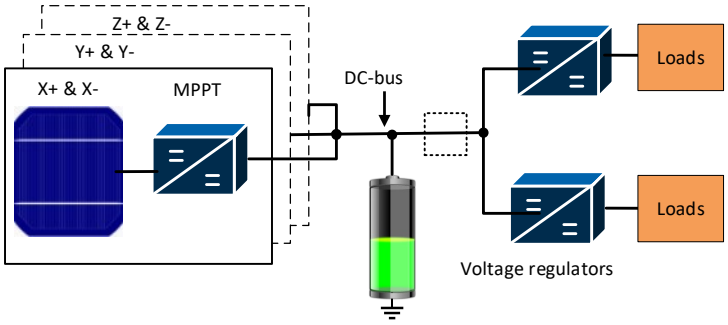

Figure 3-3: The PPT EPS architecture.

nominal output power of 4 % - 7% [37]. Due to short sunlight periods and large PV panel deployment constraints, this architecture is widely applied in CubeSat applications [51]. To distribute power to the loads, the main DC power bus can be either unregulated or regulated. In an unregulated topology, the battery voltage is tracked by the main bus, whereas, in regulated bus topologies, the main bus voltage must be fully regulated using a DC-DC converter. The PPT topology is depicted in Fig. 3-3 with unregulated bus voltages. The bus voltage can be regulated close to the reference value, by the inclusion of the DC-DC regulator shown by the dashed lines in Fig. 3-3. For peak power tracking EPS topologies, a comparison is given in [48]. The comparison claims that the architecture shown in Fig. 3-3, has the maximum efficiency for all operating modes. This architecture consists of an unregulated DC bus with a series of connected MPPT converters and, a smaller number of components.

3.2.2. POWER DISTRIBUTION ARCHITECTURES

At various steps of power conversion, isolation and voltage regulation are involved, depending on the system architecture. Galvanically isolated DC-DC converters are also great choices for integrating low-voltage renewable sources [52]. Regarding distribution two fundamental design strategies are used to distribute power in current satellites: decentralized power architecture (DePA) and distributed power architecture (DiPA) [53]. The DiPA technique is widely used to guarantee dynamic, effective, and trustworthy system performance. As seen in Fig. 3-4, this method makes use of a single isolated DC-DC converter as well as several POL converters. Non-isolated voltage regulators, known as intermediate bus converter (IBC), notably the POL converters, and isolated converter, provides partially regulated, simply unregulated, or intermediate completely regulated voltages. The IBC is physically separated from the main digital devices board due to cooling and mechanical concerns. However, each POL converter is located on a board and associated loads are close to each other, to reduce parasitic impedances. The DePA has been presented as a way to circumvent the drawbacks like losses in DiPA and the larger number of conversion stages [53]. There are two primary types of DePA, as shown in Figs. 3-5 (a) and (b): In the first

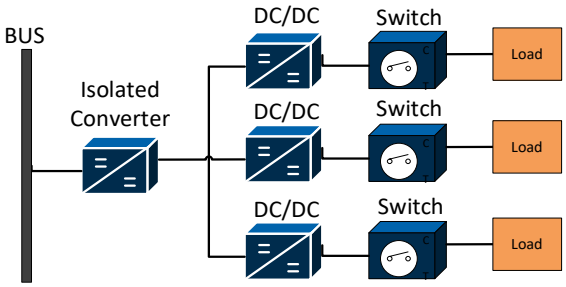

Figure 3-4: Distributed power architecture—DiPA.

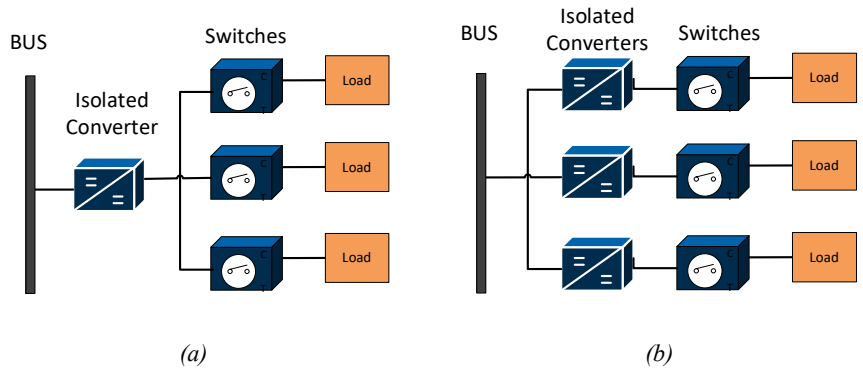

Figure 3-5: DePA power architecture which is decentralized, (a) A single input converter with multiple outputs, (b) Numerous isolated converters.

Fig [see Fig. 3-5 (a)] a single isolated converter is employed with numerous outputs which is offering completely regulated voltage levels of 1, 1.5, 2.5, 3.3, 5 V, followed by several load switches to distribute power to the loads while offering completely regulated voltage levels of 1, 1.5, 2.5, 3.3, 5 V, etc. In contrast, the second one [see Fig. 3-5 (b)] employs several independently separated controlled converters to produce completely regulated voltages and various outputs necessary for the satellite load operations. Because of its lower losses and lighter weight Compared to DiPA this architecture is favorable, where at each stage of the conversion process the power is wasted.

3.3. LATEST CONVERTER TOPOLOGIES

The fundamental components of the SmallSat EPS that guarantee consistent and effective delivery of power to the subsystems are DC-DC converters. For delicate onboard equipment to function flawlessly, the design of the converter must have the ability to maintain despite input disturbances a consistent output voltage. At the converter power stage, high-efficiency field-effect transistors (FETs) are typically used as the switching components due to their straightforward drive circuits, low ON-state resistance, and small gate charge [54] - [56]. The EPS is heavily segmented, and each segment is typically provided by a specific boost or buck DC-DC converter with a piece of appropriate switching equipment [57]. A large percentage of the usual CubeSat onboard equipment is between 3-6 V voltage ranges. The loads nature can be RF, analog or digital, and these sections are well fragmented to overcome the ripple and noise issues [58]. Relatively applying COTS components for the space applications EPS design the high-reliability requirements are difficult to estimate. The compatibility of the electromagnetic interface (EMI), radiation effects, the environment of vacuum, vibrations, and shock are just a few of the many limitations

that space converters must confront. Also, the stringent requirements of small mass, the demand for high-power quality, and high-efficiency requirements have narrowed down conventional converter choices. While the conventional converter with the minimum number of components has a simple structure and unproven power quality for space applications [59], [60]. To meet these requirements, it is necessary to take into account the mechanical dimensions, thermal analyses, and radiation-hardened component selection of each component. The selection of converter topologies that can support radiation and withstand space environments must be taken into account during the design and topology selection process. Various other elements are considered, including, transformer - or inductor-based designs, multistage, and single-stage power processing switch types. Based on settings and component types, converters can be categorized into various groups. However, we broadly discuss the isolated and non-isolated converter topologies for SmallSat applications.

3.3.1. NON-ISOLATED DC-DC CONVERTERS

For space applications, nonisolated DC converters offer several advantages, which include dry mass, high reliability, simple design, and a smaller number of components [61]. These converters are typically utilized for power control and conversion at various stages in SmallSat applications. The high voltage and current stress caused by the conventional converter's excessive duty cycle operations, however, results in limited controllability and significant losses [62]. In this section, the performance evaluation of various non-isolated DC converters for space applications is carried out.

3.3.1.1 Buck Converter Topologies Under Study

Two buck converter topologies have been recommended in [63], and [64], as shown respectively in Fig. 3-6 (a), a common mode noise reduction, and (b) load-side redundant buck converters for SmallSat applications [2]. The suggested common

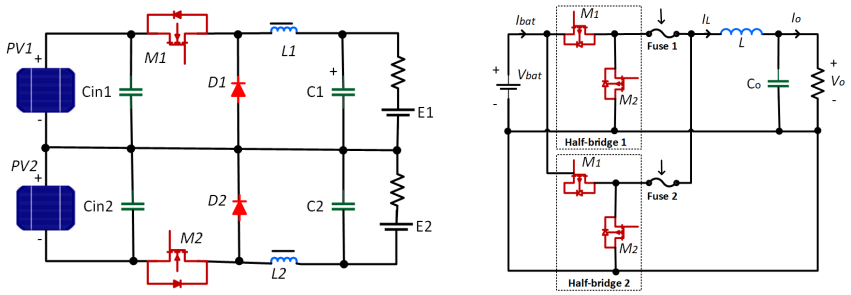

Figure 3-6: Buck converter topology for SmallSat applications: (a) common mode noise reduction converter, and (b) load-side redundant converter [J1].

mode noise reduction buck converter avoids unexpected ground bouncing problems by minimizing leakage currents at the interface between the PV panels and the satellite's power bus. While ground bounce is a delay in a transistor's ability to reach the ground following a signal change in high-density digital circuits. The most common reason why the ground bounce occurs is because of shifting magnetic flux, which can result in transients with amplitudes of volts. The suggested converter connects two buck-derived converters differentially, making sure that in the ground there is no common mode current, making it safe from modest ground bouncing, improving electromagnetic compatibility, and eliminating parasitic effects during normal operation. At the output of this converter cumulatively two inductors are linked to lessen phase current ripple and boost efficiency by lowering the number of components in the EPS. Coupled inductors provide better power density and a moderate capacity to handle transients [65]. The load-side redundant buck converter consists of an identical inductor and two separate half-bridge switching modules. For over-current protection, a fuse connects the half-bridge module and inductor. Based on the intended system for fault diagnosis, the redundant module activates in fault conditions. Due to the constrained weight and volume of smaller satellites, the viability of redundant components requires some additional effort.

3.3.1.2 Boost-based Converter Topologies Under Study

A boost power converter is used to execute MPPT in the SmallSat application when the solar array voltage is less than the bus voltage. It is extremely difficult to accomplish high-step-up DC-DC conversion, low cost, high efficiency, and due to the PV with a parallel-connected construction and low output voltage [66]. Some boost-based converter topologies have been compared and analyzed for space applications in [67]. The topologies are built and optimized by the operational voltage range, conduction emission, operational voltage, power handling capacity, and satellite solar array output impedance requirements. The power losses, control loop bandwidth, and mass have been considered in the analysis. The topology switch near-ground as depicted in Fig. 3-7 (a), the driving circuit implementation is simpler than it is for the

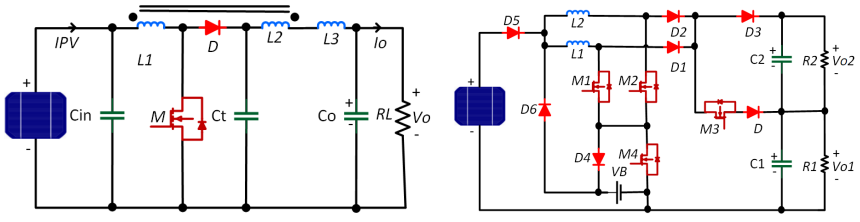

(a) *(b)*

Figure 3-7: Boost power converter:(a) switch near ground, and (b) two-input/multioutput interleaved converter [J1].

other topologies discussed, given that it grounds the power transistor. Additionally, this converter offers better efficiency when applied to a DET EPS architecture. The interleaved structure is another useful method for boosting the voltage level since it can minimize the size of passive components, lowers output current ripple, and enhances transient response [68]. For spacecraft applications, an interleaved DC-DC boost converter two-input/multioutput has been presented in [69], which is shown in Fig. 3-7 (b). The primary functions of this converter are battery charge control, MPPT power supply, and bus voltage regulation. There are three different operating modes of the proposed converter, and it uses a single compact circuit to replace three separate converters. In the first mode of operation scenario, PV supplies directly the loads, without the need for battery operation the battery supplies the loads in the second mode, and in the third operation approach, the converter combines the operation of the battery and the PV to supply the loads. In this topology the battery base is grounded which avoids battery damage and expands the battery's useful life.

3.3.1.3 Buck-boost Converter Topologies Under Study

A bidirectional power flow is provided by the buck-boost converters, and it can step up or down output voltage to a regulated level of the input voltage based on the SOC of the onboard batteries and provide charge and discharge of fully controlled [70]. The buck-buck-boost regulator (B^2R) is a step-up and step-down high-efficiency converter that is presented in [46], and has been improved in [71] as buck–buck–boost regulator (B^3R), which is shown in Fig. 3-8 (a). The converter is used when the main DC bus in DET designs with regulated or unregulated bus voltages is directly connected to the battery. In the case of MPP design implementation, the use of B^3R assists in keeping the MPP solar array voltage level and the main bus voltage close to each other, ensuring superior performance. While a single buck or boost converter cannot provide this benefit individually in the practical implementation of such configurations in SmallSat [71].

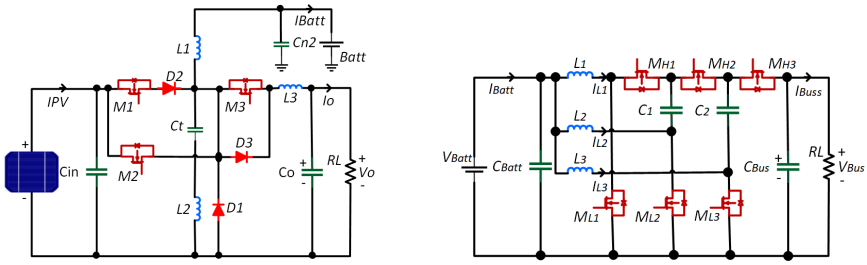

Figure 3-8: Buck-boost-based converter topologies:(a) buck–buck–boost regulator (B^3R), and (b) interleaved bidirectional PWM converter [J1].

In extreme duty cycle operations, conventional bidirectional converters present significant challenges, because of the requirements of bridging the high voltage gap between the DC bus and the battery. In addition, the converter experiences additional current stress due to the low voltage side of the battery. An interleaved bidirectional PWM converter with current balancing capabilities and high voltage conversion is suggested in [72], as shown in Fig. 3-8 (b). This converter is derived by inserting two more capacitors, C1 and C2, into the standard interleaved PWM three-phase converter. The pressures on the switches are reduced by the addition of the capacitors, which at a particular duty cycle also increase the voltage conversion ratio and balance out the inductor current. For step-up and down this converter operates for a single-cell battery-based EPS at charge/discharge of the battery and contributes to power conversion efficiently.

3.3.2. ISOLATED DC-DC CONVERTERS

Isolated converters are commonly used in a variety of forms in SmallSat applications because specialized satellite digital loads operate at low voltage supply, require a larger current (5-10 A or more) and that might be characterized by minimized fluctuations and ripple. Multiple power conversion stages are accomplished, prior to final load voltages where isolation and regulations are required [53]. Additionally, one multiport converter can be used in place of several separate converters, providing a range of advantages but at the expense of the reliability of a single point of failures such as a smaller number of components, and fewer conversion stages. The isolated converter topologies are broadly classified as Multi-Input Multi-Output topologies (MIMO), Single-Input Multi-Output (SIMO), and Single-Input Single-Output (SISO).

3.3.2.1 Single-input single-out (SISO) Converters Under Study

For SmallSat applications due to its better clamping competence, the converter of active-clamp-forward (ACF) is feasible, with fewer component counts, and a simple

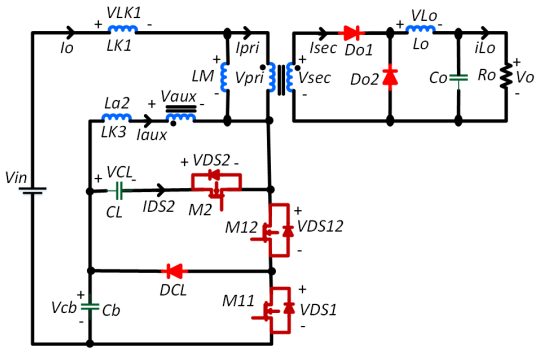

Figure 3-9: Novel ACF-SISO converter topology [J1].

structure. Though, the high pulsating current, larger di/dt, and extreme switching stress make it unfavorable [73]. To beat these drawbacks another ACF topology has been presented in [59], as can be seen in Fig. 3-9. In this converter topology, the current is continuous, and two switches are serries connected to relive the switching stress on the converter main switch. A clamping circuit and a turn-off delay are applied to avoid an imbalance in switching voltage, while both the switches are always clamped respectively to VCL and Vin. As a result, the low drain to source resistance and switches low voltage stresses the converter achieves reliability and a high-power density.

3.3.2.2 Single-input Multi-output (SIMO) Converters Under Study

A galvanic isolated magnetic feedback converter topology has been presented in [74], for space applications. The magnetic feedback forward converter which is decentralized and multioutput is illustrated in Fig. 3-10. While galvanically isolated converters with classic optocoupler feedback are instead in volatile temperatures and radiations are very sensitive. The PWM and magnetic feedback controller are more reliable because they are less susceptible to temperature variations and radiation effects in general. This converter is more effective because it has simpler circuitry than other multioutput converters and a self-resonant reset mechanism. Given that it is less complex than certain common converter topologies frequently chosen in SmallSat like the flyback multioutput converter, push-pull, full-bridge, and half-bridge. With a few small additional circuitries, this converter improves the topology with many output channels because this converter is transformer-based.

3.3.2.3 Multi-input Multi-output (MIMO) Converters Under Study

The multiport integrated converters with fewer number components, switching devices, and conversion stages. The multiport converter is smaller, more reliable, and has a lower mass in comparison to independent port converters. Additionally, there is no need for communication, and the converter's dynamic performance is improved by

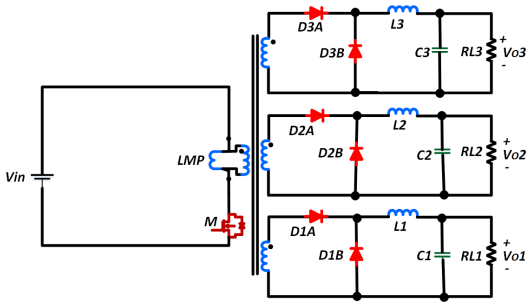

3-10: Magnetic feedback forward converter with multioutput [J1].

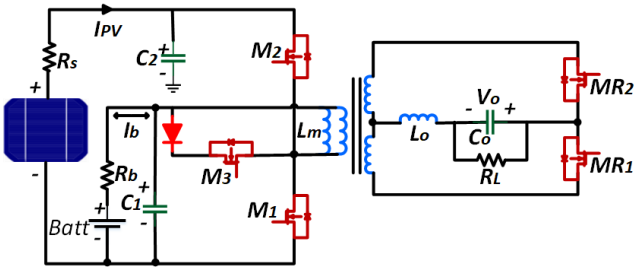

Figure 3-11: An integrated three-port converter topology [J1].

the centralized control system. For satellite applications, an integrated three-port converter has been proposed in [75], which is illustrated in Fig. 3-11. The battery, the solar input, and an isolated output port are represented by the three ports. The converter functions at MPPT during the illumination time when the battery is charging and the completely regulated power is received at loads. The half-bridge converter control is responsible for the three circuit stages, which use a constant switching cycle with modified PWM, and two independent control variables are generated respectively for *d1,* and *d2*, to operate *M1* and *M2* switches. These two independent control variables tightly regulate two converter ports, while the third port provides circuit balance. However, in contrast to conventional two-port converters, the control design necessitates more modeling efforts and is more complex.

3.4. PV TECHNOLOGIES FOR SMALLSAT APPLICATIONS

3.4.1. SPACE-QUALIFIED SOLAR CELLS

Compared to terrestrial solar cells, those utilized in space applications are capable of capturing energy from a wider range of solar radiation. The Solar cells qualified for space applications are designed for 1366.1 W/m^2 integrated power density and spectrum of AM0 (ASTME-490) [76]. But the cells for terrestrial applications are in accordance with global direct spectrums of AM1.5G (ASTM G-173) and AM1.5D, having unified 1000 W/m^2 and 900 W/m^2 power densities, respectively. Therefore, there is a greater possibility for improved solar energy harvesting, and for suitable space solar cells, a different technique is required. In SmallSat applications, the PV technologies are selected from the different available COTS component producers. The most popular solar cells used in terrestrial applications are Si-based, with up to 20% conversion rates. However, these cells in addition to their naturally low conversion rates perform considerably worse when in orbit, the radiation environment also causes them degradation of efficiency over time. For contemporary satellite applications therefore Si solar cells are not a good choice. For use in space

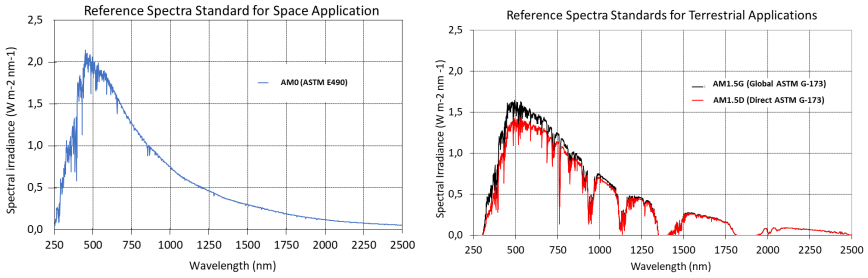

(a) *(b)*

Figure 3-12: Sunlight spectrum for standard (a) space solar cells and (b) terrestrial [J1].

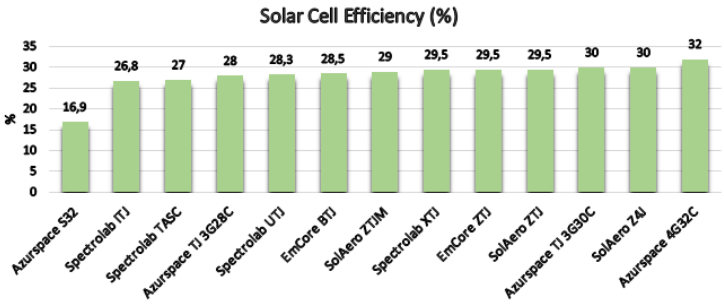

Figure 3-13: Solar cell technologies for space applications [J1].

applications to overcome the limitations of Si-cells, multijunction solar cells (MJSC) have been constructed. MJSCs are significantly more efficient than Si-based ones by over 10% [77]. In Fig. 3-12 (a) and (b) for reference the LEO and terrestrial spectra are shown. More specifically, recent research has shown that MJSCs operate with energy conversion efficiencies of 46.1% for 4-junction (4-J) and 44.4% for 3-junction (3-J) under intense sunshine [78]. Fig. 3-13 displays SmallSat applications based on suitable space solar cell technologies.

3.4.2. MJSC DESIGN AND CONSTRUCTION

An MJSC is created by stacking layers of germanium (Ge) or silicon (Si), indium gallium phosphate (InGaP), and gallium arsenide (GaAs) to catch the broadest sunlight spectrum. In Fig. 3-14 the design layers and architecture of solar cell for 3-J Ge/GaAs/InGaP is depicted. These cells perform better and are simpler to fabricate compared to other higher-order MJSCs [79]. Additionally, this solar cell has a higher cell MPP voltage and is extremely radiation-tolerant (VMPP). The three p-n junctions

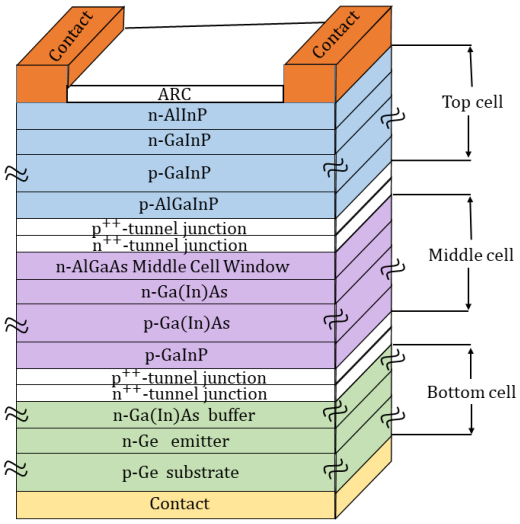

Figure 3-14: The design layers for the 3-J solar cell [J1].

that make up a 3-J solar cell are stacked one on top of the other and joined by tunnel junctions to add additional sub voltages while preserving the overall polarity of the cell. The cell radiation response is regulated by the radiation-sensitive subcell photocurrent [80]. The conversion efficiency of the 3-J solar cell had steadily increased by about 30%, at the beginning of life (BOL) [81]. Inverted metamorphic multijunction is a revolutionary cell architecture that has been proposed by recent research (IMM). In comparison to 3-J cells, IMM cells have a lower mass and are more effective [82].

3.4.3. MJSC MODELING

An ideal solar cell theoretically may be described as a current source that works in the opposite direction of a diode. Solar radiation produces a direct current, which changes because of exposing the cell to light. The model has been improved to include the effects of series and shunt resistors [83]. The circuit in Fig. 3-15 can be used to model the 3-J solar cells, for a single independent solar cell in which each sub-cell is acting. The three equivalent solar cells are set up so that they can be connected from top to bottom in series while reducing the gaps between the cells. The sum of total cells that are combined with three sub-cells can be employed to drive the electrical performance of 3-J solar cells (I–V diagram) therefore posing a similar current because of the series connected all sub-cells [84].

The current produced by each sub-cell is represented as the mathematical expression:

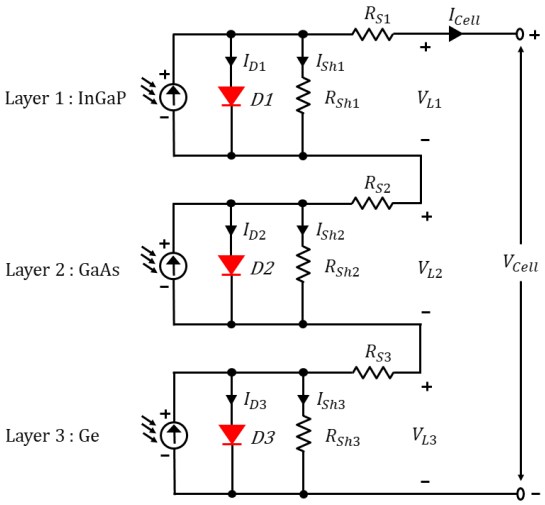

Figure 3-15: A 3-J PV cell equivalent circuit [J1].

$$I^i = I^i{}_{PV} - I^i{}_{sh}\left(e^{\frac{q\cdot(v^i + I^i R_s^i)}{a^i \cdot K \cdot T}} - 1\right) - \frac{(v^i + I^i R_s^i)}{R_{sh}^i} \tag{5}$$

The (*i=1:* top), (*i=2:* medium), and (*i=3:* bottom) where *I* am the total number of sub-cells current. I_{PV} stands for the sub-cell photocurrent, *a* stand for the Boltzmann constant, the diode inverse saturation current for the sub-cell is represented by I_s, the sub-cell temperature *T*, and electron charge *K*. The ideality factor of the diode is represented by *q*, and the R_s and R_{sh} represent respectively the series and shunt resistances [85].

$$V = \sum_{i=1}^{3} V^i \tag{6}$$

The sub-cell that generates the least amount of total current out of the three series-connected cells is represented as:

$$I = \min(I^i) \tag{7}$$

Shunt resistance R_{sh} can be disregarded since the shunt current I_{sh} is the lowest possible in the *I-V* model of the panels [86].

3.4.4. DEGRADATION ANALYSIS FOR PV UNDER RADIATION AND THERMAL ENVIRONMENT

The electrical performance of semiconductors, particularly solar cells, suffers when exposed to this radiating environment. This effect can cause mission failure and is extremely risky. The radiation response of the spacecraft's solar cells is crucial to estimate the mission's longevity. Certain electrical parameters must be determined to estimate the level of degradation of solar cells in the radiation environment, such as the maximum power reaction, short circuit current, and open-circuit voltage. The reports in [87], and [88] show the 3-J solar cell's performance evaluation and forecast under irradiation conditions. An accuracy of 5% of the degradation curves when the short-circuit current and open-circuit voltage are calculated, with the experimental data which is in good agreement. Additionally, a degradation model of the orbiting current has been presented for GaInP/GaAs/Ge 3-J solar cells in [89]. The output current is an important performance metric for defining how a solar cell model degrades. A mathematical model is built to model the output current's tendency to vary. For predicting the lifetime of 3-J solar cells the outcomes of the applied degradation model help to forecast how long the cells will last in space applications. Meanwhile, the performance of the solar cell is severely reduced by high temperatures. To provide greater performance PV back surface coatings and paint are applied as passive treatment methods. While, the backside of the solar array underwent thermal surface treatment, which significantly reduced temperature and raised overall solar cell efficiency [90].

3.5. BATTERY TECHNOLOGIES FOR SMALLSAT APPLICATIONS

The SmallSats need an ESS with batteries to keep the satellite running continuously throughout eclipse and intense load periods. The onboard satellite batteries based on their application are classified as primary and secondary batteries. Primary, such as pyro batteries, are not rechargeable; they are used for short mission requirements and are disposed of after use [91]. The secondary batteries, on the other hand, are utilized for longer missions, which are a crucial and permanent component of the EPS and are rechargeable. Therefore, the main consideration in this study is the secondary battery. The proper selection of the battery is done under the specifications of each mission such as capacity, technology, and type, which, is another crucial phase in any satellite design. For nanosatellite applications, the secondary batteries are displayed in Fig. 3-16, following their volumetric and specific energy densities. The mission duration, power/energy budgets, operational temperature range, and the available thermal management technique are the three most important factors in proper sizing and selection [92].

Under the requirements of each mission the selection of the battery technology, type, and capacity, which is undertaken, is another crucial phase in any satellite design. The

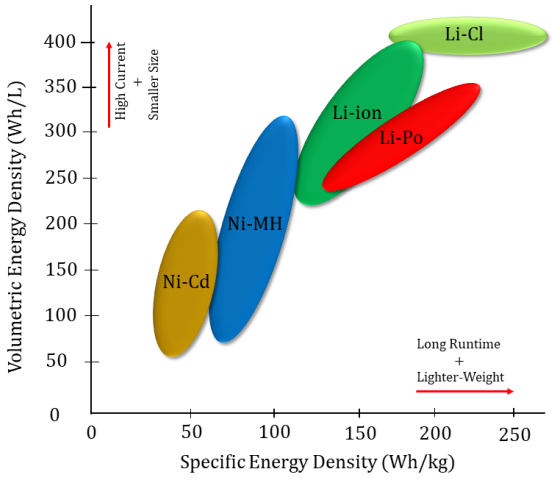

Figure 3-16: Batteries with different energy densities for SmallSat applications [J1].

mission duration, power/energy budgets, operational temperature range, and the available thermal management technique are the three most important factors in proper sizing and battery selection [92]. The harsh conditions in space need extensive design and component selection tactics. The temperatures fluctuate from −20 to −100 °C in space operating environmental circumstances which have an impact on the performance of batteries that are energy-releasing devices based on chemical reactions. The battery module may be harmed and deteriorated by excessive cooling. While for active control the application of a thin film heater is the key technique. The controller and sensors operate in a closed-loop system with the heaters, which are resistors. Additionally, to be approved for application the batteries undergo intense testing under several environmental conditions.

3.5.1. BATTERIES FOR SMALLSAT APPLICATIONS

According to a survey conducted in [93], lithium-ion batteries make up 66% of the batteries used for nanosatellite applications, compared to 16% nickel-cadmium (Ni-Cd), 12% lithium-polymer (Li-po), 4% lithium-chloride (Li-Cl), and 2% other chemistries. The development of lithium-ion technology has many advantages, including a long-li to 97% at BOL, measuring 65 mm in length and 18 mm in diameter [95], [96]. Another comparable battery technology that is proper in SmallSat Applications and is available in a pouch rather than a cylinder is the Polymer Li-ion (Li-Po), which allows for the development of thinner and lighter cell designs for specific energy accomplishment. The Li-Po cell has a 1.2–1.6 times greater gravimetric energy capacity and just 17% of the volume of a Li-ion cell in general, whereas the Li-ion cell has a higher capacity, greater life cycle, a low self-discharge rate, no memory effect, and improved working life. Li-ion batteries are widely used

TABLE 3-1: THE AVAILABLE BATTERY TECHNOLOGIES FOR SMALL SATELLITES [J1].

Maker	Name of Product	Applied Cells	Density in Energy ($Whkg^{-1}$)
ABSL	Li-ion COTS 18650 Battery	MoliCell, Sony, Samsung LG, Sanyo,	90 – 243
EaglePicher	(LP-33330) Rechargeable Space Battery	Li-ion EaglePicher	105
GomSpace	BP4NanoPower BPX Nano Power	NanoPower Li-ion GomSpace	1432- 154
Vectronic	VLB-X Li-ion Battery	Li-ion SAFT	Unkn.
Blue Canyon Technologies	BCT Battery	LiFePo4 or Li-ion	Unkn.
Canon	BP-930s	*fo*ur 18650 Li-ion cells	132
AAC Clyde	CubeSat Battery 40Whr	Li-Polymer Clyde Space	119

in CubeSats due to their tolerance of the space environment (100°C), and appropriate size. For SmallSat applications, some most recent battery technologies that are suitable are listed in Table 3-1 [35]. These upgraded cylindrical 18650 cells weigh 50 g, with an average voltage of 3.6 V, and a capacity of 3500–3600 mAh. 18650 cells have an energy density of 252 Wh/kg and 762 Wh/l, respectively [91]. Additionally, Li-ion batteries come in a variety of shapes and have minimal volume and mass [94]. The available cells have an efficiency of up

3.6. SUMMARY

This chapter reviews the SmallSat microgrid systems including the power conversion and distribution architectures. Two standard EPS unregulated bus architectures of DET and MPPT are presented with bus regulation options. The distributed and decentralized power distribution architectures have been discussed and presented with numerous output switches. The types of architecture are compared and summarized. Some important and latest converter topologies of non-isolated buck, boost, and buck-boost converter topologies for SmallSat applications have been reviewed and debated. Moreover, state-of-the-art isolated converters topologies of SISO, SIMO, and MIMO have been briefed and deliberated in SmallSat applications with a smaller number of

components, switching devices, and conversion stages. The triple junction solar cells as the appropriate energy generation technologies have been accounted for their efficiency and construction. The triple junction solar cell modeling has been also demonstrated for SmallSat applications. The Li-ion battery technologies are still a promising technology in SmallSat applications, therefore some state-of-the-art Li-ion batteries from diverse vendors are reviewed and discussed in this chapter.

CHAPTER 4. DESIGN AND DESIGN VERIFICATION OF FULL-SCALE SMALL SATELLITE MICROGRID

In this chapter, an EPS design architecture has been verified in different operating modes considering all the design requirements and main features of the mission, including power budget, orbital environment, the PV, converter, and battery designs and models. The design and sizing of key EPS elements and the coordinated control strategy have been implemented to attain efficient and stable system operation in a space volatile environment.

4.1. INTRODUCTION

The EPS relies on architectural design to harvest solar energy from body-mounted solar panels, and store the energy, but also, the reliable energy distribution must be efficiently managed in accordance with the mission's load needs. Including the provision of voltage and current specifications at subsystem needs [97]. A comprehensive and general electrical diagram of the EPS for a 3U CubeSat is shown in Fig. 4-1, and the proposed EPS is appropriately extendable for other SmallSat architecture designs A perfect EPS maximizes the harvested energy to allow the satellite to perform several tasks properly. This necessitates a strong and efficient physical design and, consequently, complex controls. The success of the CubeSat

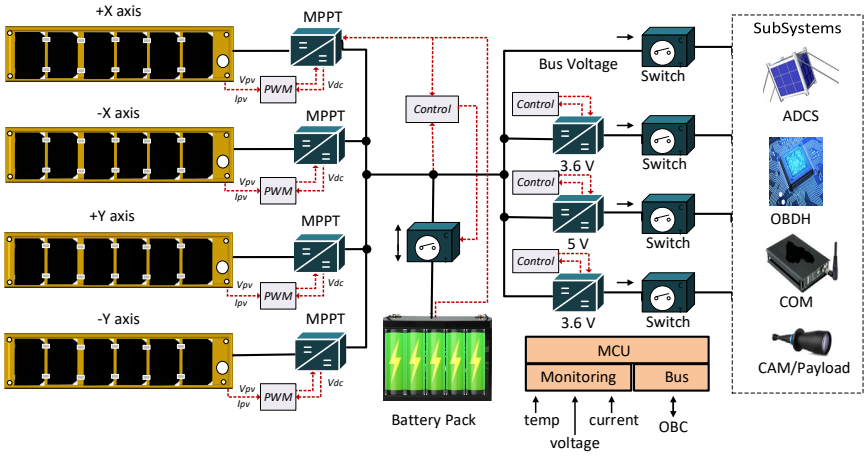

Figure 4-1: The block diagram of EPS design for a 3-U CubeSat with solar panels on X and Y axis [J2].

mission depends on the proper design of the EPS. This must take into consideration all the factors including the EPS architecture, altitude, orbit, mission duration, and inclination angle. Moreover, the load profiles, system efficiency, PV size and arrangements, battery configuration, reliability, control, resilience, and component counts are taken into consideration in the design process [98]. However, the design is complicated due to the restrictions of size and weight, the hazardous radiation environment, the wide range of temperatures, and the inexpensive components. In EPS design the most important phase is the selection of the appropriate EPS architecture, which is based primarily on a few fundamental topologies that are categorized according to main bus voltage regulation and criteria for energy transfer [48]. Peak power tracking (PPT) and direct energy transfer (DET) are two categories for energy transfer criterion based on PV panel interfacing. In the existing literature, there are some studies on design specifics for satellite EPS applications. In [99], a special satellite EPS design that takes into account CubeSat's design and operational modes is provided. In another design in [100], PPT-based EPS design, solar array dimensions, and battery parameters have been considered. The paper [99], presents a modular multi-U EPS design with several distinct PV inputs and converters to configure independent MPP channels. A design process for the satellite's PV and batteries is presented in [33]. But the EPS designs can be found in existing literature, most of them are too mission-specific and narrow in scope. Furthermore, a fine and detailed EPS with all relevant components as well as a small satellite orbital analysis model are both lacking in the current research. In this study, a complete SmallSat EPS design and design verification in different load conditions is proposed. To summarize the primary ideas in this study are given below:

- ✓ Consideration of all critical elements of EPS including, type, number, and configuration of PV and battery cells, as well as the design and sizing of the solar array and battery.
- ✓ Considering the requirements of the mission, such as the orbital duration, altitude, and inclination.
- ✓ Consideration of the operating modes, power budgets, and load profiles of the satellite.
- ✓ To ensure the execution of consistent satellite operations throughout the mission application of unregulated bus and series MPPT architecture.
- ✓ Design of control distribution unit, and point of load converters for satellite applications.

In addition, the contribution of this work is summarized as:

- o Analysis to determine the generated power from the irradiance at sun-pointing orientation scenario to find the exact PV power generation capability in this orientation.
- o Analyzing the EPS architecture with MPPT series-connected converter, battery-regulated bus, and unidirectional converter in SmallSat applications

for efficient PV power extraction, DC-regulated bus, and efficient power distribution.

- Design verification for various load conditions in different scenarios for a complete orbit in MATLAB/SIMULINK, which shows efficient energy generation, storage, and utilization.

4.2. EPS ARCHITECTURE AND DESIGN REQUIREMENTS

For the EPS design primarily the PV module, battery storage, and various switching converters and regulators are considered, which are the main components in the EPS architecture and design process. Solar panels use a space-version triple-junction Gallium Arsenide (GaAs) solar cell to convert photon energy into electrical energy. Following the 3U CubeSat structure and the design practice the PV array unit on the body-mounted satellite is divided into four sub-units according to the Cartesian coordinate system and the same as illustrated in Fig. 4-1. The PV panel, battery, and load specifications for the considered microgrid are listed in Table 4-1.

This EPS architecture houses four solar panels on its X and Y axes, this EPS architecture accommodates four solar panels, each of which is made up of six GaAs SISP solar cells with a 32% efficiency at AM0, 1Sun, 1353W/m^2, at 25°C. The six series-connected SISP 3-J PV cell average voltage at the buck MPPT converter input side is approximately 16 V. For the given X and Y axis six ISPS PV cells are series connected on each face and each face is parallelly connected to the opposite side panel. Each PV cell combination is connected to the input of their dedicated buck MPPT converter. The MPPT performance of the buck converters is intended to optimize the output power from the solar panels. Storage is provided by a Li-ion battery pack, and point-of-load converters are placed for the load supplies' voltage management. In this model 4-Li-ion 18650 cells in which each two are connected in series, and the two sets of batteries are connected in parallel. (2 series, 2 parallel) configuration. The battery pack is applied to the common DC bus and the bus voltage

TABLE 4-1: SPECIFICATIONS OF 3-U CUBESAT PV PANEL, BATTERY, AND LOADS [J2].

Name	Specifications
PV panel	Serries connected 6 SISP 32% solar cells *Voc = 16002 [mV], Isc = 19.0 [mA] *VPmax = 14100 [mV], IPmax = 18.4 [mA]
Battery	4-Li-ion 18650 cells (2 series, 2 parallel) configurations 6 to 8.4 V, 5200 mAh Vo, max = 8.3 V, Vo, crit = 6.5 V
Load voltages	Vbus = 3.6, and 5 V

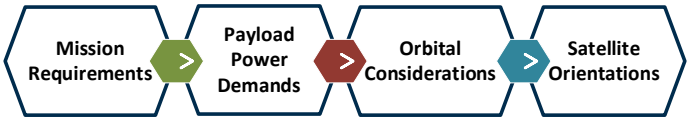

Figure 4-2: The generalized information flow required for the EPS subsystems design [J2].

is battery regulated, which is approximately about 8 V. The unregulated main power bus which follows the battery voltage is also taken into consideration. The EPS design places a strong emphasis on providing the necessary power for the satellite payloads and subsystems. The overall flow of the design information, which is depicted in Figure 4-2, is used as the basis for analysis to meet this requirement.

4.2.1. MISSION REQUIREMENTS

The majority of small satellite designs are mission-based, with objectives including but not limited to educational, research, communication, navigation, and position tracking. Many missions also involve testing technology and scientific payloads in orbit. This design case study mission is based on the data from [101], a 3U-CubeSat with a 5-year mission and a 700 km low-Earth orbit. Two scientific and one technological objective verifications are part of the mission. The mission objectives and their power consumption and voltage ratings are key to the EPS design based on that the satellite's subsystems and payloads are determined.

4.2.2. PAYLOAD POWER BUDGETS

The operating power levels of the subsystems and payloads such as attitude determination and control systems (ADCS) board, battery board, magneto torquer, transmitter (TX), battery heaters, Particle Telescope (PATE), inertial sensor modules (IMU) of attitude control, onboard computer (OBC), receiver (RX), microprocessor, and Plasma Brake (PB) are defined and displayed in Table 4-2. The satellite ADCS board, battery board, magneto torquer, TX, battery heaters, and PATE payload are supplied with a 5 V bus. While inertial sensor modules of ADCS, OBC, RX, microprocessor and PB payload are supplied from the 3.6 V regulated bus. Some critical loads like battery board, ADCS board, OBC, and RX are always in the ON state.

4.2.3. ORBITAL CONSIDERATIONS

The orbit under consideration is the most ideal low earth orbit for the SmallSat, which has a constant illumination of 1367 W/m2, at an altitude of 700 km Keplerian polar sun-synchronous orbit. To illustrate the design used for the selected case study of an altitude of 700 km orbiting in LEO with an inclination angle of 98.20° and the total

TABLE 4-2: POWER REQUIREMENTS FOR 3-U CUBE SAT SUBSYSTEMS AND PAYLOADS [J2].

Subsystems	Component	Current (A)	Voltage (V)	Power (W)
EPS	Battery Board	0.020	5.0	0.100
ADCS	ADCS Board	0.020	5.0	0.100
	IMU	0.265	3.6	0.954
	Magnetorquer	0.600	5.0	3.000
OBC	Flight Computer	0.071	3.6	0.2556
Transceiver	UHF TX	0.78	5.0	3.9
	VHF RX	0.046	3.6	0.1656
Payload	Microprocessor	0.300	3.6	1.08
	Plasma brake (PB)	0.182	3.6	0.6552
	Battery Heaters	0.400	5.0	2.000
	PATE	0.600	5.0	3.000

orbit period will be 99 min. The Sunlight period is 63.36% of the orbit, which is 62.7 minutes of the total orbit timing, while the eclipse time ratio is 36.64% of the orbit and 36.3 minutes of the total orbit timing.

4.2.4. SATELLITE ORIENTATION

The satellite orientation is Sun-pointing orientation as discussed in Chapter 2 and shown in Figure 2-3 (a) and (b). The 3U face of the satellite which is labeled as X- is the one that is receiving the most energy from the Sun. To meet the scientific requirements and to avoid the solar panel developing hotspots due to constantly facing the Sun, the spacecraft spins its axis at a rate of 4 rpm during the orbital period. Figure

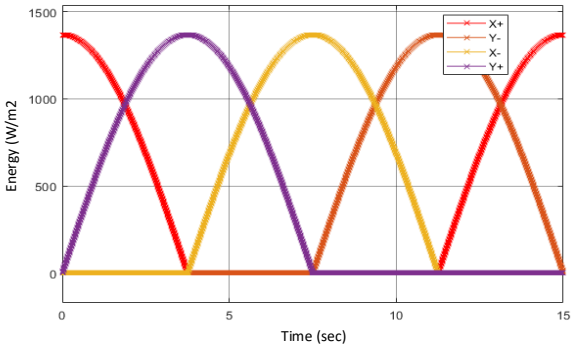

Figure 4-3: The harvested energy in each spin by the PV panels [J2].

4-3 shows the gathered irradiation and the energy produced by the PV panels in each spin.

4.3. PV PANEL DESIGN

The preferred solar cells for CubeSat applications are the available triple-junction (3-J) solar cells from several manufacturers, each with a distinct price level and degree of efficiency. At present, the available commercial-of-the-shelf (COT) SISP triple-junction solar cells for space applications must achieve up to 32% efficiency [102]. Once the solar cells are selected, the number of solar cells in every array installed on the body of the CubeSat should be known. Though a generalized approach is to install solar cells on the entire available body. However, this approach results in more weight and expenses. The famous strategy to determine the number of appropriate cells required in a solar panel is the energy balancing method. The energy balance method is to match the power demand of the subsystems and loads to the generated power of the satellite. In the considered case study, each PV panel consists of six triple junctions of SISP solar cells exposed to temperature and irradiance. The solar cells are series connected in each panel and this configuration is used for the simulation. Although at solar panel design process the mission life, the PV parameters (voltage, current, and generated power) at the End of Life (EOL), and the energy required by loads in each orbit are taken into account. These requirements are achieved by considering accurate sun-tracking, effective MPPT extraction, and optimal converter utilization. Various standard limitations and the simple design adaptation limit the solar panel affixing area because solar panels are typically body mounted on CubeSats. Therefore, to maximize the possible generation, high-efficiency solar cells are implemented to achieve maximum power.

The power generated by solar panel systems relies on the irradiance profile, cell type, cell efficiency, number of cells in each PV module, and series-parallel cell arrangements. The performance of the solar panel can be confirmed by using the datasheet of 3-J PV cells provided by the makers and the exponential mathematical models of the solar panel. The considered solar cell is the SISP 3-J cell and the cell properties are illustrated in Table 4-3. While the I-V and P-V curves of the PV panels are shown in varying irradiances and temperatures, as shown in Fig. 4-4 (a) and (b), respectively. There is a maximum likelihood of three CubeSat faces being exposed to solar radiation at any given time based on CubeSat appearance. As a result, it is crucial to design an appropriate setup for solar panels that continuously modifies its configuration in response to the environment. An example of the irradiance profile for the 3U CubeSat considered in this case study has been created for the relevant sides as can be seen in Fig. 4-1 and the resultant harvested energy is illustrated in Fig. 4-3.

The current of the PV panel is derived by the equation given in Eq. (8):

TABLE 4-3: THE PROPERTIES OF THE SISP TRIPLE JUNCTION SOLAR CELL [J2].

PV Parameters	Values
voltage at open circuit V_{OC}	2667 [mV]
At max. power voltage VPmax	2350 [mV]
Density of the short circuit current ISC	19.0 [mA]
Density of the current at max. Power IPmax	18.4 [mA/cm2]
Cell dimensions	30.15 [cm2]
Maximum cell efficiency ηmax	32 [%]

$$I_{pv,i}(V) = \frac{pI_x}{1-exp\left(\frac{-1}{b}\right)}\left[I - exp\left(\frac{V}{sbV_x} - \frac{1}{b}\right)\right] \quad (8)$$

Where V stands for voltage and b for the panel's characteristic constant. The parallel and series connections shown by the letters p and s enable the design simulation of multiple solar panels. Based on information from the PV datasheet, short circuit current I_x and short circuit voltage V_x are obtained.

The generated output power P_{pv} is derived from Eq. (9).

$$P_{pv,i}(V) = \frac{VpI_x}{1-exp\left(\frac{-1}{b}\right)}\left[I - exp\left(\frac{V}{sbV_x} - \frac{1}{b}\right)\right] \quad (9)$$

The available energy per orbit of the body-mounted satellite is calculated with Eq. (10).

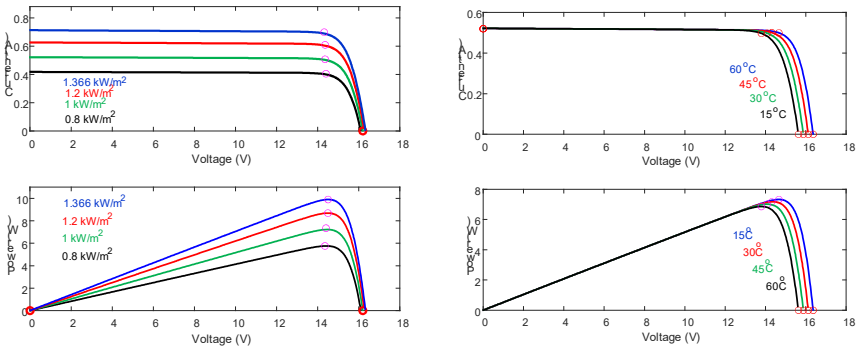

Figure 4-4: The solar panel I-V and P-V curves: (a) at varying irradiance; (b) at varying temperature [C1].

$$E_{pv,i}(V) = \int_{o}^{T_{Sun}} P_{pv,i}(V)_{dt} \quad (10)$$

Where T_{sun} is the length of the day and P_{pv}, $i(V)$ is the power that was instantaneously harvested.

The maximum power output of a typical solar panel is depicted as indicated in (11).

$$P_{mppt} = \left(N_s V_{mppt} - V_d\right) - \left(N_p A J_{mppt}\right) \quad (11)$$

Where A is the cell's area, N_s and N_p are the number of cells in series and parallel, V_d is the reverse diode voltage drop, J_{mppt} is the peak power current per unit area, and V_{mppt} is the voltage at peak power.

4.4. BUCK CONVERTER

A higher voltage source is converted into a lower, regulated voltage level via the buck converter. The most common DC-DC converter architecture is the buck converter in the microprocessor voltage regulator (VRM) and applications of power management. These applications require quick-to-line and load transient responses in addition to outstanding efficiency across a wide load current range [103]. The test and simulation parameters are listed for input and load side buck converters in Table 4-4.

By assuming two stages, the Buck converter can be analyzed and examined: the first stage corresponds to the MOSFET's ON state, and the second stage to its OFF state. The relationship between the input voltage (Vs) and the output voltage (Vo), while the buck converter is in Continuous Conduction Mode (CCM) operating. As shown in Fig. 4-5 (a), For steady state (stage 1) the average voltage across the inductor in one cycle can be represented as, Eq. (12).

$$(V_L)_{ON} * T_{ON} + (V_L)_{OFF} * T_{OFF} = 0 \quad (12)$$

In the case of stage 2 for diode ON and MOSFET is OFF as shown in Fig. 4-5 (b):

TABLE 4-4: BUCK CONVERTER TEST AND SIMULATION PARAMETERS [J2].

Parameters	Buck 1	Buck 2	Buck 3
Inductor (L)	147.5 μH	10.5 μH	10.5 μH
Capacitor (C)	15.7 μF	200 μF	200 μF
Switching Frequency (F)	100 kHz	100 kHz	100 kHz
Voltage in	16 V	8 V	8 V
Voltage out	8 V	5 V	3.6 V

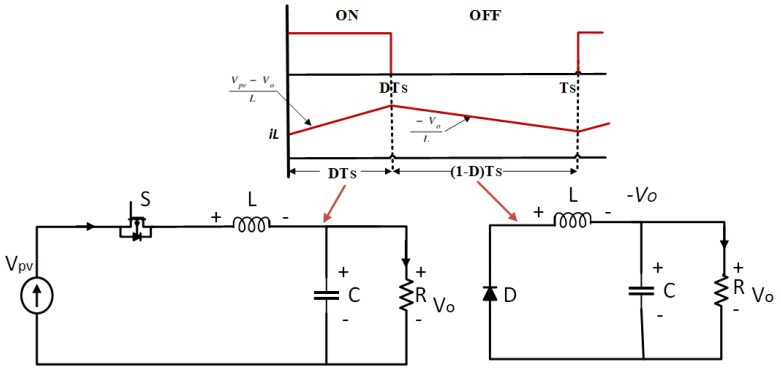

Figure 4-5: Two operation stages of the buck converter: (a) when the MOSFET is ON; (b) when the MOSFET OFF [J2].

$$(V_{pv} - V_o) * DT_S + (-V_o) * (1 - D)T_S \quad (13)$$

By simplification:

$$DV_{pv} - DV_o - V_o + DV_o = 0 \quad (14)$$

Then,

$$V_o = D * V_{pv} \quad (15)$$

The differential equations related to state variables considering the parasitic resistances of filter capacitor and inductance are presented as:

$$V_{pv}(t) = V_o(t) + L\frac{di_L(t)}{dt} + r_L i_L(t) \quad (16)$$

$$i_L(t) = \frac{1}{L}\int(V_{pv}(t) - V_o(t) - r_L i_L(t)) \quad (17)$$

$$V_o(t) = 1/C \int(i_C(t)\,dt + i_C(t) * r_C) \quad (18)$$

Applying KCL and KVL in Fig. 4-5 we can get the following:

$$i_C(t) = i_L(t) - R(t) = \frac{CdV_C(t)}{dt} \quad (19)$$

Where,

TABLE 4-5: TWO STATE OPERATIONS DESCRIPTION OF BUCK CONVERTER [J2].

T	D	f means (sign (i_L))
ON	OFF	1 → for $i_L > 0$ (MOSFET is ON)
OFF	ON	0 → for $i_L < 0$ (MOSFET is OFF)
OFF	OFF	0

$$V_C(t) = V_o(t) - r_C i_C(t) \tag{20}$$

$$V_o(t) = \frac{1}{C}\int(\, i_L(t)dt - \frac{1}{C}\int(\frac{V_o(t)}{R})dt + r_C i_C(t) \tag{21}$$

The buck converter operates in two states while functioning in CCM since it is a switching device. Using a logical variable f as a switching function with the values 0 and 1, these two states are taken into consideration. Table 4-5 provides a detailed explanation of the two-state operations of the buck converter for MOSFET ON/OFF.

Therefore Eq. (12) will be modified to express the state equation of the proposed buck converter, which is represented by the mathematical model.

$$V_L(t) = (V_{pv}(t) - V_o(t) - r_L i_L(t) * f - V_o(t) * sign(i_L(t)) * \bar{f} \tag{22}$$

Since Fig. 4-5 depicts the switching function as a periodic square signal, it is possible to create an expression based on the Fourier Series that looks like this:

$$f = D + \sum_{n=1}^{\infty} \frac{2}{n\pi} \sin(nD\pi)\cos(n\omega t) \tag{23}$$

where ω the angular switching frequency and D represents the duty cycle.

4.5. BATTERY DESIGN AND SIZING

Various subsystems of the satellite require a continuous power source for the duration of the operation, an appropriate storage device design is crucial to mission planning. The storage device covers periods of both maximum and average load as well as when the satellite is in eclipse. Rechargeable batteries are the subject of this effort because batteries are the second source of energy used to power satellite systems. For use in SmallSat storage system applications, batteries with various chemistries, including nickel-hydrogen (Ni-H2), nickel-cadmium (Ni-Cd), lithium polymer (Li-Po), and lithium-ion (Li-Ion), have been evaluated, and verified over the years [2]. But as of late, Li-ion battery cells are now trending in the majority of SmallSat EPS.

4.5.1. BATTERY DESIGN

For this case study, the basis is taken for the 3U-CubeSat battery architecture with 4-Li-ion 18650 cells (2 series, 2 parallel) combinations. Table 4-6 [104] lists the battery cell specifications. Rechargeable Li-ion batteries were chosen because of their extended lifespan, high energy density, and capacity. It may also generate bursts of huge energy without endangering the cell thanks to its wide operating temperature range and distinct working cycle. The generalized equation that expresses the power from battery storage is described in the paragraphs that follow [105].

$$P_{storage}(k) = (S.P(k))_{BS,i} \tag{24}$$

Where $(S)_{BS,i}$ denotes the battery storage's operational condition and$(S.P(k))_{BS,i}$ denotes the storage capacity offered by the battery.

Energy can either be delivered (generation side) or absorbed from storage systems (load side). To be more specific, the CubeSat storage device's charging and discharging mechanism can be described as [106].

$$(S)_{BS,i} = \begin{cases} 1, & P_{gen}(k) < P_{load}(k) \quad Discharge \\ -1, & P_{gen}(k) > P_{load}(k) \quad Charge \\ 0, & P_{gen}(k) = P_{load}(k) \quad Iddl \end{cases}$$

Where, when the power generation is greater, less, or equal to the load demand, the CubeSat storage devices balance the power accordingly.

Fig. 4-6 creates and shows a model of an electrical battery circuit [107]. Where respectively, $i_{Batt,}$ $v_{Batt,}$ and SOC stands for input battery current, internal battery voltage, and battery state of charge. Using the Kirchhoff law for current and voltage in Fig. 4-6, the dynamic equations for the internal voltage can be stated as follows:

TABLE 4-6: LI-ION 18650 BATTERY BASIC CHARACTERISTICS [J2].

Parameters	Values
Nominal voltage	3.7V
Rated capacity	2.6Ah
Initial SOC	50%
Fully charged voltage	4.2V
Nominal discharge current	0.52A
Cut-off voltage	3.0V

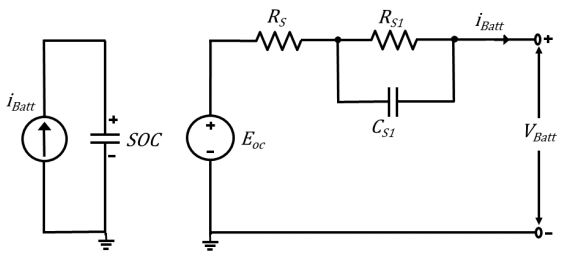

Figure 4-6: Battery equivalent electric circuit model [J2].

$$i_{Batt} = C_{S1}\frac{d}{dt}V_{Batt}C_{S1} - \frac{1}{R_{S1}}V_{Batt}C_{S1} \tag{25}$$

$$V_{Batt} = E_{oc}(SOC, i_{Batt}) + R_{S1}\, i_{Batt} - V_{Batt}C_{S1} \tag{26}$$

Where by combining the battery current while taking the battery's internal temperature, T_B, into consideration, the SOC is derived, where R_{S1} and C_{S1} are the internal resistance, capacitance, and open circuit voltage, and E_{oc} is a non-linear function of SOC and battery current i_{Batt}.

$$\frac{d}{dt}SOC = \frac{1}{C_{S1}(i_{Batt}, T_B)}\, i_{Batt} \tag{27}$$

Additionally, the SOC% is also used to indicate the battery's remaining energy storage capacity. It can be said in the following way:

$$SOC_{min} \leq SOC\ (k) \leq SOC_{max} \tag{28}$$

This means that when the SOC falls below the minimal level, it will be disconnected and start to charge again by the PV system when it is operating beyond its maximum capacity.

4.5.2. BATTERY SIZING

The determination of the battery size is very crucial for the successful the mission's success. While choosing battery size two very important things must be considered. The first is the amount of energy consumed for the eclipse, and the second is DOD [51]. The percentage of the battery's total capacity depends on the number of charge/discharge cycles (DOD) that are spent in each cycle, which affect in turn, the lifetime of the satellite depends on battery life. The battery cell's DOD needs to be limited to under 30% [100].

In the scenario taken into consideration for this design, the period is (99 min) 1:39h, meaning that the satellite makes 15 revolutions around the planet in a day. The mission

duration is 5 years, and the satellite's total number of rotations is estimated to be around 26650. In the eclipse period, the worst case is expected to consume the energy of 0.6 Wh. Thus, the battery packs minimum capacity is:

$$C_{min} = \frac{E_{ecl}/v_B}{DOD} = \frac{0.60/3.6}{0.3} = 0.556\ mAh \quad (29)$$

Where E_{ecl} is the required power at the eclipse phase, which might be less than the accumulated power needed for battery charging.

The difference (without a margin) between the power generated and the power required for the mission during periods of sunlight and eclipse is used to calculate the E_{acc}, which is the power needed to charge the battery, according to [108]:

$$E_{acc} = E_{prod} - E_{day\_needs} \quad (30)$$

4.6. RESULTS AND DISCUSSION

The considered microgrid design is a 3U-CubeSat illustrated in Fig. 4-1, and the payload ON/OFF states are considered as a case study to verify the design at different operating modes. While the rest of the subsystems are in idle and operation modes as given in Table 4-7, with their specific power consumption as illustrated in Table 4-2.

TABLE 4-7: POWER BUDGET OF 3-U CUBE SAT SUBSYSTEMS, AND THE PAYLOADS ON/ OFF OPERATING MODES [J2].

Subsystems	Component	Avg Duty Cycle (%)	Six Satellite Operation Modes in One Orbit (99 min)					
			1st (15 min)	2nd (17 min)	3rd (17.5 min)	4th (16.5 min)	5th (16 min)	6th (17 min)
EPS	Batt Board	100%	ON	ON	ON	ON	ON	ON
ADCS	ADCS Board	100%	ON	ON	ON	ON	ON	ON
	IMU	30%	OFF	ON	ON	OFF	OFF	OFF
	Magnetorquer	15%	OFF	OFF	ON	OFF	OFF	OFF
OBC	Computer	100%	ON	ON	ON	ON	ON	ON
Transceiver	UHF TX	30%	OFF	ON	ON	OFF	OFF	OFF
	VHF RX	100%	ON	ON	ON	ON	ON	ON
Pay loads	Processor	15%	ON	OFF	OFF	OFF	OFF	OFF
	PB	15%	ON	OFF	OFF	OFF	OFF	OFF
	Heaters	10%	OFF	OFF	OFF	OFF	OFF	ON
	PATE	35%	OFF	ON	ON	OFF	OFF	OFF
Power in operation modes (W)			2.559	8.475	11.475	0.621	1.142	2.621

The simulation of a full orbit has been carried out in six operation modes according to different load conditions.

Based on the harvested energy in each spin (15 sec) of the satellite, the PV power, as well as the instantaneous total power and the current from X and Y sides of the 3U CubeSat are shown in Fig. 4-7 (a) and (b) respectively. On each X and Y face, a sinusoidal pattern can be seen, indicating that the PV power is being tracked correctly under the irradiance pattern of Fig. 4-3. The graph of PV-generated power in Fig. 4-8 (a) shows that, due to the satellite moving into an eclipse after 62.7 minutes (3762 sec), power generation immediately stops. Additionally, the change of various load

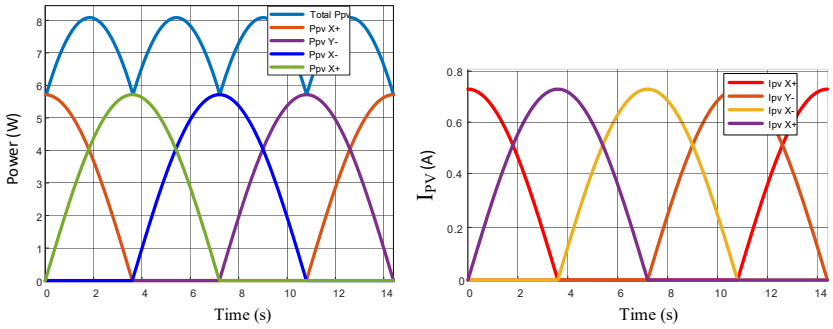

(a) *(b)*

Figure 4-7: The PV generated (a) power and, (b) current from X and Y sides of the 3U CubeSat [J2].

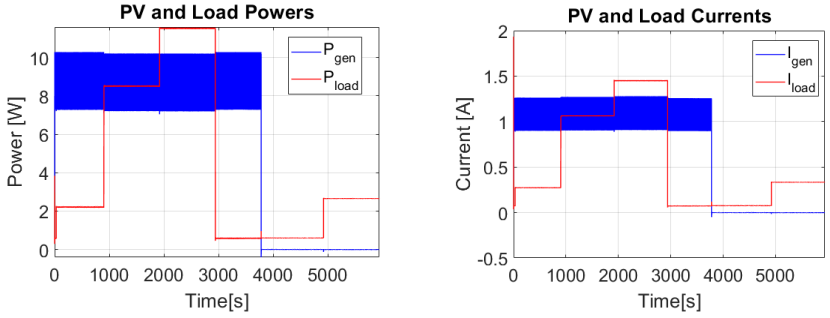

(a) *(b)*

Figure 4-8: The load conditions in different operation modes, and (a) PV generated and load powers, (b) PV and load currents [J2].

conditions in different operation modes of the satellite can be observed in Fig. 4-8 (a) from the PV and load powers. The PV and load currents are demonstrated in Fig. 4-8 (b) which are following the load conditions and satellite operation modes in eclipse and irradiance. Fig. 4-9 (a) and (b) demonstrate the battery voltage and current respectively. In the first operation mode for 15 minutes (0 – 900 sec) the battery voltage is slowly increasing, and the battery current is negative.

It can be observed that the loads are demanding less power in the first operation mode than the PV-generated power while the battery is charging. In the second operation mode for 17 minutes (900 – 1920 sec) the battery voltage is constant to its rated voltage and the battery current is zero which shows that the generated PV power is exactly sufficient for the load demands. In the third operation mode for 16.5 minutes (1920 – 2970 sec), the battery voltage is negative, and the battery current is positive, which indicates that the generated PV power is not sufficient in peak power conditions, and the battery backups the maximum PV generation at excessive load conditions. In the fourth operation mode for 17.5 minutes (2970 – 3960 sec), it can be observed that the battery voltage is at maximum level and the battery current is negative, it indicates that the battery is compensated to its maximum SOC before it goes to the eclipse. At the fifth operation mode for 16 minutes (3960 – 4920 sec), at eclipse condition, the battery is discharging slowly to power the critical loads which are always ON, and the battery voltage drops while the battery current increases. At the sixth operation mode for 17 minutes (4920 – 5940 sec), when battery heaters are turned ON, the battery voltage drops more, and the battery discharges current increases till the satellite again comes to the irradiance in the second orbit. Fig. 4-10 (a) demonstrates the variation in SOC of the battery according to each mode of operation and (b) represents the regulated voltage levels of 5 and 3.6 V for load buses. In this design verification, the SOC of the battery only varies about 8%, and it is a sign that in this design there is the capability to handle furthermore power-thirsty loads

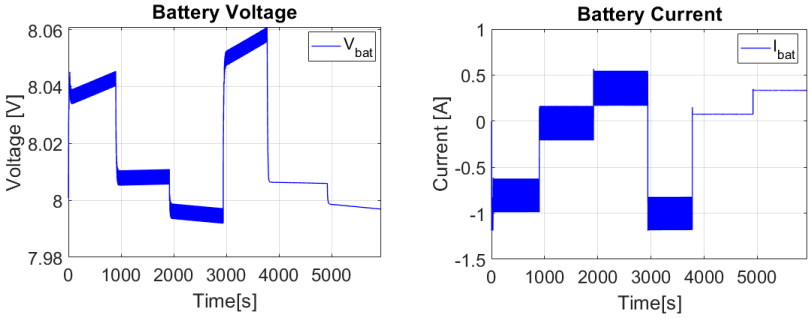

(a) *(b)*

Figure 4-9: A demonstration of (a) battery voltage and (b) the battery current, in different load operation modes [J2].

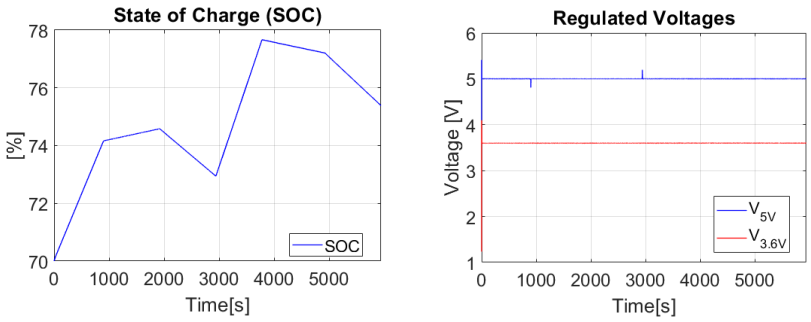

(a) *(b)*

Figure 4-10: Demonstration of (a) SOC of the battery, and (b) regulated voltage levels at 5 and 3.6 V for the 3U CubeSat in different operation modes [J2].

in the 3U CubeSat. From the results, the steady voltages at the desired levels despite variations in loads and continuously variable irradiance serve as proof that the controllers are operating correctly. Both during the eclipse and in full daylight, the DC bus voltage remains constant, demonstrating the effectiveness of maintaining stable DC bus voltage by the battery management and control algorithm.

4.7. SUMMARY

The SmallSat mission success mostly depends on the proper design of the SmallSat microgrid. A comprehensive and general electrical diagram of the EPS for a 3U CubeSat has been considered in this design verification in this chapter. The mission important parameters have been considered including the mission duration, the satellite altitude, orientation, and payload power requirements in this design. The PV panels are designed and modeled considering the SISP triple-junction solar cells for space applications which achieve up to 32% efficiency. For the battery storage system design the battery cell specifications rechargeable Li-ion batteries were chosen because of their extended lifespan, high energy density, and capacity. Moreover, the battery sizing has been considered to meet mission-specific requirements. From the results, it has been proved that the design is very efficient, and the controllers are operating correctly. Both during the eclipse and in full daylight, DC bus voltage remains constant, demonstrating the effectiveness in maintaining stable DC bus voltage.

CHAPTER 5. AN OPTIMIZED MPPT CONTROL FOR SMALL SATELLITE MICROGRID

In this chapter, some MPPT techniques such as, perturbed and observe (P&O), incremental conductance (IC), and ripple correlation control (RCC) have been considered in a comparative study for SmallSat microgrid applications. While the important orbital parameters and space environment scenarios have been considered for optimal power extraction.

5.1. INTRODUCTION

We know from the studies in the past chapters that the Small Sat microgrid is restrained by some regulation of mass and volume yet the power is produced by the solar panels mounted on the body. The typical SmallSat microgrid is shown in Fig. 5-1. Under the demands and goals of the mission, each LEO NanoSat retains a certain orbit within one of three orientations: Sun-pointing, nadir-pointing, and free

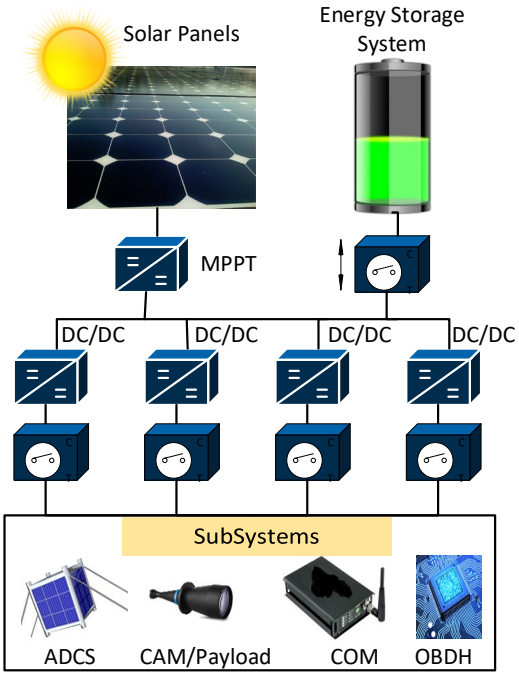

Figure 5-1: A typical NanoSat microgrid [C1].

orientation [41]. The solar radiation drastically fluctuates in each orientation on the satellite's face, which causes Nanosat's angle with the Sun to continuously change its position [109]. The rapid change in position and irradiance will affect the PV maximum power extraction. Therefore, the solar array at Maximum Power Point Tracking (MPPT) appears to be the most appropriate choice for these operating conditions, in contrast to the Direct Energy Transfer (DET) option [51]. For small satellites, deep-space probes, experiment platforms for satellites, etc., several maximum power point tracking approaches (MPPT) have recently been verified. In paper [110], an MPPT controller is developed to get the most power possible out of a photovoltaic (PV) array deployed on an orbiting spacecraft. A fuzzy logic controller (FLC) is employed in the construction of the proposed MPPT to estimate at the maximum power point (MPP) the reference voltage of the PV array, and an adaptive mechanism is used as the reference model to adjust for variations between the PV system. The P&O approach, a quick method with high reliability has been developed to reduce output power oscillations without the use of temperature and light sensors [111]. This study uses a fuzzy algorithm to track the maximum power point. As per the simulation results, the output power is less irregular when the fuzzy approach is used, and more power is generated from the same PV. In [112], based on DSP and LabVIEW, a set of integrated MPPT control and online monitoring system is designed. In this integrated system, the parallel PV array's output characteristics can be effectively controlled and managed under various environmental conditions. Effective improvements are made to digital control's reliability when the integrated system is used in commercial aerospace. In [113], two alternative MPPT algorithms, an analog oscillating MPPT, and an analog global MPPT have been developed, described, compared, and used in the experimental validation for microsatellite Solar Array Regulation (SAR). The P&O approach owing to its simplicity, tracking accuracy, and low complexity, is particularly very popular for LEO SmallSat applications. However, this technique counters with a series of problems, including oscillation close to the maximum power. As a result, the investigation of other important approaches in SmallSat applications, particularly incremental conductance (IC) and ripple correlation control (RCC) seems very valuable [114].

From the above literature review, this work proposes a comparative study in two different scenarios of the conventional P&O, IC, and RCC. The first scenario examines the effects of sudden shifts in temperature and irradiance in a transient condition. In the second scenario, a 3U nano CubeSat with a 4 rpm spin and standard irradiance of 1367 W/m2 is examined in Sun-pointing orientation.

5.2. SYSTEM DESCRIPTION AND PARAMETERS

The system is composed of a few key components as illustrated in the suggested schematic layout in Fig. 5-2. Including (a) power generation and (b) a DC-DC boost converter, (d) a DC resistive load, and the three MPPT techniques-IC, RCC, and P&O.

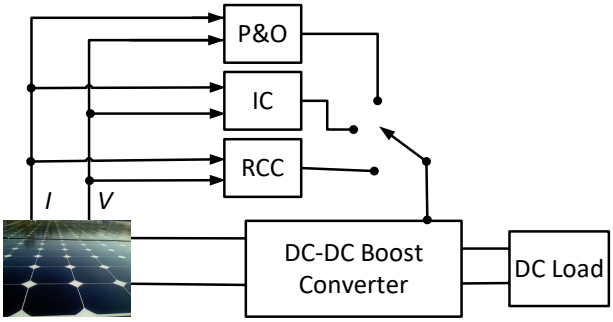

Figure 5-2: The under test schematic diagram of the system [C1].

5.2.1. ORBITAL CONSIDERATIONS

The orbit under consideration is a Keplerian polar Sun-synchronous orbit at an altitude of 700 km, making it the ideal low-earth orbit for the NanoSat, which has a consistent illumination of 1367 W/m2.

5.2.2. PV ARCHITECTURE

In this study, each of the four solar panels on the Nano Sat EPS architecture is placed at the X and Y axes. The considered solar cells are 6 triple junctions (3-J) GaAs SISP solar cells with 32% efficiency at AM0, 1 Sun, with an average temperature of 28°C under the conditions of 1367W/m^2. The description of the solar panels is listed in Table 5-1.

5.2.3. ORIENTATION OF THE SATELLITE

The considered satellite orientation is Sun-pointing orientation, as discussed in Section 2.2.2. The spacecraft spins the axis at a rate of 4 rpm throughout the orbit period to meet the objectives of the mission and prevent PV cells from being damaged by constant irradiance and temperature. This motion made possible the solar energy

TABLE 5-1: SPECIFICATIONS OF 3-U CUBESAT PV PANEL [C1].

Name	Specifications
PV-panel	Serries connected 6 SISP 32% solar cells *Voc = 16002 [mV], Isc = 19.0 [mA] *VPmax = 14100 [mV], IPmax = 18.4 [mA]

harvested by PV panels mounted on the X and Y axes of the NanoSat, as shown in Fig. 4-3.

5.2.4. MPPT CONVERTER

The DC-DC converters are power electronic circuits that alter the applied input voltage level into another adapted level at the converter's output. These converters are comprised of capacitors and inductors and semiconductor devices, through which the applied input voltage level is converted. In this proposed system, a boost converter is positioned at the back end to function as a power electronic interface for the MPPT to each of its associated PV Panels. Therefore, the input voltage is enhanced corresponding to the duty ratio offered by the controller. The boost converter and the linked control system can be seen in the DC-DC boost converter's circuit illustrated in Fig. 5-3. Since the capacitor, inductor, diode, and switch don't use energy under ideal circumstances, two basic conservation principles apply between the input and the output. The input energy may be equal to the output energy, according to the first energy balancing law. The input charge must be equal to the output charge for the second law of charge balance to operate.

Since, when the switch is open, during (1-d) T in one T-period, the input current can only provide charge to the output side. For the first and second laws, the equations are given in (4) and (5), respectively.

$$P_{in} = P_{out} \rightarrow I_{in}V_{in} = I_{out}V_{out} \tag{31}$$

$$Q_{in} = Q_{out} \rightarrow I_{in}(1-d)T = I_{out} \tag{32}$$

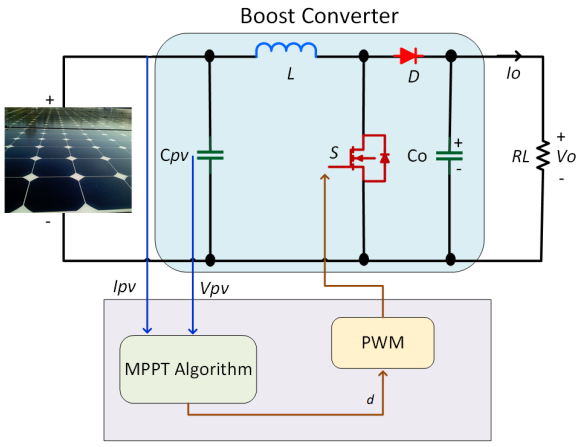

Figure 5-3: Global system scheme for MPPT [C1].

Eq. (4) and (5) can be used to calculate the fundamental relationship between the input and output voltages

$$V_{out} = \frac{V_{in}}{1-d} \tag{33}$$

According to this relationship, it is seen that $V_{out} > V_{in}$, where the duty cycle d is a positive number less than 1.

5.3. APPLIED MPP TRACKING TECHNIQUES

The primary goal of adopting MPPT techniques is to extract and track the maximum power of solar cells under a specific radiation level by controlling the system voltage. As a result, summaries of P&O, IC, and RCC approaches are provided in this section.

5.3.1. PERTURB AND OBSERVE TECHNIQUE

This technique is the most widely used in practice because it is straightforward, simple to use, and can be implemented at a cheap cost while yet providing good performance. However, the P&O algorithm becomes confused at times when the environment is changing quickly [115]. This method involves periodically changing the resulting PV current or voltage to observe their impact on PV characteristics to produce maximum power. While, by either boosting (+ve) or decreasing (-ve) current or voltage of the PV array the system's operational point is moved nearer the MPP. Before reaching the peak value, when there is no difference in power. The direction of the subsequent step is in the same direction if $\Delta V>0$ leads to $\Delta P>0$; otherwise, it is in the other direction, as shown in Table 5-2 [116]. The main procedures for the P&O algorithm are presented in detail in [116].

5.3.2. INCREMENTAL CONDUCTANCE CONTROL

The greater tracking efficiency and accuracy of this method, make it extensively used in PV power generation systems. The flowchart in Fig. 5-4, describes the general idea behind this approach.

TABLE 5-2: TRUTH TABLE FOR P&O MPPT METHOD [C1].

Perturbation ($\Delta \boldsymbol{V}$)	Power change ($\Delta \boldsymbol{P}$)	Next perturbation
+	+	+D
+	-	-D
-	+	-D
-	-	+D

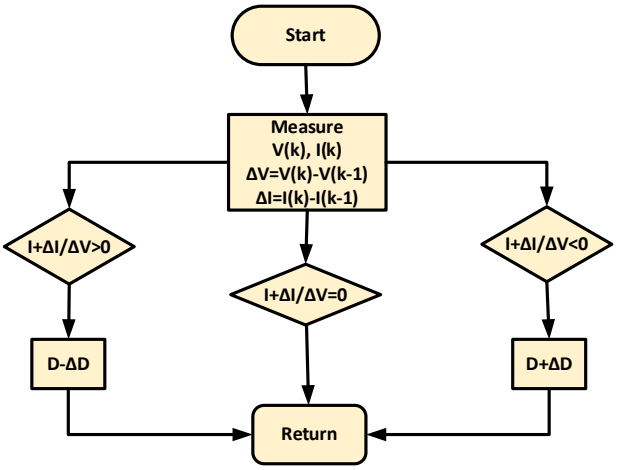

Figure 5-4: Flowchart of incremental conductance algorithm [C1].

The IC algorithm utilizes the PV array's derivative P~V characteristics (conductance). While, based on the instantaneous and incremental conductance, the terminal voltage of the PV system under consideration is determined [117].

$$P = VI$$

By applying the chain rule for products derivatives

$$\frac{\partial P}{\partial V} = \frac{[\partial(VI)]}{\partial V} = I \times \frac{\partial V}{\partial V} + V \times \frac{\partial I}{\partial V} = I + V\frac{\partial I}{\partial V} \tag{34}$$

And it can be as:

$$\frac{\partial P}{\partial I} = \frac{[\partial(VI)]}{\partial V} = I \times \frac{\partial V}{\partial I} + V \times \frac{\partial I}{\partial I} = V + I\frac{\partial V}{\partial I} \tag{35}$$

When reaching the MPP, this means that the $\frac{\partial P}{\partial V} = 0$

The boost converters associated with PWM signals are controlled by the MPPT until $\partial(I)/\partial(V) + (I/V) = 0$ is assured from Eq. (31). The module's max power is set by its incremental conductance, which is > 98%. For $\frac{\partial P}{\partial V}$, three basic conditions must be taken into consideration: the first, when $\frac{\partial P}{\partial V} > 0$, signifies that some adjustments must be done to the right side because the panel is operating on the MPP on the left side. Second, when $\frac{\partial P}{\partial V} < 0$, corresponds to the operational point being on the right side of the MPP, necessitating some adjustments to the left. In the third condition, when the

change $\frac{\partial P}{\partial V} = 0$, in this case, so no requirement to make any change because the solar panel is working exactly at the MPP [118].

5.3.3. RIPPLE CORRELATION CONTROL

The ripple correlation control approach is based on the boost converter's input current, which has a ripple component and a DC component called I_L. Regarding the temperature and radiation levels, the I_L is set. The output power is a combination of ripple and means components that fluctuate nonlinearly with I_L, as shown in Fig. 5-5 [119]. The objective is to force I_L to track $I_L{}^*$corresponding to the MPP irrespective of other variances, temperature, and irradiance [120]. in Fig. 5-6, the RCC block diagram is demonstrated. Therefore, to correlate the inductor's current I_L towards $i_L{}^*$ the idea here is to achieve the MPP so it should specify whether I_L is low/high then $I_L{}^*$. In case, $I_L < I_L{}^*$ it shows that the ripple for current and power are in phase so the $\frac{dp}{dt} \times \frac{di_L}{dt}$ is positive (>0). Likewise, in the case of $I_L < I_L{}^*$, it signifies that $\frac{dp}{dt} \times \frac{di_L}{dt}$ is negative (< 0). In this technique for separation of the DC component, a high pass filter is applied. Due to the inherent ripples encountered during the converter's switching operation, the time derivatives of the current and power are not equal to zero, and the following conclusion can be drawn [120]:

$$d = k. \int \frac{dp}{dt} \times \frac{di_L}{sdt}\, dt \tag{36}$$

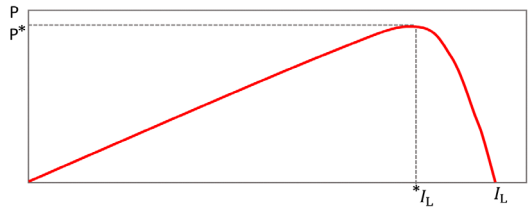

Figure 5-5 PV array average current and power [C1].

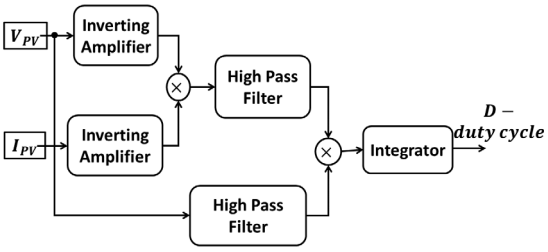

Figure: 5-6 RCC block diagram [C1].

where d and k are the duty cycle and the constant (+ve gain) respectively. depending on the duty cycle d, the inductor current decreases and increases, allowing the appropriate d to be adjusted for the achievement of *IL*.

5.4. SIMULATION RESULTS AND DISCUSSION

5.4.1. DYNAMIC RESPONSE OF PV AND MPPT CONTROL: SCENARIO 1

In this case, sequence irradiance perturbations and temperature levels are taken into consideration when examining the suggested techniques, as can be seen in Fig. 5-7. The initial standard irradiance at the beginning was considered 1367 W/m2; however, after 1.2 seconds a sudden decrease occurred and the irradiance level falls to 1200 W/m2, before increasing once again to 1300 W/m2 level at 2.45 seconds. Therefore, the MPP also suddenly changes according to the irradiance level change, and the extracted PV power is adjusted accordingly with the operating voltage and current.

It can be seen from the voltages and currents demonstrated in Fig. 5-8, and 5-9 that, all three offered MPPT strategies track the change according to the irradiance levels.

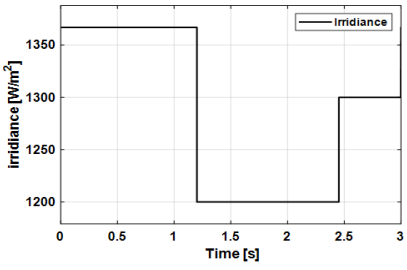

Figure: 5-7 Change in different irradiance levels [C1].

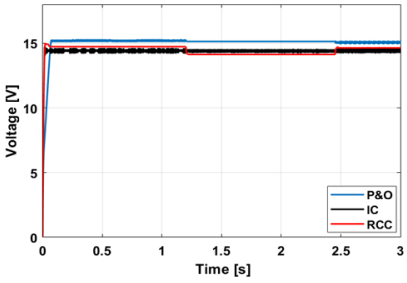

Figure: 5-8 Comparison of output Voltages [C1].

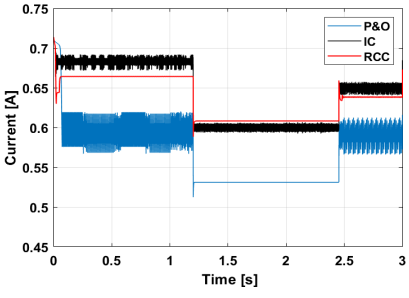

Figure: 5-9 Comparison of output currents [C1].

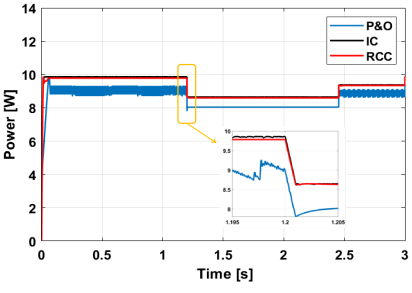

Figure: 5-10 Comparison of output powers [C1].

In Fig. 5-10 power tracking levels of all three techniques are demonstrated, however, the performance of each MPPT technique varies from one another. In comparison to the RCC, which offers greater and smoother power, and the IC, which delivers an even higher power but with some oscillation, P&O has poorer performance attained, and less power has been taken from the PV. Additionally, as demonstrated in Fig. 5-10, the RCC and IC responses stabilize more quickly (faster convergence rate) throughout the time of radiation fluctuations. The changes in power and voltage for all irradiance variations are shown in Table 5-3. The final finding approves that the RCC has a higher convergence rate than the traditional P&O and IC approaches.

5.4.2. DYNAMIC RESPONSE OF PV AND MPPT CONTROL: SCENARIO 2

In the second case, the suggested methods are tested for a 3U CubeSat spinning at 4 rpm in a Sun-pointing orientation. While the spacecraft rotates in its axis, the irradiance level varies on the faces of the satellite simultaneously. Fig. 5-11 displays the combined average extracted irradiance from the X-, X+, Y-, and Y+ faces of the

TABLE 5-3: THE CHANGES IN POWER AND VOLTAGE OF P&O, IC AND RCC IN VARIOUS IRRADIANCE LEVELS [C1].

Irradiance level (w/m2)	Switching time (s)	Method	Power (W)	Voltage (V)	Current (A)
1367	At the beginning t= 0 s	P&O	9.1	15.2	0.6
		IC	9.87	14.5	0.683
		RCC	9.78	14.75	0.664
1200	t = 1.2 s	P&O	8.04	15.14	0.53
		IC	8.64	14.4	0.6
		RCC	8.61	14.13	0.608
1300	t= 2.45 s	P&O	8.9	15.1	0.59
		IC	9.38	14.64	0.65
		RCC	9.35	14.44	0.64

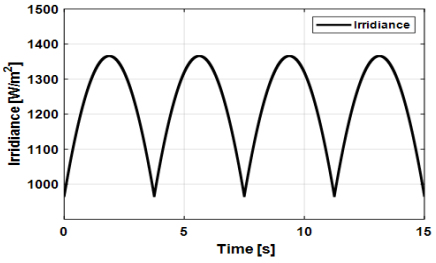

Fig: 5-11 Combined average extracted irradiance from X-, X+, Y-, and Y+ faces of the satellite in each spin [C1].

satellite in each spin. The initial average irradiance when the satellite starts moving was 1000 W/m2, however, in the spinning condition, once the satellite moved after 2.15 sec, the Y-side was entirely on the standard irradiance of 1367 W/m2. After the satellite, Y-side faced the standard irradiance and moved to its axis the irradiance level subsequently reduced once more after t=4.25 sec to 1000 W/m^2.

The X+, Y+, and X- faces exhibit a similar pattern of behavior in each spin. Therefore, the MPP changes in a similar pattern, and due to variations in the operating voltage and current, the output power extracted from the solar PV arrays also is modified. This change in voltage, current, and extracted power can be seen in Fig. 5-12 (a), (b), and (c) simultaneously. In addition, it can be noticed in Fig. 5-12 (c), that all the examined MPPT techniques track the variations of the power, but the effectiveness of each tracking methodology varies from each other. Compared to the other two approaches, the P&O extracts less power while oscillating more frequently. In contrast to RCC and P&O, the IC method extracts greater power. While the RCC is smoother and offers fewer oscillations as compared to the IC method. Additionally, in the event of radiation fluctuations, IC and RCC reactions stabilize more quickly (greater convergence rate) than the P&O. The result confirms that RCC and IC have a higher

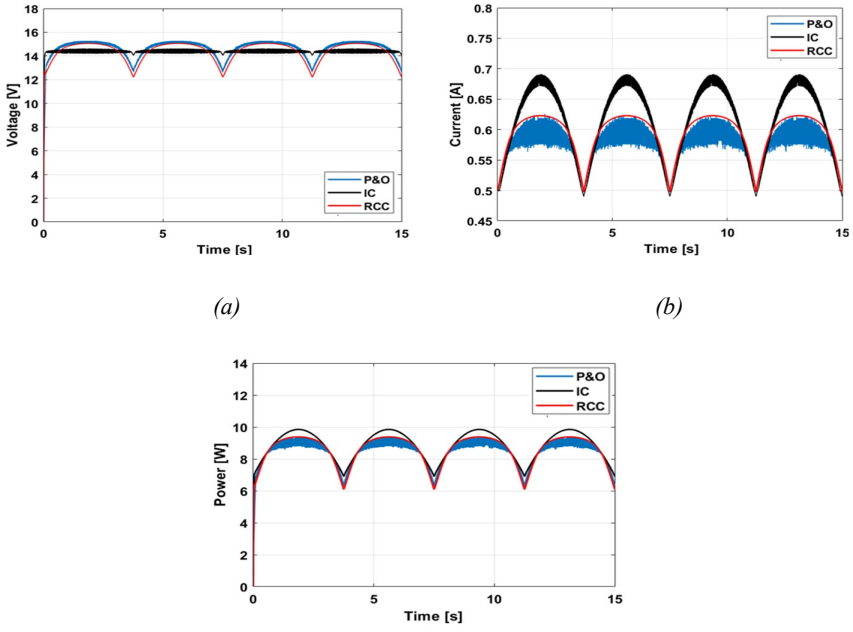

Figure: 5-12 Comparison of outputs from the PV extracted, (a) voltage, (b) current, and (c) power under P&O, IC and RCC at NanoSat spin of 360^0 in 15 sec [C1].

convergence rate than the traditional P&O approach, hence, the superiority of RCC and IC is approved compared to the P&O for SmallSat applications.

5.5. SUMMARY

In this chapter, important MPPT techniques like P&O, IC and RCC have been implemented for SmallSat applications under the Sun-pointing orientation scenario where the satellite is spinning in its axis with rpm. Two different scenarios have been taken for analysis, where in the first case the examination has been done under the effect of temperature and irradiance sequence perturbations considering only the Sun-pointing position. In the second scenario, the analysis has been done considering the same MPPT techniques while the satellite is in the spin of 4 rpm, where the irradiance varies according to the satellite spin. In both cases, P&O is not more efficient than the IC and RCC. ICC power level is higher as compared to the RCC but with high oscillations, however, the RCC has low oscillations and is smoother than the IC technique. Hence, RCC is an optimal MPPT solution for SmallSat applications.

CHAPTER 6. POWER MANAGEMENT AND CONTROL OF SMALL SATELLITE MICROGRID

In this chapter, a novel adaptive control algorithm for battery and load management has been introduced to achieve coordinated and efficient resource utilization in SmallSat applications. The adaptive control algorithm is in charge of battery voltage regulation and the control coordination to shift MPPT mode to load current control for PV power curtailment purposes.

6.1. INTRODUCTION

The primary energy source of a SmallSat during the illumination period is solar photovoltaic (PV) panels and the access energy is used to charge the batteries. The stored energy is utilized, when the satellite is operating under heavy strain and when solar irradiance is often unavailable at the eclipse. Based on the incident payloads and operational requirements of the CubeSat, the load profiles generally vary from satellite to satellite [121]. While any failure of the EPS might leads to a total loss of the satellite which potentially results in the mission failure. Therefore, for the lifespan and success of CubeSat missions, the crucial aspects are the availability, controllability, and reliability of EPS. Due to improper coordination between the satellite's many parts several space missions have failed, such as the power control units, solar array, and batteries. The primary causes are power system malfunctions, inadequate power bus connections with solar panels and/or batteries, voltage fluctuations, overcurrent protection deficiencies and a lack of generated power for transmitter operation, and degradation of the battery [122]. With the use of strong management techniques and carefully managed coordination between the EPS components, EPS failure can be largely prevented. To counter the EPS potential malfunctions, microgrid technologies have recently demonstrated their promise as a contender option for electric power generation, nearby secure and reliable delivery [123]. This new idea in terrestrial applications like the remote region where grid structure is unavailable, electrification and telecommunication operations, and the microgrids which are islanded have successfully provided power system solutions [124]. Researchers and practitioners working with space power systems have been pushed to think about their EPS functioning as a microgrid operating in the islanded mode because of the successful islanded microgrids demonstration due to their increased dependability, robustness, and controllability.

To prove their suitability for CubeSat EPS operation, this study work draws inspiration from methodologies developed for the control and management of

microgrids. Mashood et al. [125], developed a microgrid architecture that is solar PV-based and made up of a collection of several microgrids with the ability to coordinate their interactions with one another. Since the individual microgrid design shown in [125], is essentially what the EPS of the CubeSat is like, the control algorithms can be successfully repeated as long as the environmental factors are taken into account for the applications of the satellite.

In support of this claim, in this work, the coordination of the CubeSat microgrid has been considered among the PV-generated power, loads, and battery storage. Since overcharging leads to degradation of life and SOH of the battery [126], hence, the recommended controller switches from MPPT to voltage control mode at the battery voltage level with its reference of SOC, and battery overcharging is prevented. This will cause a suboptimal curtailment of the solar resources that are currently available and battery discharging, resulting in PV power generation that is lower than load requirements. Alternately, this work has presented a control method that can switch between load power curtailment mode and solar PV generation between MPPT. The suggested controller will smoothly switch from MPPT to load the mode of current control, which decreases the incident output of the PV to the load requirements locally while maintaining a steady level of battery SOC. As a result, the proposed energy management and control system has the potential to curtailment per the requirements between MPPT and the loads. Therefore, from excessive overcharging the battery life is conserved.

6.2. CUBESAT MICROGRID ARCHITECTURE FOR CASE STUDY

The primary power source in SmallSat microgrid is the solar panel. Typically, solar cells are arranged in pairs on all six sides of the CubeSat so that at least three of its sides are always exposed to light during every movement other than the interval of

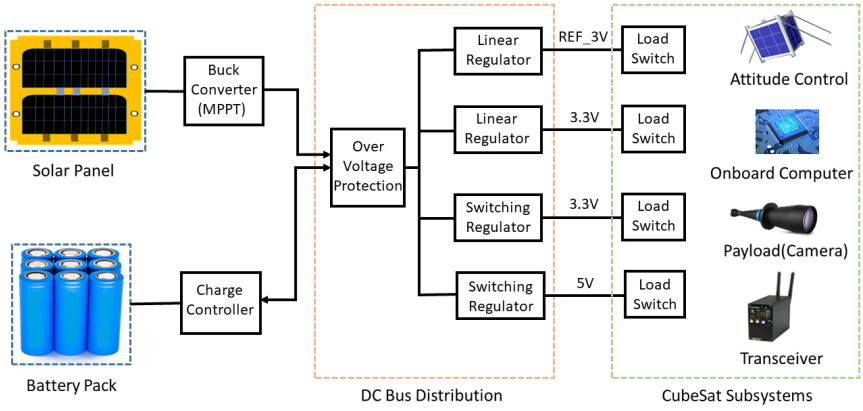

Figure: 6-1 A simple architecture of the CubeSat microgrid [C2].

the eclipse [127]. For CubeSat microgrid analysis, we have lumped in the shape of a compact solar panel several solar cells. The general architecture of the CubeSat microgrid has been depicted in Fig. 6-1, where the solar panel is the illustration of the lumped PV panel. The solar panel is interfaced with a DC-DC converter, which is in charge to extract the maximum power out of the incident light and charging the batteries. Depending on the selection of PV module characteristics, battery, bus voltage levels, and the DC-DC converter the buck, buck-boost, or a simple boost converter is applied. The battery storage system is provided by a Li-ion battery, which also controls the DC bus voltage. By applying the DC-DC converters to the DC bus, subsystems including payloads are integrated as shown in Fig. 6-1. The load profiles for the CubeSat system are typically dynamic and range from limited mode operation to the operation of full load. For mission operation the high-power system might be turned on at times, putting the CubeSat under full load. Occasionally, parts of the loads are turned off, and CubeSat operates in a mode with limited functionality. Likewise, some critical loads like the receiver and onboard computer need to be powered continuously. There has been a detailed discussion with load profiles about various mission modes in [2]. Although different loads may require different voltages and require DC-DC converters to operate. In the scope of this present study, the lumped load on the DC bus is only considered but actual details of the point of load (POL) converters have not been taken into consideration for analysis. In actual cases, the DC bus voltage compared to the battery voltage may be either greater or lower; But, in this case, the DC bus voltage is maintained typically at the battery voltage level to reduce further converter requirements. depending on the incident irradiance, the battery is charged by the solar power PS or either meets the load demand PL. Since there is no longer any incident irradiance when the CubeSat enters the eclipse the load demands are met by the battery discharge. An ideal energy balance in a time interval Δt is given by (34), where the resistive losses and the battery charge/discharge efficiency are neglected.

$$p_s \Delta t = p_L \Delta t + \int_0^T V_B \, (I_S - I_L) dt \tag{37}$$

Here, the bus or battery voltage is VB, at which CubeSat loads IL is connected and which is the lumped load also. The generated solar current is IS which is managed by the DC-DC buck converter. The control algorithm with its mode of operations is used to determine the battery state of charge (SOC) and switch between MPPT and current control mode. This strategy of MPPT to the current control mode will be taken into consideration by this energy balance. According to the battery's initial SOC_i and ampere-hour (Ah) capacity, the overall change in battery SOC is represented by (35).

$$SOC = SOC_i + \frac{1}{C} \int_0^T (I_S - I_L) dt \tag{38}$$

A control algorithm based on SOC for optimal PV power extraction is designed for solar power conditions and scenarios of load demands. The following section goes over the control algorithm and the energy management system.

6.3. CONTROL AND MANAGEMENT SYSTEM DESIGN

As the case study the specifications are considered as from [127], where for interfacing the solar panels and batteries a buck DC-DC converter is required because voltages at their maximum power points VMP of the PV panel is greater than the battery voltage VB on the DC bus. The CubeSat microgrid under-considered power architecture is shown in Fig. 6-2. The battery SOC may take different values, based on the varying profile of generated solar power and the requirements of the load. The MPPT control will take over the duty of extracting the most power possible from the incident solar energy during the Sun illumination period. The battery's SOC will tend to increase if during this time the load demand is not too large; as a result, to reduce the risk and possibility of overcharging a maximum SOCmax threshold is defined. Similar to this, when no solar power is available during the eclipse, a mechanism is set to shut down non-critical loads; as a result, to prevent deep discharge of the battery an SOC_{min} a lower threshold is also set. The controller, which supervises the SOC functioning in either the current control or MPPT mode, via an internal communication link receives the information from the SOC. As depicted in Fig. 6-2 the power electronics interface circuit supports both modes of operation, and future discussion is conducted in accordance with this.

In PV power systems, the MPPT algorithms are employed to draw the greatest amount of power possible from the incident solar irradiance. In the maximum power transfer method to match the loads, a DC-DC switch-mode converter is connected in series with the solar array to dynamically regulate the output impedance of the array. Hence, the solar array operating current or voltage in MPPT approaches can either manipulate to drive it to its operational point by regulating the switching converter operation between the load and PV. Several parameters affect the location of MPP like the type

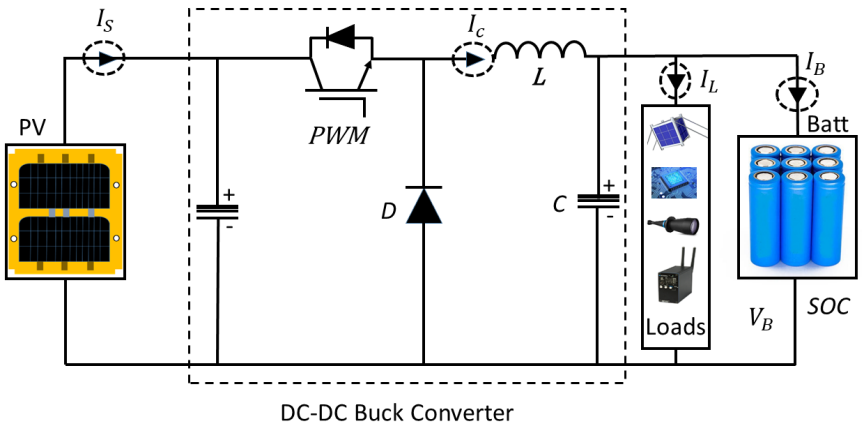

Figure: 6-2 The power electronic interface of CubeSat Microgrid under consideration [C2].

of cell being used, the temperature, the total amount of solar irradiation reaching the surface, and the position of the solar cell to the Sun [128]. As for the CubeSat solar panel placements, three power points at once can be tracked at the satellite, three different MPPT converters are installed within the CubeSat to accommodate the solar panels mounted on six sides. Each solar panel is parallelly connected to its opposite side panel and the same DC-DC converter. In this case, a single MPPT tracker has been utilized since the solar cells in the form of modules have been lumped out. Different MPPT algorithms are discussed and reviewed in [127], which states that the most frequently employed MPPT algorithms are O&O, the hill-climbing method, and the method of incremental conductance (IC).

For photovoltaic systems, global MPPT of numerous sophisticated and complex methods in addition to the simpler ones under rapidly changing atmospheric conditions are also proposed as the corresponding irradiance and temperatures [129]. In this work, the P&O algorithm has been used because of its simplified implementation, inherent simplicity, and the least computational complexity. In Fig. 6-3, a detailed and comprehensive flowchart of the P&O technique is depicted. Whenever the operating voltage of the solar array VS is perturbed in a particular direction the drawn power PS of the solar module increases. Then it will appear that the operating point in the direction of MPP has switched, since as a consequence, in the same direction the operating voltage must also be perturbed. Or else, if the drawn power of PV falls, there is a shift in the driving point from MPP, and therefore, in the operating voltage perturbation's direction, a change is necessities. Based upon the incident irradiance and the loading profile between the input and output the net influx of power difference either SOC tends to decrease or increase as determined in Eq.

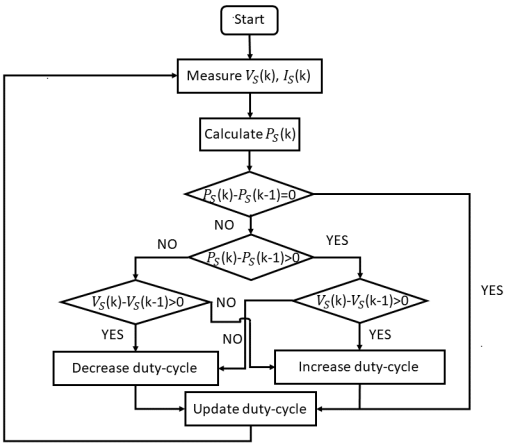

Figure: 6-3 MPPT flowchart using P&O technique [C2].

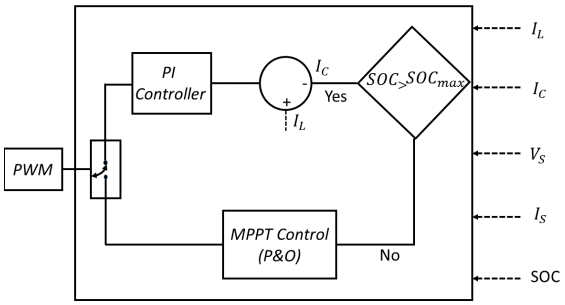

Figure: 6-4 Control mode switching scheme for SOC [C2].

(35). If the battery's SOC is not limited, it could overcharge, which would then cause gasification and cause a rapid decline and degradation in battery life. Thus, the battery switches its mode from MPPT mode to the current-controlled mode upon approaching the maximum level of SOC_{max}. The load variation information is communicated through the link of internal communication that is devoted to SOC-related information. The buck converter generates a duty cycle following Eq. (36), to shift its mode to the current control mode, as shown in Fig. 6-4.

$$d = k_p(I_L - I_C) + k_i \int_0^T (I_L - I_C)\, dt \tag{39}$$

Where the converter duty cycle is d and the current extracted by the converter IC with its associated PWM from the solar PV accurately match-up the incident load requirements IL. The proportional and integrational control constants on which the PI controller is tuned are kp and ki.

It is important to note that the battery will be able to regulate the DC bus voltage since is already getting close to its maximum state of charge, with power curtailment that is exactly equivalent to the load conditions leaving solar power just to supply the load. Given that the load requirements are now being met in full by solar PV power, under (35), the net energy will be zero which is entering the battery, and during this operation mode, the net change will also be zero in battery SOC. For the time being, the maximum utilizable power the control scheme will optimally extract from solar PV, the battery life will not get impacted, therefore.

6.4. SIMULATION RESULTS AND DISCUSSION

6.4.1. UNDER STUDY CASE 1

The specifications take into consideration for the proposed control and EMS validation intended for low earth orbit are from ESTCube-1. additionally, incident

TABLE 6-1: PARAMETERS OF SIMULATED CASE STUDY [C2].

Parameters	Values
Solar Module Lumped Power	10Wp@1000W/ m^2
Voltage at Maximum Power V_{MP}	9 V
Power Current at Maximum I_{MP}	1.1 A
Capacity of Battery C	2200 mAh
Voltage of Battery V_B	8V
Power at full-load P_L	13.4 W
Load Limited Functionality P_L	6.7 W
SOC_{max}	80%
SOC_{min}	40%
Low Earth Orbit Incident Solar in Irradiance	1300 W/m^2
Constants for Control *kp, ki*	0.2, 13
Inductance of Buck Converter L	1.3 mH

irradiance values during the flight are gathered from [127], for varying load profiles of different subsystems. For the sake of simplification, the specific simulation parameters for the case study are listed and grouped in Table 6-1. The incident irradiance conditions and the simulation results for various load scenarios are displayed in Fig. 6-5. In low earth orbit, the incident irradiance during eclipse and light mode is shown in Fig. 6-5 (a). The satellite continues in sunlight from t = 0 up to t = 0.4 sec, and remains at the eclipse period starting from t = 0.4 up till 0.5 sec. A 10Wp peak panel generates substantially more power in space than on the earth's surface because incident irradiance there is (1367 W/m2), rather than (1000 W/m2), higher due to the lower air mass. For the satellite, the time-varying lumped load profile in Fig. 6-5 (b), has corresponded. Where the satellite is operating in Full-load mode from t = 0 to 0.2 sec. In this state, all the subsystems are functional including the payloads. While it can be seen in the load profile figure, that the satellite shifts from full load operating condition at t = 0.2 to 0.5-sec limited functionality mode. In this condition, the critical subsystems are ON only.

The solar energy extracted by the buck converter is shown in Fig. 6-5 (c). At the beginning of the simulation, it is apparent that to harvest the maximum amount of energy from the incident solar light the MPPT mode of the buck converter is functioning, since the CubeSat is at full load and there is a high PV irradiance

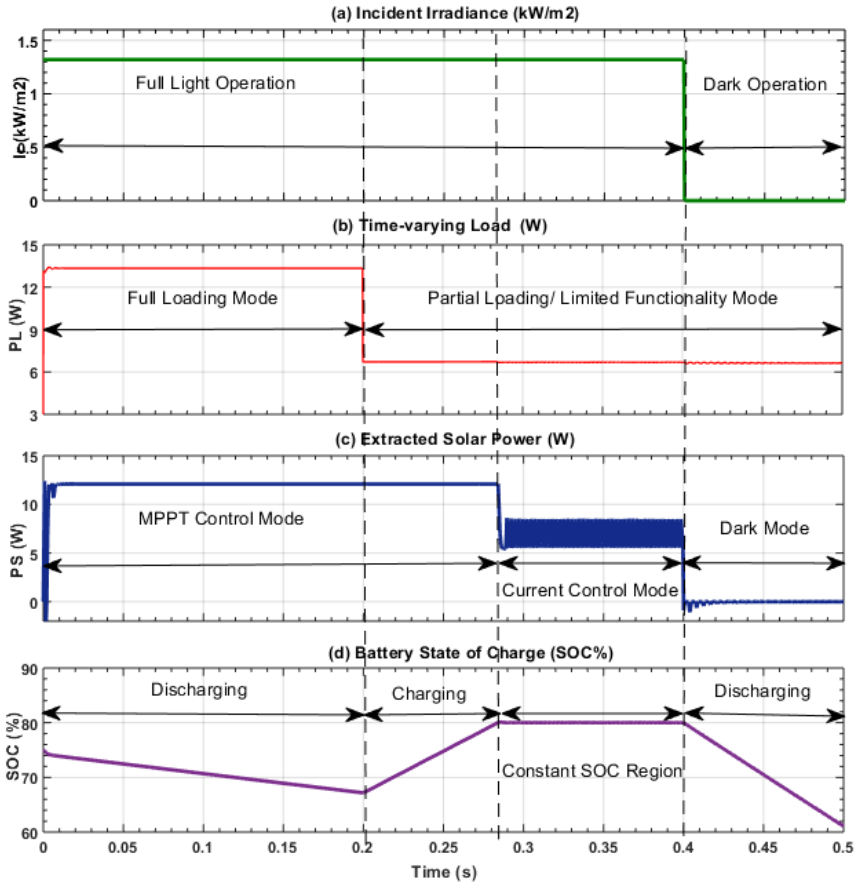

Figure: 6-5 Simulation results, (a) low earth orbit profile of incident irradiance, (b) profile of time-varying loads, (c) profile for extraction of solar power (d) profile under varying solar and loads for battery SOC [C2].

available. Although the maximum amount of power is extracted, it is still insufficient to meet the load requirement using solely solar power; as a result, to the net load power demand the battery also contributes, because of which, can be seen in Fig 6-5 (d), that at the beginning of the simulation SOC starts decreasing. The CubeSat switches at t = 0.2 sec, to reduced functionality mode from full load operation. Since the converter is already in MPPT mode and there is irradiance, to extract the maximum amount of power it will continue, using some of it to charge the batteries and the rest to meet load requirements. At this period the battery's SOC rises under these circumstances until it hits SOCmax, which can be seen in Fig. 6-5 (d). At SOCmax condition, despite the entire irradiance being available, the solar converter switches as the battery get close to SOCmax from MPPT to the mode of current control, limiting its output under

incident load needs. In the current control mode, at t = 0.28 sec the average power exactly matches the load requirements taken from the sun and continues through t = 0.4 sec, as can be seen in Fig. 6-5 (c). Consequently, curtailment is accomplished through the current control strategy. In Fig. 6-5 (d) this is also visible, the battery SOC stays set at 80% during this time frame and does not change when in the current control mode, the solar converter is working. As a result by applying the management algorithm, curtailment of optimal power has been achieved. When CubeSat reaches the eclipse at t = 0.4 and 0.5 seconds, there is no irradiance. Based on battery energy availability, the battery then starts delivering power to the loads, as the solar power is dropping to zero. Thus, from the results, it can be observed that the suggested control strategy permits the optimal power extraction of solar PV in the energy management system.

6.4.2. UNDER STUDY CASE 2

To validate the control and power management system the specifications considered are taken from Chapter 4 of this thesis "Design Verification of a Full-scale Small Satellite Microgrid". The considered case study is a 3U-CubeSat at a low-earth orbit of 700 km with a mission duration of 5 years. The simulation of a full orbit has been carried out in six operation modes according to different load conditions following the simulation model of the satellite illustrated in Fig. 4-1. The operation modes are given with their average duty cycles in Table 4-7. The analysis has been carried out on the basis of SOC_{max} and SOC_{min} defined as the upper and lower limits of the battery SOC.

In Fig. 4-9 it is demonstrated that the payload ON/OFF periods considered for the design verification are normal loads and the battery SOC value varies from 70 to 78% in the peak load conditions. Therefore, in the case of validation of the controlled power management system, the upper and lower limits for the battery SOC have been set at 90 and 87.5% respectively to constrain the SOC limits and note the effectiveness of the power management system. The simulation results for controlled power management system effectiveness in different satellite modes of operations are discussed below.

The simulation result of PV and load power for various operation modes in incident irradiance and eclipse conditions are displayed in Fig. 6-6. It can be seen in Fig. 6-6 that the satellite is in Sun illumination for 62.7 minutes and 36.3 minutes during the eclipse. At the illumination period time t = 0 to 900 sec some critical loads are only connected it can be seen in Fig. 6-7 that the battery SOC is increasing and at t = 700 sec the battery SOC reaches 90% which is the maximum SOC limit defined. It can be noticed in Fig. 6-6 that, at t = 700 sec the control and power management system curtail the PV power for 50 seconds. Based on the SOC limits the PV power operates at MPPT and PV power curtailment modes until at t = 900 sec when another operation

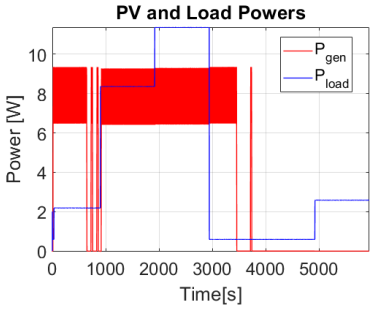

Figure: 6-6 PV and load powers at power management condition [C1].

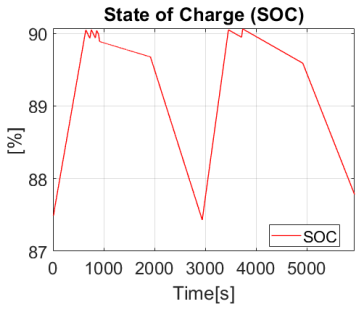

Figure: 6-7 Battery SOC at various load conditions and at control management [C1].

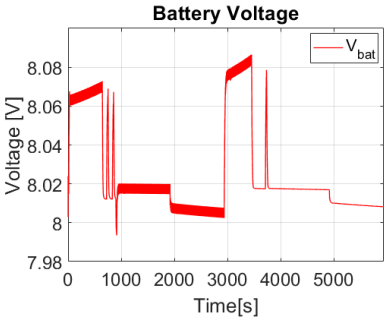

Figure: 6-8 Battery voltage in loads and controlled management situations [C1].

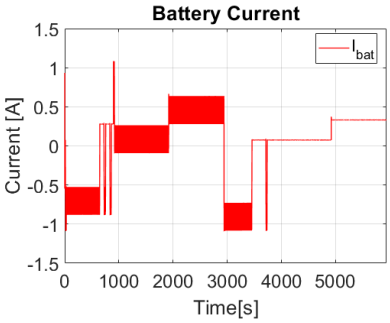

Figure: 6-9 Battery voltage in Loads and controlled management situations [C1].

mode starts, and the load power is nearly the PV generated power level. In the second operation mode at t = 900 – 1920 sec, it can be noticed in Fig. 6-7, that the battery SOC is slowly declining to compensate for the power demand exceeded by the generated PV power. At the third operation mode when t = 1920 – 2970 sec, the satellite is at peak load condition while PV and storage system both are fulfilling the load requirements which can be noticed in Fig. 6-6 and battery SOC in Fig. 6-7. In the third operation mode, it can be noticed in Fig. 6-7 that the battery discharges up to the lower limit of 87.5% SOC level at t = 2970 sec, and the non-critical satellite loads are disconnected by the control and management system. At the fourth operation mode at t = 2970 – 3960 sec only the critical nature of loads is connected, and the battery SOC starts increasing until it reaches again in maximum SOC limits at 3500 sec. At maximum SOC limits again the effective can be noticed in Fig. 6-7. In the fifth and sixth operations modes, only some low power loads are connected, and the satellite is in eclipse conditions. The battery current and voltage can be observed in Fig. 6-8 and 6-9 for various loads and control management conditions. Fig. 6-10 shows the two voltage buses of 5 and 3.6 voltage levels which are regulated at the required load

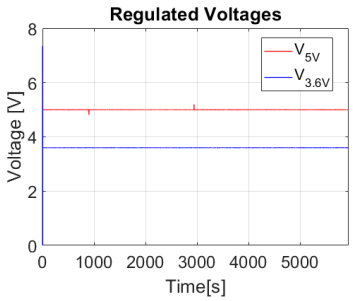

Figure: 6-10 The 5 and 3.6 regulated Voltage buses [C1].

levels of the satellite voltage-sensitive loads. The outputs that come from Fig. 6-8 and 6-9 prove that the controlled power management system is working accordingly to the variations of the loads and PV power generation. The battery SOC limits are completely followed by the controlled management system.

6.5. SUMMARY

An adaptive control algorithm has been presented in this chapter for SmallSat microgrid applications to extract optimal power from the PV and properly manage the battery from overcharging and over-discharging. The proposed control and management system is capable of optimal battery charging by which the battery life enhancement is achieved. The analysis in two case scenarios with and without considering the Point of Load (POL) converters shows through the results that the power conversion converter switches to the MPPT mode and PV power curtailment modes based on the SOC threshold. The battery SOC remains nearly at a constant level when the PV power is curtailed irrespective of the incident irradiance and the non-critical loads are disconnected soon after the battery SOC reaches a minimum threshold. The proposed power management and control systems hold the capability to extract maximum power under load demands and curtail the power when the battery is at maximum SOC level. Moreover, disconnects the non-critical loads soon after the battery reaches the minimum battery SOC threshold. The MPPT, PV power curtailment, and non-critical load disconnection operations are performed by the incident load conditions to avoid over and under-charging of the satellite battery which enhances the satellite's overall life span.

CHAPTER 7. CONCLUSIONS AND FUTURE WORK

The overall Ph.D. project contributions and future perspectives are presented in this section.

7.1. CONCLUSIONS

The curiosity of humans from the beginning has been to explore planets beyond the reach of humans and too deep into space for the exploration of space resources. In this regard, many steps have been taken and among them, the small satellites industry has seen a huge surge in the number of missions recently. The particular class CubeSat in this category is booming with several launches due to its specific shape and cost. The CubeSat consists of some subsystems among which The EPS is the most crucial one. Many missions have failed due to a lack of tested and state-of-the-art designs, components, and control and coordination among the satellite EPS components. Therefore, this Ph.D. research project is based on the investigation and analysis of the design, development, and coordination between the RES and ESS technologies for a reliable and efficient SmallSat microgrid.

This thesis first presents a general introduction and background of SmallSat and Its importance for the exploration of space resources. In addition to that, an overview of EPS, the EPS main challenges, and some potential solutions including recent research and advancements have been discussed. Considering the main challenges is SmallSat design due to low power, simple EPS architecture, and satellite-constrained size the next part of this dissertation, investigates the overall system configuration and control systems holistically, including orbital parameter, satellite orientations, power conversion and distribution architectures of SmallSat. The system architectures, onboard functional blocks, and some of the important topologies i.e., non-isolated, and isolated, converter topologies have been reviewed in the second part. The discussion of cutting-edge solar power generating technologies and the solar cells suitable for SmallSat applications has been carried out, including the 3-J solar cell circuit standard design layers. In addition to that, different battery technology characterization and state-of-the-art battery technologies are reviewed for SmallSat applications.

The third section of this work presents a generalized and full-scale EPS design of COTS components, which considers modeling the distinctive features and examining the power supply and demand of the satellite. The proposed design considers EPS architecture and design requirements, load profile, operating modes, and altitude. Additionally, the main components of this EPS like the PV module, the battery

storage, and several switching converters and regulators are considered. This design also suggests the control technique for power management to monitor the maximum PV power point (MPP) and battery state of charge (SOC) limits. The main components of this EPS system are the PV module, the battery storage, and several switching converters and regulators. The design has been verified for different load and environment conditions, which shows promising results in realistic space weather conditions. In line with this design and the design verification, some important MPPT techniques have been investigated in the next section among P&O, IC, and RCC to verify the optimal power extraction strategy for SmallSat applications in space volatile environments and satellite specific orientations. In the case of sequence perturbations of irradiance and changing temperature condition the MPP also get changed. In this condition all the under-test MPPT method work but differently. The P&O is performing lower with less power extraction compared to ICC and RCC. RCC and IC respond faster, however, IC provides an oscillated power compared to RCC. The same MPPT strategies in a 4-rpm spin for a 3 U CubeSat application under changing irradiance levels perform similarly discussed sequence perturbations of irradiance conditions. Hence RCC technique is the optimal MPPT strategy for SmallSat applications under volatile space and satellite operating conditions.

Finally, a novel robust power management strategy for coordination has been presented in this thesis. The coordinated control has been implemented including generation, battery energy storage, and loads to avoid battery overcharging and to overcome SOH issues. The proposed controller shifts the MPPT voltage level to the regulated voltage level of the battery. In addition to that, when the battery reaches maximum SOC level, the solar PV generation is switched by the control mechanism from MPPT mode to power curtailment mode. The results verify the effectiveness of the proposed approaches.

7.2. FUTURE WORK

During the period of the development of this thesis, many research gaps require further research in relation to SmallSat EPS design, development, and operations under harsh space conditions. Potential future works are listed as follows:

1. Identification of optimized and state-of-the-art technologies for SmallSat applications. The SmallSat mostly consists of COTS components which lack the configuration requirements for EPS designs due to mission individual constraints of power generation, mass, and volume. The selection of up-to-date multi-junction PV and battery storage technologies must be analyzed and tested for space temperature and irradiance environment.

2. EPS design for several satellite orientation scenarios, maximum load conditions, and change in session factors. In the existing designs and design verifications, there is a lack of consideration of all satellite possible orbital parameters, orientations, and

variations of irradiance and temperatures according to the sessions of the year. The validation of the designs for various load conditions and different orientations, considering real orbital conditions for all sessions should be carried out.

3. Experimental test. Experimental setups and CubeSats should be built for implementation and validation of the abovementioned aspects in a laboratory environment.

LITERATURE LIST

Bibliography

[1] A. Lashab, M. Yaqoob, Y. Terriche, J.C. Vasquez and J.M. Guerrero, "Space microgrids: New concepts on electric power systems for satellites," *IEEE Electrification Magazine,* vol. 8, no. 4, pp. 8-19 2020.

[2] M. Yaqoob, A. Lashab, J. Vasquez, J.M. Guerrero, M. Orchard and A. Bintoudi, "A comprehensive review on small satellite microgrids," *IEEE Transactions on Power Electronics* vol. 37, no. 10, pp. 12741-12762, Oct. 2022.

[3] A. Bermudez-Garcia, P. Voarino and O. Raccurt, "Environments, needs and opportunities for future space photovoltaic power generation: A review," *Appl.Energy*, vol. 290, pp. 116757 2021.

[4] J.M. Logsdon. (July 15, .). *"space exploration." Encyclopedia Britannica,* [Online]. available: https://www.britannica.com/science/space-exploration.

[5] E. Kulu, "Nanosats database," *URL: https://www.nanosats.eu/cubesat* 2019.

[6] A. Mann, "Starlink: SpaceX's satellite internet project," *Space.com, updated May*, vol. 28 2021.

[7] J.R. Kopacz, R. Herschitz and J. Roney, "Small satellites an overview and assessment," *Acta Astronaut.* 2020.

[8] Anonymous (June 28,). *Small Satellite Missions* [Online]. available: https://www.nasa.gov/directorates/heo/home/CubeSats_initiative.

[9] Anonymous *Planet Labs, Planet spacecraft operations and ground control Accessed date: 2 June 2017* [Online]. available: https:// www.planet.com/docs/spec-sheets/spacecraft-ops/.

[10] B. Cotten, I. Bennett and R.E. Zee, "On-orbit results from the CanX-7 drag sail deorbit mission," in *Proceedings of the AIAA/USU Conference on Small Satellites, Year in Review*, 2017.

[11] Anonymous *Space Flight 101, AAUSAT 4, Space Flight 101,* [Online]. available: http://spaceflight101.com/ spacecraft/aausat-4.

[12] S. Gao, Y. Rahmat-Samii, R.E. Hodges and X. Yang, "Advanced antennas for small satellites," *Proc IEEE*, vol. 106, no. 3, pp. 391-403 2018.

[13] M. Chan, J. Bultitude, D. Faber, D. Hawes and O. Fab, "Productization of CubeSat rendezvous and docking solutions," *In Proceedings of the AIAA/USU Conference on Small Satellites*, Utah State University, Logan, UT. 2019.

[14] T. Wekerle, J.B. Pessoa Filho, L.E.V.L.d. Costa and L.G. Trabasso, "Status and trends of smallsats and their launch vehicles—An up-to-date review," *Journal of Aerospace Technology and Management*, vol. 9, no. 3, pp. 269-286 2017.

[15] T. Pultarova and C. Henry, "OneWeb weighing 2,000 more satellites," *SpaceNews.com.SpaceNews*, vol. 24 2017.

[16] C. Poly, "CubeSat design specification (CDS) rev 13," *Cal Poly SLO* 2015.

[17] C.E. Gonzalez, C.J. Rojas, A. Bergel and M.A. Diaz, "An architecture-tracking approach to evaluate a modular and extensible flight software for CubeSat nanosatellites," *IEEE Access*, vol. 7, pp. 126409-126429 2019.

[18] P. Bugryniec, "Cubesat: The need for more power to realise telecommunications," *final report of mini project, University of Sheffield* 2016.

[19] P.B. De Selding, "Google-backed global broadband venture secures spectrum for satellite network," *Spacenews, May*, vol. 30, pp. 2014 2014.

[20] J. Brodkin, "With latency as low as 25ms, SpaceX to launch broadband satellites in 2019," *Ars Technica, May* 2017.
[21] A. Poghosyan and A. Golkar, "CubeSat evolution: Analyzing CubeSat capabilities for conducting science missions," *Prog.Aerospace Sci.*, vol. 88, pp. 59-83 2017.
[22] L. Alminde, J. Christiansen, K. Kaas Laursen, A. Midtgaard, M. Bisgard, M. Jensen, B. Gosvig, A. Birklykke, P. Koch and Y. Le Moullec, "Gomx-1: A nano-satellite mission to demonstrate improved situational awareness for air traffic control," *In 26th Annual AIAA/USU Conference on Small Satellites,* 2012.
[23] M. Langer and J. Bouwmeester, "Reliability of cubesats-statistical data, developers' beliefs and the way forward," *In Proceedings of the 30th Annual AIAA/USU Conference on Small Satellites,* Logan, UT, USA, 6–11 August 2016.
[24] S.Y. Kim, J. Castet and J.H. Saleh, "Spacecraft electrical power subsystem: Failure behavior, reliability, and multi-state failure analyses," *Reliab.Eng.Syst.Saf.*, vol. 98, no. 1, pp. 55-65 2012.
[25] T.L. Vandoorn, J.C. Vasquez, J. De Kooning, J.M. Guerrero and L. Vandevelde, "Microgrids: Hierarchical control and an overview of the control and reserve management strategies," *IEEE industrial electronics magazine*, vol. 7, no. 4, pp. 42-55 2013.
[26] C. Marnay, S. Chatzivasileiadis, C. Abbey, R. Iravani, G. Joos, P. Lombardi, P. Mancarella and J. von Appen, "Microgrid evolution roadmap," in *2015 international symposium on smart electric distribution systems and technologies (EDST)*, 2015, pp. 139-144.
[27] D. Homan and Q. Young, "The challenges of developing an operational nanosatellite," *22nd Annual AIAA/USU Conference on Small Satellites,* North Logan, Utah 2008.
[28] Small Spacecraft Systems Virtual Institute. (October). *State-of-the-Art Small Spacecraft Technology* [Online]. available: https://ntrs.nasa.gov/api/citations/20210021263/downloads/2021_SOA_final_508_updated.pdf.
[29] E. ESA, "Tailored ecss engineering standards for in-orbit demonstration cubesat projects," *ESA, ESTEC: Noordwijk, The Netherlands* 2016.
[30] NASA Education. *Understanding Space Radiation* [Online]. available: https://go.nasa.gov/2A474ER.
[31] Scott Thornton. *Tin whiskers: What happens when they spontaneously erupt?* [Online]. available: https://www.microcontrollertips.com/when-tin-whiskers-spontaneously-erupt-faq/.
[32] C. Leonard, "Challenges for electronic circuits in space applications," *Analog Devices, Inc.Available online: https://www.analog.com/media/en/technical-documentation/tech-articles/Challenges-for-Electronic-Circuits-in-Space-Applications.pdf (accessed on 1 July 2018)*.
[33] O. Khan, M. El Moursi, H. Zeineldin, V. Khadkikar and M. Al Hosani, "Comprehensive design and control methodology for DC-powered satellite electrical subsystem based on PV and battery," *IET Renewable Power Generation*, vol. 14, no. 12, pp. 2202-2210 2020.
[34] A. Edpuganti, V. Khadkikar, M.S. Elmoursi, H. Zeineldin, N. Alsayari and K. Al Hosani, "A comprehensive review on CubeSat electrical power system architectures," *IEEE Transactions on Power Electronics* vol. 37, no. 3, pp. 3161-3177, 2022.
[35] B.D. Yost, D.J. Mayer, C.D. Burkhard, S.V. Weston and J.L. Fishman, "Small spacecraft systems virtual institute's federated databases and state of the art of small spacecraft technology report," 2018.

[36] A.D. Bintoudi, C. Timplalexis, G. Mendes, J.M. Guerrero and C. Demoulias, "Design of Space Microgrid for Manned Lunar Base: Spinning-in Terrestrial Technologies," in *2019 European Space Power Conference (ESPC)*, 2019, pp. 1-8.
[37] M.R. Patel, "Spacecraft power systems", *CRC press,* 2004.
[38] K. Woellert, P. Ehrenfreund, A.J. Ricco and H. Hertzfeld, "Cubesats: Cost-effective science and technology platforms for emerging and developing nations," *Advances in Space Research*, vol. 47, no. 4, pp. 663-684 2011.
[39] S.L. Rickman, "Introduction to On-orbit thermal environments," in *Thermal and Fluids Analysis Workshop*, 2014.
[40] S. Dahbi, A. Aziz, S. Zouggar, N. Benazzi, H. Zahboune and M. Elhafyani, "Design and sizing of electrical power source for a nanosatellite using photovoltaic cells," in *3rd International Renewable and Sustainable Energy Conference (IRSEC)*, 2015, pp. 1-6.
[41] S. Sanchez-Sanjuan, J. Gonzalez-Llorente and R. Hurtado-Velasco, "Comparison of the incident solar energy and battery storage in a 3U CubeSat satellite for different orientation scenarios," *Journal of Aerospace Technology and Management*, vol. 8, no. 1, pp. 91-102 2016.
[42] J. Bester, B.B. Groenewald and R. Wilkinson, "Electrical power system for a 3U CubeSat nanosatellite incorporating peak power tracking with dual redundant control," *Przeglad Elektrotechniczny,* vol. 88, pp. 300–304, 2012.
[43] A.D. Bintoudi, C. Timplalexis, G. Mendes, J.M. Guerrero and C. Demoulias, "Design of Space Microgrid for Manned Lunar Base: Spinning-in Terrestrial Technologies," in *2019 European Space Power Conference (ESPC)*, 2019, pp. 1-8.
[44] O. Shekoofa and E. Kosari, "Comparing the topologies of satellite electrical power subsystem based on system level specifications," in *2013 6th International Conference on Recent Advances in Space Technologies (RAST)*, 2013, pp. 671-675.
[45] C. Clark and A. Lopez, "Power system challenges for small satellite missions," in *Proceedings of the 2006 Small Satellites, Systems and Services Symposium, D. Danesy, Ed. The Netherlands: ESA*, 2006.
[46] O. Mourra, A. Fernandez and F. Tonicello, "Buck boost regulator (B 2 R) for spacecraft solar array power conversion," in *2010 Twenty-Fifth Annual IEEE Applied Power Electronics Conference and Exposition (APEC)*, 2010, pp. 1313-1319.
[47] T.M. Lim, A.M. Cramer, J.E. Lumpp and S.A. Rawashdeh, "A modular electrical power system architecture for small spacecraft," *IEEE Trans.Aerospace Electron.Syst.*, vol. 54, no. 4, pp. 1832-1849 2018.
[48] A. Edpuganti, V. Khadkikar, H. Zeineldin, M.S. El Moursi and M. Al Hosani, "Comparison of peak power tracking based electric power system architectures for CubeSats," *IEEE Trans.Ind.Appl.*, vol. 57, no. 3, pp. 2758-2768 2021.
[49] J. Bouwmeester and J. Guo, "Survey of worldwide pico-and nanosatellite missions, distributions and subsystem technology," *Acta Astronaut.*, vol. 67, no. 7-8, pp. 854-862 2010.
[50] J.A. Carrasco, F.G. de Quirós, H. Alavés and M. Navalón, "An analog maximum power point tracker with pulsewidth modulator multiplication for a solar array regulator," *IEEE Transactions on Power Electronics*, vol. 34, no. 9, pp. 8808-8815 2018.
[51] L. Peng, Z. Jun, Y. Xiaozhou and C. Luping, "Design and validation of modular MPPT electric power system for multi-U CubeSat," in *2017 3rd IEEE International Conference on Control Science and Systems Engineering (ICCSSE)*, 2017, pp. 374-377.
[52] A. Chub, D. Vinnikov, F. Blaabjerg and F.Z. Peng, "A review of galvanically isolated impedance-source DC–DC converters," *IEEE Transactions on Power Electronics*, vol. 31, no. 4, pp. 2808-2828 2015.

[53] Manuel Padial Pérez. (April 8,). *"Secondary Power Distribution In Satellites"https://www.doeeet.com/content/eee-components/draft-secondary-power-distribution-in-satellites. [date retrieved August 17, 2020].* [Online]. available: https://www.doeeet.com/content/eee-components/draft-secondary-power-distribution-in-satellites/.

[54] M. D'Antonio, C. Shi, B. Wu and A. Khaligh, "Design and optimization of a solar power conversion system for space applications," *IEEE Trans.Ind.Appl.*, vol. 55, no. 3, pp. 2310-2319 2019.

[55] M. Forouzesh, Y.P. Siwakoti, S.A. Gorji, F. Blaabjerg and B. Lehman, "Step-up DC–DC converters: A comprehensive review of voltage-boosting techniques, topologies, and applications," *IEEE transactions on power electronics*, vol. 32, no. 12, pp. 9143-9178 2017.

[56] R.R. Gopi and S. Sreejith, "Converter topologies in photovoltaic applications–A review," *Renewable and Sustainable Energy Reviews*, vol. 94, pp. 1-14 2018.

[57] S. Oprea, C. Radoi, A. Florescu, A. Savu and A. Lita, "Power architectures and power conditioning unit for very small satellites," in *Energy Harvesting and Energy Efficiency,* Springer, 2017, pp. 491-539.

[58] A. Ali, S.A. Khan, M.U. Khan, H. Ali, M. Rizwan Mughal and J. Praks, "Design of modular power management and attitude control subsystems for a microsatellite," *International Journal of Aerospace Engineering*, vol. 2018, 2018.

[59] B. Hoang, S. White, B. Spence and S. Kiefer, "Commercialization of Deployable Space Systems' roll-out solar array (ROSA) technology for Space Systems Loral (SSL) solar arrays," in *2016 IEEE Aerospace Conference*, 2016, pp. 1-12.

[60] N. Lee, J. Lee, Y. Cheon, S. Han and G. Moon, "A high-power-density converter with a continuous input current waveform for satellite power applications," *IEEE Trans.Ind.Electron.*, vol. 67, no. 2, pp. 1024-1035 2019.

[61] P.C. Adell, A.F. Witulski, R.D. Schrimpf, F. Baronti, W.T. Holman and K.F. Galloway, "Digital control for radiation-hardened switching converters in space," *IEEE Trans.Aerospace Electron.Syst.*, vol. 46, no. 2, pp. 761-770 2010.

[62] K. Yao, M. Ye, M. Xu and F.C. Lee, "Tapped-inductor buck converter for high-step-down DC-DC conversion," *IEEE Transactions on Power Electronics*, vol. 20, no. 4, pp. 775-780 2005.

[63] J. Faujdar, D.K. Gautam and V. Verma, "A New Converter for Common Mode Noise Reduction for EPS of a Nano satellite," in *2020 IEEE First International Conference on Smart Technologies for Power, Energy and Control (STPEC)*, 2020, pp. 1-6.

[64] A. Edpuganti, V. Khadkikar, M.S. Elmoursi, H. Zeineldin and M. Al Hosani, "A Novel EPS Architecture for 1U/2U Cubesats with Enhanced Fault-Tolerant Capability," in *2020 IEEE Industry Applications Society Annual Meeting*, 2020, pp. 1-6.

[65] P. Wong, P. Xu, P. Yang and F.C. Lee, "Performance improvements of interleaving VRMs with coupling inductors," *IEEE Transactions on Power Electronics*, vol. 16, no. 4, pp. 499-507 2001.

[66] W. Li and X. He, "Review of nonisolated high-step-up DC/DC converters in photovoltaic grid-connected applications," *IEEE Trans.Ind.Electron.*, vol. 58, no. 4, pp. 1239-1250 2010.

[67] O. Garcia, P. Alou, J.A. Oliver, D. Diaz, D. Meneses, J.A. Cobos, A. Soto, E. Lapena and J. Rancano, "Comparison of boost-based MPPT topologies for space applications," *IEEE Trans.Aerospace Electron.Syst.*, vol. 49, no. 2, pp. 1091-1107 2013.

[68] K. Hwu and Y.T. Yau, "An interleaved AC–DC converter based on current tracking," *IEEE Trans.Ind.Electron.*, vol. 56, no. 5, pp. 1456-1463 2008.

[69] J.G. Gorji, K. Abbaszadeh and F. Bagheroskouei, "A New Two-input And Multi-output Interleaved DC_DC Boost Converter For Satellites Power system," in *2019 10th International Power Electronics, Drive Systems and Technologies Conference (PEDSTC)*, 2019, pp. 236-241.

[70] O.C. Onar, J. Kobayashi, D.C. Erb and A. Khaligh, "A bidirectional high-power-quality grid interface with a novel bidirectional noninverted buck–boost converter for PHEVs," *IEEE transactions on vehicular technology*, vol. 61, no. 5, pp. 2018-2032 2012.

[71] O. Mourra, A. Fernandez, F. Tonicello and S. Landstroem, "Multiple port DC DC converter for spacecraft power conditioning unit," in *2012 Twenty-Seventh Annual IEEE Applied Power Electronics Conference and Exposition (APEC)*, 2012, pp. 1278-1285.

[72] M. Uno, M. Inoue, Y. Sato and H. Nagata, "Bidirectional interleaved PWM converter with high voltage-conversion ratio and automatic current balancing capability for single-cell battery power system in small scientific satellites," *energies*, vol. 11, no. 10, pp. 2702 2018.

[73] F. Belloni, P.G. Maranesi and M. Riva, "DC/DC converter for the international space station," *IEEE Trans.Aerospace Electron.Syst.*, vol. 46, no. 2, pp. 623-634 2010.

[74] P.K. Rampelli, R. Deekshit, D.S. Reddy, B.K. Singh, V. Chippalkatti and T. Kanthimathinathan, "Multiple-output magnetic feedback forward converter with discrete PWM for space application," in *2012 IEEE International Conference on Power Electronics, Drives and Energy Systems (PEDES)*, 2012, pp. 1-6.

[75] A. Pukniel, V. Coverstone, R. Burton and D. Carroll, "The dynamics and control of the CubeSail mission: A solar sailing demonstration," *Advances in Space Research*, vol. 48, no. 11, pp. 1902-1910 2011.

[76] Standard Solar Spectra. [Online]. available: https://www.pveducation.org/pvcdrom/appendices/standard-solar-spectra.

[77] R. Cariou, J. Benick, P. Beutel, N. Razek, C. Flötgen, M. Hermle, D. Lackner, S.W. Glunz, A.W. Bett and M. Wimplinger, "Monolithic two-terminal III–V//si triple-junction solar cells with 30.2% efficiency under 1-sun AM1. 5G," *IEEE Journal of Photovoltaics*, vol. 7, no. 1, pp. 367-373 2016.

[78] N. Miyashita, Y. He, T. Agui, H. Juso, T. Takamoto and Y. Okada, "Inverted lattice-matched triple junction solar cells with 1.0 eV GaInNAsSb subcell by MOCVD/MBE hybrid growth," *IEEE Journal of Photovoltaics*, vol. 9, no. 3, pp. 666-672 2019.

[79] Loren Grush. (Aug 17,). *NASA is prepared if a battery ever explodes in space* [Online]. available: https://www.theverge.com/2018/8/17/17681422/nasa-lithium-ion-batteries-thermal-runaway-human-spaceflight.

[80] M. Stan, B. Cho, B. Guzie, G. Smith, P. Sharps and T. Varghese, "Air Force ManTech qualification of the 30% class GaInP2/Ga (In) As/Ge solar cell to the AIAA S-111 standard: results and recommendations," in *2010 35th IEEE Photovoltaic Specialists Conference*, 2010, pp. 2625.

[81] S. Pandey, "Ge/GaAs/InGaP triple-junction solar cells for space exploration,".

[82] M. Alia-Novobilski. Advanced multi-junction solar cells deliver high efficiency, reduced costs for space" [Online]. available: *Advanced-multi-junction-solar-cells-high. html https://phys.org/news/2018-01*.

[83] J.A. Gow and C.D. Manning, "Development of a photovoltaic array model for use in power-electronics simulation studies," *IEE Proceedings-Electric Power Applications*, vol. 146, no. 2, pp. 193-200 1999.

[84] S. Chtita, Y. Chaibi, A. Derouich and J. Belkadid, "Modeling and Simulation of a Photovoltaic Panel Based on a Triple Junction Cells for a Nanosatellite," in *2018 International Symposium on Advanced Electrical and Communication Technologies (ISAECT)*, 2018, pp. 1-6.

[85] J.A. Ramos-Hernanz, J.J. Campayo, E. Zulueta, O. Barambones, P. Eguía and I. Zamora, "Obtaining the characteristics curves of a photocell by different methods," in *International Conference on Renewable Energies and Power Quality*, 2013, pp. 1-6.

[86] A. Zekry, A. Shaker and M. Salem, "Solar cells and arrays: Principles, analysis, and design advances in renewable energies and power technologies," pp. 3-56. Elsevier, 2018.

[87] G. Xin, F. Zhan-Zu, C. Xin-Yu, Y. Sheng-Sheng and Z. Lei, "Performance evaluation and prediction of single-junction and triple-junction GaAs solar cells induced by electron and proton irradiations," *IEEE Trans.Nucl.Sci.*, vol. 61, no. 4, pp. 1838-1842 2014.

[88] S. Sato, H. Miyamoto, M. Imaizumi, K. Shimazaki, C. Morioka, K. Kawano and T. Ohshima, "Degradation modeling of InGaP/GaAs/ge triple-junction solar cells irradiated with various-energy protons," *Solar Energy Mater.Solar Cells*, vol. 93, no. 6-7, pp. 768-773 2009.

[89] J. Meng, J. Feng, Q. Sun, Z. Pan and T. Liu, "Degradation model of the orbiting current for GaInP/GaAs/ge triple-junction solar cells used on satellite," *Solar Energy*, vol. 122, pp. 464-471 2015.

[90] H.K. Kim and C.Y. Han, "Analytical and numerical approaches of a solar array thermal analysis in a low-earth orbit satellite," *Advances in space research*, vol. 46, no. 11, pp. 1427-1439 2010.

[91] V. Knap, L.K. Vestergaard and D. Stroe, "A review of battery technology in CubeSats and small satellite solutions," *Energies*, vol. 13, no. 16, pp. 4097 2020.

[92] B. Abdi, A. Alimardani, R. Ghasemi and S. Mirtalaei, "Energy storage selection for leo satellites," *International Journal of Machine Learning and Computing*, vol. 3, no. 3, pp. 287 2013.

[93] J. Bouwmeester and J. Guo, "Survey of worldwide pico-and nanosatellite missions, distributions and subsystem technology," *Acta Astronaut.*, vol. 67, no. 7-8, pp. 854-862 2010.

[94] V. McLaren, C. Clark, E. Simon and B. Hendel, "Lithium-ion polymer cell for small satellites," in *Proceedings of the NASA Battery Workshop*, 2008.

[95] C. Yeh, S. Wu, T. Huang, Y. Tsai, J. Juang and K. Wu, "Certification of Lithium-ion Cells with Electrical Power Subsystem for CubeSat," in *7th Nano-Satellite Symposium and the 4th UNISEC-Global Meeting*, 2016.

[96] B.T. Schneidegger, "Performance characterization of high energy commercial lithium-ion cells," *NASA/TM—2010-216926*, 2010.

[97] L. Kessler Slongo, S. Vega Martinez, B. Vale Barbosa Eiterer and E. Augusto Bezerra, "Nanosatellite electrical power system architectures: Models, simulations, and tests," *International Journal of Circuit Theory and Applications*, vol. 48, no. 12, pp. 2153-2189 2020.

[98] D. Del Corso, C. Passerone, L. Reyneri, C. Sansoe, S. Speretta and M. Tranchero, "Design of a university nano-satellite: The PiCPoT case," *IEEE Trans.Aerospace Electron.Syst.*, vol. 47, no. 3, pp. 1985-2007 2011.

[99] L. Peng, Z. Jun and Y. Xiaozhou, "Design and on-orbit verification of EPS for the world's first 12U polarized light detection CubeSat," *International Journal of Aeronautical and Space Sciences*, vol. 19, no. 3, pp. 718-729 2018.

[100] A. Aoudeche, X. Zhao and K.D. Kerrouche, "Design of a high-performance electrical power system for an earth observation nano-satellite," in *Proceedings of the 2018 International Conference on Electronics and Electrical Engineering Technology*, 2018, pp. 140-146.

[101] K. Cheremetiev, "Design of reliable electrical power system for foresail-1 small satellite," *Master Thesis School of Electrical Engineering Aalto University*, 2020.

[102] SISP 32% Solar Cells [Online]. available: http://en.811sisp.com/newsinfor/p3_351.html?&pageid=3&_id=351&r=0.
[103] M.H. Rashid, *Power electronics: circuits, devices, and applications*, Pearson Education India, 2009.
[104] E.L.B. Datasheet—LIR18650, "Lithium-ion battery," *2600 mAh*.
[105] K. Lamichhane, M. Kiran, T. Kannan, D. Sahay, H.G. Ranjith, S.R. Hegde and S. Sandya, "Operational flow of twin satellite mission," in *2015 IEEE Metrology for Aerospace (MetroAeroSpace)*, 2015, pp. 362-366.
[106] R. Darbali-Zamora, E.I. Ortiz-Rivera and A.A. Rincon-Charris, "Dynamic Real-Time Simulation Approach to Power Management Modelling for CubeSat Applications," in *2019 IEEE 46th Photovoltaic Specialists Conference (PVSC)*, 2019, pp. 2792-2797.
[107] E. Mostacciuolo, L. Iannelli, S. Sagnelli, F. Vasca, R. Luisi and V. Stanzione, "Modeling and power management of a LEO small satellite electrical power system," in *2018 European Control Conference (ECC)*, 2018, pp. 2738-2743.
[108] K.D.E. Kerrouche, A. Seddjar, N. Khorchef, S.A. Bendoukha, L. Wang and A. Aoudeche, "CubeSat project: Experience gained, and design methodology adopted for a low-cost electrical power system," *Automatika*, vol. 63, no. 4, pp. 695-717 2022.
[109] A. Ali, A. Massoud, M.O. Hasna, T. Khattab, T. Jabban and M.A. Nema, "Modeling of CubeSat orientation scenario and solar cells for internet of space provision," in *2019 9th International Conference on Recent Advances in Space Technologies (RAST)*, 2019, pp. 541-546.
[110] S. Noroozi, H. Shayanfar and M. Nasirian, "Design of an intelligent MPPT for a PV array mounted on a satellite considering outer space," *International Transactions on Electrical Energy Systems*, vol. 31, no. 9, pp. e12984 2021.
[111] A. Balal and M. Murshed, "Implementation and comparison of perturb and observe, and fuzzy logic control on maximum power point tracking (MPPT) for a small satellite," *Journal of Soft Computing and Decision Support Systems*, vol. 8, no. 2, pp. 14-18 2021.
[112] Y. Xu, G. Wang, C. Zhang, X. Li and Q. Xu, "Research on Integrated MPPT Control and Online Monitoring System of Microsatellite," in *2021 IEEE 5th Advanced Information Technology, Electronic and Automation Control Conference (IAEAC)*, 2021, pp. 344-348.
[113] C. Torres, A. Garrigós, J.M. Blanes, P. Casado, D. Marroquí and C. Orts, "Analog MPPT Comparison for Interplanetary Small Satellites Missions," in *24th European Conference on Power Electronics and Applications (EPE'22 ECCE Europe)*, 2022, pp. 1-9.
[114] M. Lawan, A. Aboushady and K.H. Ahmed, "Photovoltaic MPPT techniques comparative review," in *9th International Conference on Renewable Energy Research and Application (ICRERA)*, 2020, pp. 344-351.
[115] N. Femia, G. Petrone, G. Spagnuolo and M. Vitelli, "Optimization of perturb and observe maximum power point tracking method," *IEEE transactions on power electronics*, vol. 20, no. 4, pp. 963-973 2005.
[116] S. Panda, S. Singh, R. Sharma and P.R. Satpathy, "Tracking Comparison of P&O and INC based MPPTs under varying weather conditions," in *2nd International Conference on Data Science and Business Analytics (ICDSBA)*, 2018, pp. 198-203.
[117] D. Sera, L. Mathe, T. Kerekes, S.V. Spataru and R. Teodorescu, "On the perturb-and-observe and incremental conductance MPPT methods for PV systems," *IEEE journal of photovoltaics*, vol. 3, no. 3, pp. 1070-1078 2013.
[118] S.U. Ramani, S.K. Kollimalla and B. Arundhati, "Comparitive study of P&O and incremental conductance method for PV system," in *2017 International Conference on Circuit, Power and Computing Technologies (ICCPCT)*, 2017, pp. 1-7.

[119] A. Trivedi, A. Gupta, R.K. Pachauri and Y.K. Chauhan, "Comparison of Perturb & Observe and Ripple correlation control MPPT algorithms for PV array," in *2016 IEEE 1st International Conference on Power Electronics, Intelligent Control and Energy Systems (ICPEICES)*, 2016, pp. 1-5.

[120] T. Esram, J.W. Kimball, P.T. Krein, P.L. Chapman and P. Midya, "Dynamic maximum power point tracking of photovoltaic arrays using ripple correlation control," *IEEE Transactions on power electronics*, vol. 21, no. 5, pp. 1282-1291 2006.

[121] M. Yaqoob, A. Hussain, J. Maurilio, A. Lashab, J. C. Vasquez, J. M. Guerrero, "Design and power management of a full-scale LEO small satellite microgrid," *Submitted in IEEE Access*, 2022.

[122] M. Swartwout, "The first one hundred CubeSats: A statistical look," *Journal of small Satellites*, vol. 2, no. 2, pp. 213-233 2013.

[123] M. Soshinskaya, W.H. Crijns-Graus, J.M. Guerrero and J.C. Vasquez, "Microgrids: Experiences, barriers and success factors," *Renewable and sustainable energy reviews*, vol. 40, pp. 659-672 2014.

[124] M. Nasir, M. Anees, H. Abbas Khan and J.M. Guerrero, "Dual-loop control strategy applied to the cluster of multiple nanogrids for rural electrification applications," *IET Smart Grid*, vol. 2, no. 3, pp. 327-335 2019.

[125] M. Nasir, Z. Jin, H.A. Khan, N.A. Zaffar, J.C. Vasquez and J.M. Guerrero, "A decentralized control architecture applied to DC nanogrid clusters for rural electrification in developing regions," *IEEE Transactions on Power Electronics*, vol. 34, no. 2, pp. 1773-1785 2018.

[126] M.H. Lipu, M.A. Hannan, A. Hussain, M.M. Hoque, P.J. Ker, M.M. Saad and A. Ayob, "A review of state of health and remaining useful life estimation methods for lithium-ion battery in electric vehicles: Challenges and recommendations," *J.Clean.Prod.*, vol. 205, pp. 115-133 2018.

[127] M. Pajusalu, E. Ilbis, T. Ilves, M. Veske, J. Kalde, H. Lillmaa, R. Rantsus, M. Pelakauskas, A. Leitu and K. Voormansik, "Design and pre-flight testing of the electrical power system for the ESTCube-1 nanosatellite," *Proceedings of the Estonian Academy of Sciences*, vol. 63, no. 2, pp. 232 2014.

[128] P. Chen, B. Yan, C. Liu, S. Wang and Y. Liu, "A comparative study on MPPT for photovoltaic generation systems," in *IEEE 2nd International Future Energy Electronics Conference (IFEEC)*, 2015, pp. 1-6.

[129] M. Nasir and M.F. Zia, "Global maximum power point tracking algorithm for photovoltaic systems under partial shading conditions," in *16th International Power Electronics and Motion Control Conference and Exposition*, 2014, pp. 667-672.

Part 2

Selected Papers

Journal Paper 1

A Comprehensive Review on Small Satellite Microgrids

Mohammad Yaqoob, *Student Member, IEEE*, Abderezak Lashab *Member, IEEE*, Juan C. Vasquez *Senior Member, IEEE*, Josep M. Guerrero, *Fellow, IEEE,* Marcos E. Orchard, and Angelina D. Bintoudi, *Student Member, IEEE*

The paper has been published in *IEEE Transactions on Power Electronics*, vol. 37, no. 10, pp. 12741-12762, 2022.

Journal Paper 2

Design and Power Management of a Full-scale LEO Small Satellite Microgrid

Mohammad Yaqoob *Student Member*, José Maurilio Raya-Armenta *Student Member*, Hussein Abubakr *Student Member, IEEE*, Abderezak Lashab *Member, IEEE*, *Josep* M. Guerrero, *Fellow, IEEE,* Juan C. Vasquez *Senior Member, IEEE*

The paper has been submitted in *IEEE Access*, vol. XX(X), pp. XXX-XXX, 2022.

Conference Paper 1

A Comparative Study of MPPTs for Nano-Satellite Microgrid Applications under Spinning Flight Scenarios

Mohammad Yaqoob, *Student Member, IEEE*, Hussein Abubakr *Student Member, IEEE*, Jose Matas Alcala *Senior Member, IEEE*, Abderezak Lashab *Member, IEEE*, Juan C. Vasquez *Senior Member, IEEE*, Josep M. Guerrero, *Fellow, IEEE*

The paper has been presented in *48th Annual Conference of the Industrial Electronics Society, IECON,* pp. X-X, 17 - 20 October 2022, Brussels, Belgium.

Conference Paper 2

Self-directed Energy Management System for an Islanded Cube Satellite Nanogrid

Mohammad Yaqoob, *Student Member, IEEE*, Mashood Nasir *Member, IEEE*, Juan C. Vasquez *Senior Member, IEEE*, Josep M. Guerrero, *Fellow, IEEE*

The paper has been published in *IEEE Aerospace Conference,* pp. 1-7, 07-14 March 2020, Big Sky, MT, USA.

ISSN (online): 2446-1636
ISBN (online): 978-87-7573-777-2

AALBORG UNIVERSITY PRESS